Teknillinen korkeakoulu
Laivalaboratorio

Helsinki University of Technology
Ship Laboratory

Espoo 2003

M-280

THE EVOLUTION OF RIDGED ICE FIELDS

Mikko Lensu

M-280

THE EVOLUTION OF RIDGED ICE FIELDS

Mikko Lensu

Dissertation for the degree of Doctor of Philosophy to be presented with due permission for public examination and debate in Auditorium K216 at Helsinki University of Technology, Espoo, Finland, on the 11th of June 2003 at 12 noon.

ISBN 951-22-6558-3
ISSN 1456-3045

Helsinki University of Technology
Ship Laboratory

Teknillinen korkeakoulu
Laivalaboratorio

Espoo 2003

ABSTRACT

Ridges are elongated ice cover features created by local deformation. In the Baltic the visible part of the ridge, the sail, is typically 1-3 m high while the bulk of the ridge volume is contained to the 5-15 m deep subsurface keel. In larger scales ridging creates ridged ice fields. The modeling of ridges and ridged ice fields is important for dynamic ice drift models, for ice navigating ships, and for the estimation of ice loads exerted against offshore structures.

Ridge fields are quantified in terms of ridge heights and ridge spacings which are distances between ridge sails. The present work formulates an equation governing the evolution of ridge spacing distribution. The usual lognormal and exponential distribution models for spacing distributions are obtained as solutions. The equation also explains several statistical features found in the analysis of ice surface profile data from the Baltic and from the Kara Sea. Conservation equations for continuum fields of spacing distributions are formulated. These can be included in dynamic ice forecast models.

The parameterisation links the evolution to the decrease of ice area and to the fields of concentration and strain rate. An estimate for the equivalent thickness of ridge rubble is thereby obtained and is much larger than the values estimated previously. The parameterisation requires cross-sectional modelling of the ridges. A new type of feature, a ridge cluster, is introduced to describe ridges in keel contact. Concepts to describe cluster structure and cluster occurrence are developed.

The spacing equation is a specific formulation of the Kolmogorov-Feller equation which is the basic equation governing discontinuous Markov processes. Another specific formulation is the equation governing the evolution of ice thickness distribution. A general presentation of discontinuous Markov processes is given. It can be used to construct evolution equations for ice morphological quantities. In the present context it is used to formulate alternatives to the spacing equation. The most applicable of these alternatives govern the distribution of ridge sail number, or the number of sails on line segments.

PREFACE

This work belongs to ice cover geophysics which constitutes an essential body of background knowledge for arctic marine technology. It was triggered by my considerations on changing ice floe size in the Finnish Institute of Marine Research in early 1990's. I realised that the relevance of the adopted methods extended beyond that specific problem and a wish to formulate an applicable general approach to changing ice cover geometry emerged. After moving to Ship Laboratory ridged ice fields became a natural application for the theory.

I am especially grateful to my supervisor, Professor Kaj Riska, who's enthusiasm and open-mindedness towards new ideas I appreciate. Poincaré stated that "nothing is more practical than a good theory" but from Prof. Riska I learned that this includes also skills of clear and precise communication. Almost as much I am indebted to Professor Jukka Tuhkuri with whom I had during several years almost daily discussions on ice research. He also read carefully my manuscripts and his sound comments helped me a great deal forward. I also wish to thank Professor Petri Varsta who's friendly attitude has let me understand that he considers my work as beneficial to Ship Laboratory.

Special thanks go to Professor Matti Leppäranta who gave the initial impetus to this work. I also wish to thank all colleagues with whom I have worked in Finland and around the Arctic. A special mention goes to Dr. Christian Haas, with whom I have shared several enjoyable field expeditions, and to Dr. Mark Hopkins who has helped me to see ridge science as a noble enterprise. Finally I wish to thank my wife Leena for remaining herself during this work.

Degerby, May 2003
Mikko Lensu

> The great Danish author appears to have had his own thoughts on stochastic ice science:
>
> *He dragged some sharp, flat pieces of ice to and fro, and placed them together in all kinds of positions, as if he wished to make something out of them; just as we try to form various figures with little tablets of wood which we call a Chinese puzzle. Kay's fingers were very artistic; it was the icy game of reason at which he played, and in his eyes the figures were very remarkable, and of the highest importance; this opinion was owing to the piece of glass still sticking in his eye.*
>
> H.C. Andersen, "The Snow Queen"

CONTENTS

RECURRENT NOTATIONS

Basic notations

$X,Y,\ldots;\mathbf{X},\mathbf{Y},\ldots$	Morphological variables (univariate; multivariate)
$x,y,\ldots;\mathbf{x},\mathbf{y},\ldots$	Values of morphological variables
n	Value of discrete variable; event number
t	Time
$\mathbf{r}$, $\mathbf{v}$	Horizontal coordinate, velocity field
σ, $\dot{\varepsilon}$	Stress, strain rate
μ,ρ	Measure, measure density
f, g	Morphological distributions
k	Discrete morphological distribution; event number distribution
Λ	Lognormal distribution
δ	Dirac delta function
(;)	Separating variables and parameters
$\langle\ \rangle$	Expectation, mean value, averaging
Var , Std	Variance, standard deviation
μ,σ	Geometric mean, geometric standard deviation
$(\ \vert x)$, $\langle\ \vert x\rangle$	Conditioning on x
Δ	Integration domain
R, S	Region, ridge sail field
A	Area
C	Concentration
L	Length, length scale
N,M	Number
V	Volume

Evolution equations

α	Event rate
a	Relative Poisson rate
β	Intensity factor of event rate
$\rightarrow$	Transition
B	Transition probability
b	Probability distribution defined on [0,1]
κ	Progeny production
Ψ	Mechanical evolution
θ	Continuous process rate
γ^e,γ^d	Emergence and destruction terms

F,K,Φ	Integral transforms
s	Integral transform variable
ρ	Correlation

Ridge fields

H	Parent ice thickness, block thickness
H_{eq}	Equivalent thickness of ridge rubble
h_{cs} , h_l	Cross-sectional ridge sail height, ridge sail link height
h_0	Sail height cutoff value
w_{cs} ,w_l	Cross-sectional ridge keel width, ridge link keel width
c	Ice consumption
v^*, w^*, c^*	Reductions of ridge volume, ridge width and ice consumption
$\bar{d}$, d	Length of ridge sail per unit area, ridge sail density
X,x	Ridge sail spacing
X,x	Spacing cross-section variable
V,v	Spacing cross-section volume
c_s	Spacing consumption
Y_n ,y_n	Length of sail spacing n-concatenation
Y^+,Y^-, y^+, y^-	Length of threshold concatenation
Z,z	Ice thickness
L_i	Segment length
n_i	Sail number
φ	Ice area decrease function

Subscripts

i,j,k	Scale indices in sail numbers
l	Pertaining to ridge link cross-section
cs	Pertaining to ridge cross-sections
s	Pertaining to sail spacings
as	Asymptotical
eq	Equivalent

1. INTRODUCTION

1.1. The scope of the work

The main focus of the present work is on the time evolution of ridge spacing distribution. Spacings quantify the distances between ridges. The aim is to formulate conservation equations which yield the observed spacing distributions as solutions and make possible the incorporating of spacing distribution evolution into dynamic ice models. This task is analogical to that taken by Thorndike et al. (1975) in their approach to ice thickness distribution. Therefore the present study focuses also more generally on distributions describing ice cover. The aim is to show that the equations for spacing and thickness distributions are specific formulations of a more general approach that can be applied also to other ice morphological distributions.

Ridges are elongated pileup features in the ice cover. In the Baltic the visible part of the ridge, the sail, is typically 1-3 m high while the bulk of the ridge volume is contained to the 5-15 m deep keel. The study of ridges and the ridging process is important for general ice cover characterisation, for dynamic ice drift models, for the estimation of ice loads exerted against ships and offshore structures, and for the calculation of ship speed in a ridged ice field. There are three main study areas that are relevant here: ridge buildup process, ridge properties, and ridged ice fields. Ridge buildup sets on when the local compressive forces in the ice cover exceed local ice cover strength. The forces required to drive the buildup further increase with the size of the growing ridge. This usually results into the termination of the buildup process through the failing of the ice cover elsewhere. The characterisation of buildup sequence, and the relation of the buildup forces to local ice thickness and ice mechanical parameters are central questions. Completed ridges have certain mechanical and structural properties. The structural properties describe the geometry of the ridges and their internal composition. The mechanical properties depend on the structural properties and with them determine the forces that a ridge may exert on a ship or an offshore structure.

In a larger scale ice cover compression creates ridge fields. Dynamically these relate to ridge buildup events like statistical physical systems composed of a large number of subsystems. Also structurally they are described by the statistics of the individual ridges. The size and occurrence of the ridges in the field vary considerably and are most conveniently described by statistical distributions. In surface characterisation this is usually done by ridge sail height and ridge sail spacing distributions. If the field is compressed further its area decreases as more level ice is heaped into ridges. At the same time the spacing distribution changes. To relate the ice area decrease to the spacing distribution change constitutes the main parameterisation task of the present study. This is approached in longer time

scales where the buildup of a ridge can be considered as an instantaneous event. The relation between area decrease and spacing distribution change depends on the size of ridges and involves thus both sail height distribution and ridge structure models.

The required ridge structural concepts and distributions are defined in Chapter 2. The main novelty is the introduction of ridge clusters or groups of ridges with keel contact. Chapter 3 presents an evolution theory for ice morphological distributions. It is based on the theory of discontinuous Markov processes, originally formulated by Kolmogorov (1931). As an application of the general theory Chapter 4 presents evolution equations for ridge spacing distributions. Alternative approaches to describe ridge field evolution are also considered. Analytical solution methods for the presented equations are given in Chapter 5, and the usual distribution models for spacing distribution are obtained as solutions. The theory predicts several statistical features pertaining to the clustering of ridges. These are compared with observations in Chapter 6. The incorporating of spacing evolution to dynamic ice models is considered in Chapter 7 and a parameterisation based on available data is given.

1.2. Review of earlier research

The present work is a synthesis of two lines of research, the theory of discontinuous Markov processes and the study of ridged ice fields. The theory of discontinuous Markov processes was formulated by Kolmogorov (1931) and Feller (1936), and the main equation of the theory is called the Kolmogorov-Feller equation. The equation itself is a continuous and usually linear integral-differential equation. It soon found applications in various fields. These usually have a particulate process context where the particles may fragment or coagulate. In 1975 Thorndike, Rothrock, Maykut and Colony published a paper in which they formulated an equation governing the temporal change of ice thickness distribution. The equation is of the Kolmogorov-Feller type although this was not recognised. Their formulation was also nonlinear. Later approaches have largely taken the equation of Thorndike et al. (1975) as such and sought better parameterisations and amendments through the consideration of different processes of thickness change (Hibler 1980). The theoretical developments are few. Thorndike (1992) gave a discrete matrix formulation of the thickness equation and noted that it constituted a discrete Markov process. Timokhov (1998) noted that the floe size distribution is governed by an equation that is mathematically similar to the thickness equation. Pritchard (1998) suggested a bivariate oriented thickness equation, and Marchenko (1999) suggested another bivariate formulation where the other variable described the degree of damage in

the ice. However, none of this work is connected to the main field of research around the Kolmogorov-Feller type equations and their applications.

The parameterisation of the thickness equation of Thorndike et al. (1975) is done by considering different processes of thickness change. The equation is thus implicitly related to the ridging process. It has been incorporated to few ice models (Hibler 1980, Flato and Hibler 1995, Thomas et al. 1996, Bitz et al. 2001). The thickness in dynamic ice models is generally described by a number of thickness or ice type categories. The two-type description (Hibler 1979) includes ice concentration and average ice thickness. Adding more thickness categories brings the thickness description closer to the thickness equation which has a continuous range of thickness categories. Adding more ice types brings the thickness description towards the methods of present approach, where the ridge distributions can be interpreted as describing a continuous range of ice types. In a three-type description the third type is usually ridged or deformed ice (Leppäranta 1981 c, Flato and Hibler 1991, Harder and Lemke 1994, Haapala and Leppäranta 1996). The volume of ridged ice can be converted into ridge field parameters by using ridge structure models. This is, however, not usually done. The model equations can also use ridge field parameters instead of ridged ice volume (Leppäranta 1981 c). Another approach was adopted by Steiner et al. (1999) who interpreted a certain fraction of energy dissipated in the ice cover as energy used in ridge buildup. This parameter was then converted into ridge field parameters using ridge models. More categories can be added in order to separate ridged ice more accurately from other deformed ice types, for example rafted ice and rubble ice (Haapala 2000).

Studies that can be used to parameterise ridge fields and their evolution are numerous. Ridge structure research started both in the Baltic and in Arctic in 1970's (Palosuo 1975, Keinonen 1976, Kovacs 1970). Later also the strength of ridges was measured in full scale (Leppäranta and Hakala 1992, Hoyland et al. 2000) and thermal processes were monitored (Leppäranta et al. 1995). Kankaanpää (1997) has analysed or reviewed most Baltic structural data and a reanalysis of all available Arctic data sets was done by Timco and Burden (1997). A major motivation of structural studies has been the modelling of loads exerted by ridges against offshore structures (Chao 1992). Another important application is the calculation of the resistance experienced by ridge penetrating ships (Keinonen 1979). Ship trials in ridged ice have usually been accompanied by ridge structure measurements (Mäkinen et al. 1975, Nyman et al. 1999). Another application is the modelling of SAR backscattering from ridge sails (Manninen 1997).

Surface profiling measurements with a laser are the main source of sail height and spacing distributions. In the Baltic a laser profilometer was first mounted to a ship

(Leppäranta 1981 a) and later carried by a helicopter (Lewis et al. 1993). Arctic and Antarctic laser profile data sets have been analysed in Tucker et al. (1979), Wadhams (1980, 1981), Kreider and Thro (1981), Weeks et. al (1989), Dierking (1995), and Granberg and Leppäranta (1999). From the ice draft profile ridge keel depth and spacing distributions are determined. The central arctic draft profile has been recorded by upward looking sonars during numerous submarine cruises. Only a part of this data very large data source has been free for analysis (Wadhams and Horne 1980, Wadhams 1981, McLaren 1989). The sonars may also be moored for long term monitoring (Vinje et. al 1998) The ridge distributions are also required in the estimation of speed and damage risk of ships navigating in a ridged ice field (Kujala 1994).

Ridge formation models have suggested several mechanisms of initialisation, failure and buildup (Parmerter and Coon 1972, Kovacs and Sodhi 1980, Sayed and Frederking 1988). Recently discrete element modelling has been applied to ridge buildup (Hopkins 1998) and also to ice cover ridging in larger scales (Hopkins 1996). Ice tank tests provide an important comparison to these studies (Timco and Sayed 1986, Hopkins et al. 1999).

The evolution theory of ridge fields creates a focal point of all these fields of study. The equations formulated in the theory are parameterised by the ridge structure and ridge formation models, the resulting ridge field statistics is compared with profile data, and finally the validated theory can be used to predict changes in ridging and to calculate ice loads and travel times of ice navigating ships.

2. DESCRIPTION OF RIDGED ICE FIELDS BY RIDGE SAILS

2.1. Introduction

Parameters characterising ridged ice fields are defined in the present chapter together with their associated distributions. The parameters and distributions are defined so that they are suitable to the characterisation of a dynamically changing ridge field. Commonly applied parameters are critically discussed. Ridge link is defined to serve as the decomposition unit of ridge fields. When new ridges are formed, a certain area of non-ridged ice is heaped into ridges. The ridge formation relates also to certain movements in the ice cover. Special attention is paid to these two aspects. Another general feature of the approach is the description of ridge fields in terms of surface observable parameters. Several new concepts are introduced. Most of these are related to the clustering of ridges, or the occurrence of groups of ridges which are in keel contact. In spacing evolution context the clustering is described in terms of a new structural entity, spacing cross-section.

The main motivation to consider clustering is to model its effect in spacing evolution and ice volume balance. However, the importance of ridge clusters as ice features is evident. Therefore alternative characterisations of clustering are also given. The clusters introduce a new dimension in contexts where ridge structural modelling is applied. Wide deformation features that usually are interpreted as large ridges become quantifiable in terms of well defined parameters. In application contexts, especially when ice going ships are considered, the alternative characterisations of clustering are more suitable.

When the new structural concepts are brought into the statistical context of ridge fields new distributions are required. These describe ridge links, spacing cross-sections, and ridge clusters. Several distributions related to ridge clustering are introduced. The most useful of these is the ridge sail number distribution which is a versatile alternative to the sail spacing distribution. The averaged ridge structure parameters are also related to other parameters describing ridged ice fields. The most important of these is the equivalent thickness of ridge rubble.

2.2. Ridge structure and ridged ice fields

2.2.1. Ridge formation

A region in an ice covered sea area is considered. It is assumed that there is no ice flux across boundaries while the shape of the region and its area A may change in time. Such region is called a Lagrangian region. In the region the average ice concentration is C, the area of ice is CA, the volume of ice is V, and the average

ice thickness is V/CA. The ice volume per unit area, V/A, which often is taken as the definition of average ice thickness, will not be used in the present context. A time period during which thermal ice growth or melting can be neglected is considered. A mechanical thickness increase process is then any process where the average ice thickness increases, that is, the ice area decreases while the ice volume remains unchanged. On the other hand, V/A need not increase in a mechanical thickness increase process and may also change without such process, and is therefore not suitable for present purposes.

Figure 1. Ongoing ridge formation process. The sail height is 1-1.5 m.

A mechanical thickness increase process manifests as local processes. These can be classified by three process types which are rubble compression, finger rafting and ridging. In rubble compression an aggregate of loose ice pieces or small floes is compressed into larger average thickness. In finger rafting the ice sheet fails along a linear fault and the opposing sheets are forced into two layers. The vertical order of the layered sheets alternates creating a pattern of fingers. In ridge formation the ice cover fails along a linear fault, or the process is initiated from a pre-existing fault, like a crack or an interface between floes. This is followed by a compressive movement between the opposing ice sheets. These are broken into blocks which are heaped above and below the water level. An ongoing ridge formation process is seen in Figure 1. The ridge formation process terminates

when the forces required to continue the process exceed the local driving forces present in the ice cover. The result is a narrow, long formation roughly following the direction of the original fault. The visible part is called sail and the underwater part keel (Figure 3). In a larger ice areas the ridging manifests as creation of ridge fields (Figure 2).

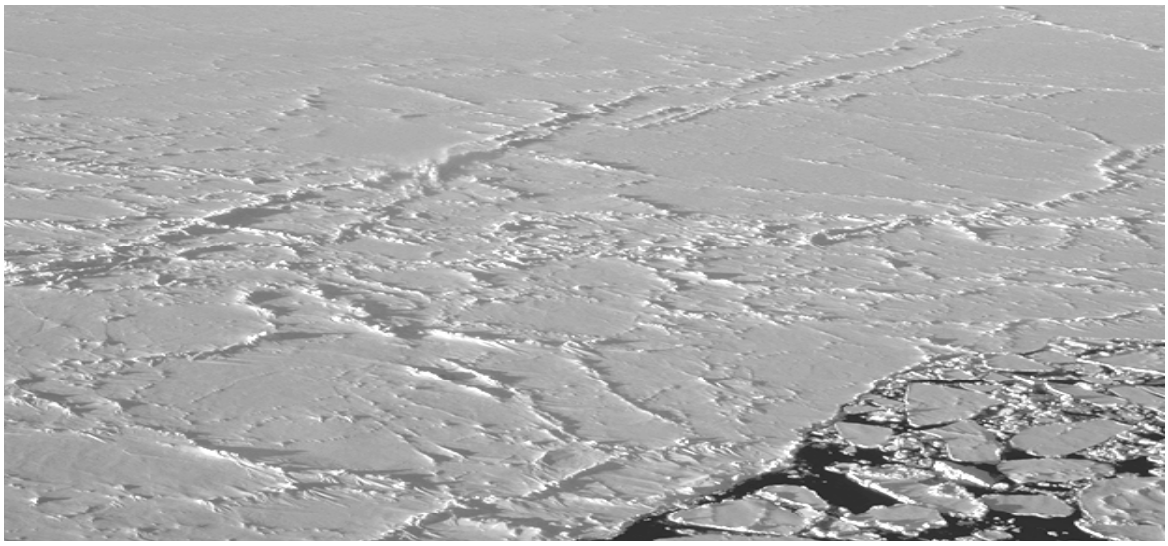

Figure 2. A central arctic ridge field as seen from a helicopter. Ridge sails are 1-3 m high.

2.2.2. Ridge creating ice cover movements, ridge direction, and ridge links

It is apparent from Figure 2 that 'ridge' understood as an elementary unit feature of a ridge field is an ambiguous concept. The ridgelike formations have very different lengths, meet and intersect other similar formations, and are intermittent and zigzagging. Ridge links are defined to serve the need of having such elementary linear features with direction and two endpoints. However, the relation of the observed ridge link direction to the ridge creating ice cover movement is problematic and is discussed first.

Figure 3 shows an idealised ridge created by uniaxial compression the direction of which is perpendicular to the initial rectilinear fault. The direction of the created ridge follows the fault direction, and the direction perpendicular to it defines ridge normal direction. The compressive movement in the ridge normal direction is considered as differential movement where one sheet is stationary and the opposing sheet moves. The ice from which the ridge blocks are formed is called

parent ice. The total magnitude of the differential compressive movement between the ice sheets is called parent ice consumption.

However, the direction of the compressive movement may also have an oblique angle with the direction of the ridge. This may be due to the oblique angle of the initial fault, for example. With respect to the ridge direction, the differential movement has then a compressive component normal to the ridge direction, and a shearing component aligned with the ridge direction. It is also possible that there is differential rotational movement between the ice sheets. If the lower end of the cut in Figure 3 acts as a hinge, and the right hand sheet is rotated counterclockwise around it, a ridge with size increasing along its direction is created.

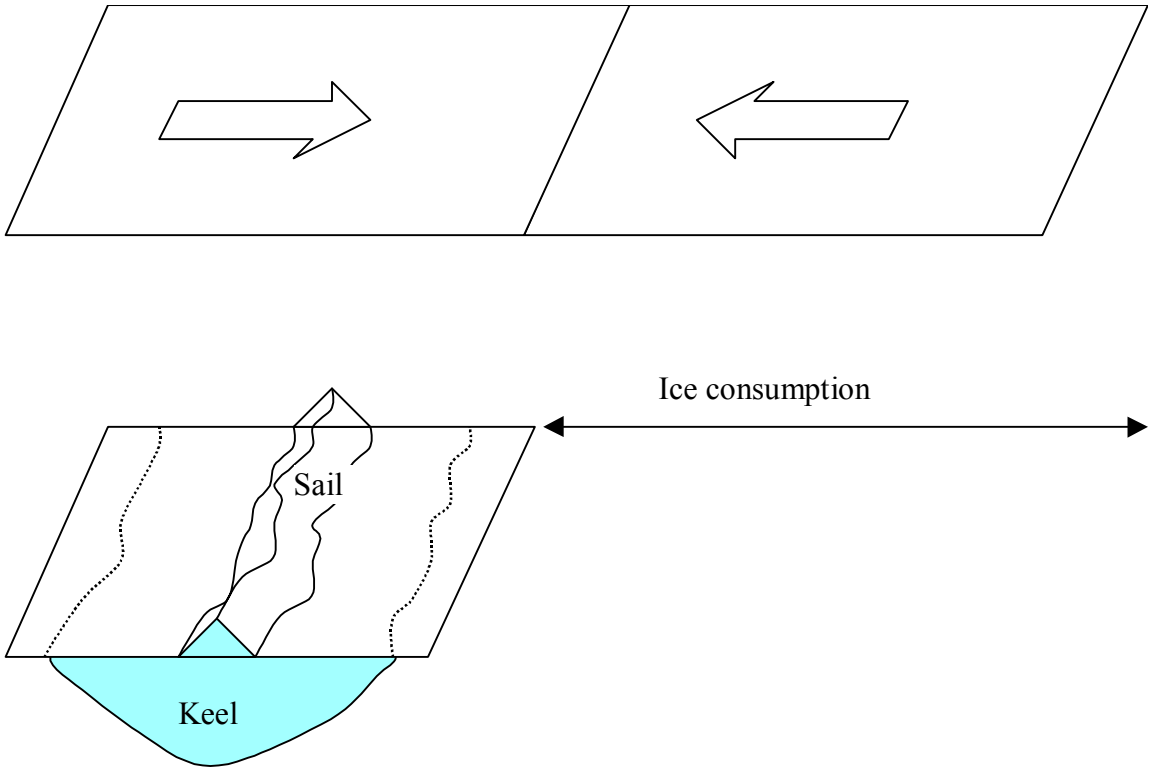

Figure 3. An idealised ridge formation event in uniaxial compression. The initial fault is perpendicular to the differential movement. The ice consumption is not in scale.

A schematic uniaxial compressive ridge formation event in a larger scale is shown in Figure 4, where three visually estimated ridge directions are also shown. Direction 1 appears as the overall direction of the ridge, while Directions 2 and 3 pertain to local segments. With respect to these directions, the differential

movement has a different shearing components in each case. The local segment running in Direction 2 appears as a pure compressive ridge while the local segment in Direction 3 would be termed as a shear ridge.

It would be unambiguous to define ridge direction to be perpendicular to the compressive movement. The zigzagging of the ridge would then not count. Direction 1 is in Figure 4 related to the initial fault which makes a certain angle with the compressive movement. The initial geometry is not determined by forcing only, but also by random factors which are due to pre-existing flaws and other ice cover structure. In addition, it has been observed in ice tank tests that the direction of the ridge with respect to the compression may change during the formation (Tuhkuri and Lensu 1998, 2002). These tests compressed two 6 m wide sheets of model ice into ridges, starting from an initial cut. Their initial configuration was similar to Figure 3. In the tests the random factors were due to the random thickness variation of the model ice. Three ridges were created from each sheet of model ice and had in several cases very dissimilar appearances although the test arrangements were identical.

Thus it is not straightforward to relate the directions of the bygone differential movements to observed ridge directions. The defining of the ridge direction in terms of the ridge creating movement is not applicable in practice. Therefore, the ridges are decomposed to segments with have sufficiently linear keels so that the direction of the segment is determined by its keel. Following Hibler et al. (1972) these segments are called ridge links. Link normal direction is perpendicular to the link direction. The ridge link length is variable. Thus in Figure 4 the Directions 2 and 3 define ridge links. The magnitude and direction of the differential movement that creates the ridge link is assumed to be uniform along the link. This includes the assumption that the rotational component of the differential movement is negligible in link formation.

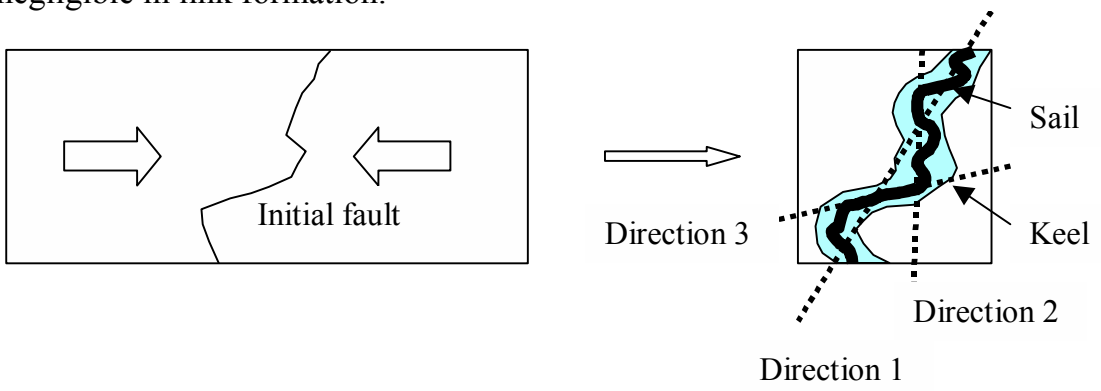

Figure 4. A compressive ridge formation event shown in a larger scale. If a section of a forming ridge is not perpendicular to the compressive movement, then with respect to the section direction the movement has a shearing component.

2.2.3. Ridge cross-section

A ridge cross-section is a two-dimensional vertical cut from a ridge link in the link normal direction. Cross-sections constitute the basic field data on ridge structure. They are decomposed by the water level to sail and keel cross-sections. The highest elevation of the sail cross-section defines cross-sectional ridge sail height h_{cs}, and the deepest draft of the keel cross-section defines cross-sectional keel depth d_{cs}. The corresponding locations are called cross-sectional sail maximum and cross-sectional keel maximum. In an idealised ridge link the cross-sectional sail maximum belongs to a linelike crest of the sail. The sail crest need not be straight but may undulate.

Cross-sectional ice volume v_{cs} is defined in units of volume per unit width. The remaining main cross-section parameters are porosity or relative void content $\kappa_{cs}(t)$ and keel width w_{cs}. In freezing conditions the voids in the upper keel layer close. This decreases porosity and increases ice volume which may also change by melting. However, in the present study only the initial volume is relevant and the thermal processes are not considered. Therefore the convention is adopted that v_{cs} refers to the cross-sectional volume at the time of ridge formation.

2.2.4. Ridge link cross-section

Ridge link cross-section is an averaged cross-section pertaining to the link. The ordinary cross-section parameters vary as the cross-section location changes and a single cross-section represents the link only approximately. Instead, the link is described by averaged cross-sectional parameters which are link cross-section volume v_l, link sail height h_l, link keel depth d_l, and link keel width w_l. These refer to the geometry of an averaged cross-section, called a link cross-section (Figure 5). Thermal processes are not considered and v_l refers to the time of link formation.

In sections to follow longer cross-sections containing both level ice and several ridge cross-sections need be considered. The ridge cross-sections will then be described by ridge link cross-section parameters. On the other hand, the along link variation of cross-sectional height h_{cs} is essential in the interpretation of pencil beam profiling measurements. The link height h_l is not obtainable from such measurements. Instead, they observe from a link a randomly chosen height value h_{cs} which is statistically related to h_l.

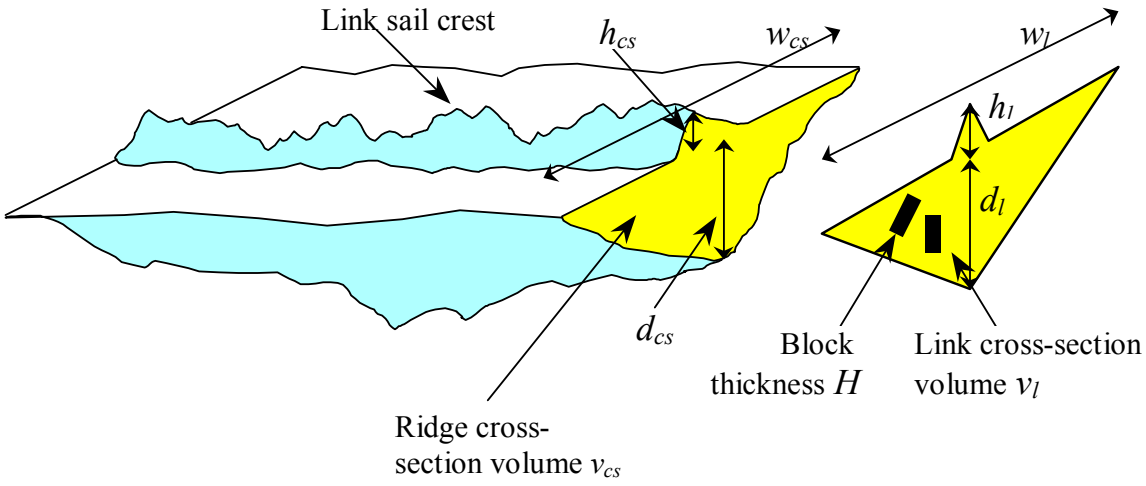

Figure 5. Ridge link, ridge cross-section, and link cross-section.

2.2.5. Ice consumption

The ice consumption c is a measure of the amount of ice pushed into the link. It is defined through the volume conservation relation

$$cH = v_l - Hw_l \qquad (1)$$

in terms of link cross-section parameters and the average thickness H of parent ice. If the link is created with no shear as in Figure 3, an ice sheet of length $c+w_l$ and with parent ice thickness H is compressed into a ridge of width w_l. The parent ice thickness equals then the average block thickness in the ridge. However, the relation (1) is applied also to cases where the ridge creating movement has a shearing component. The magnitude and direction of the link creating differential movement is assumed to be uniform across the link width. With some additional assumptions considered below, c is the compressive component of this differential movement.

The shear ridge section of Figure 4 is selected and modeled as a ridge link (Figure 6). In the direction of the differential movement, a parallelogram shaped ice area is compressed into a parallelogram shaped ridge segment A. From a ridge formation viewpoint this segment would be a good choice for a ridge link. However, the direction of the differential movement cannot usually be known. Therefore all ridge links are considered as if they were formed by the compressive component of the differential movement. The link is thus in Figure 6 modeled as a rectangular

area of width w_l. It is thought of as created from a rectangular parent ice area which then has length $c+w_l$. The following are evident from the inspection of Figure 6:

1. The shearing component of the differential movement induces flux of ice over the link end boundaries. In the definition (1) c is the compressive component of the differential movement if this flux does not affect the link volume.
2. The ice consumption c and volume v_l of the link are proportional to the ratio of compressive component to the total differential movement. Thus c and v_l depend on link direction.

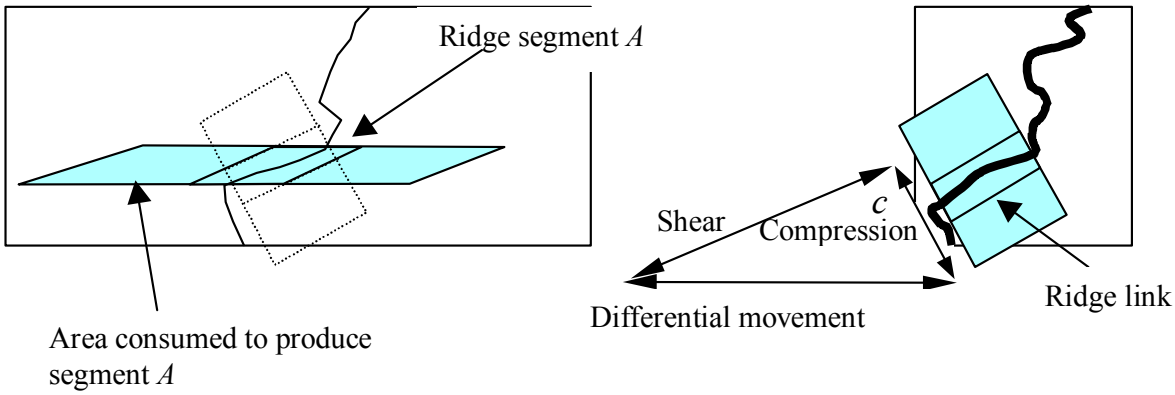

Figure 6. Formation of a ridge link in the Figure 4 case. The differential movement has a shearing component aligned with the link. As this component is usually not known, the link is modeled as created from a rectangular ice sheet in uniaxial compression.

2.2.6. Link cross-section model

A cross-section model is a set of relations between cross-sectional parameters. The present approach seeks to parameterise ridge links by link height h_l and parent ice block thickness H. These parameters can be measured or estimated from the surface. The link cross-section volume v_l and width w_l are related to them with the model. The relations are statistical and the use of approximate functional relations is discussed here. The statistical variation should not be large if the functional relations are applied to individual ridges. However, each of the following may have considerable variation:

1. The differential movement in a link formation.
2. The relative magnitude of compression which then determines the ice consumption c.
3. For a given value of c, the thickness H of the parent ice.
4. For given values of c and H, the link width w_l.
5. For given values of c, H and w_l, which determine v_l, the link height h_l.

Thus the statistical variation of parameter relations is expected to be large. Therefore functional relations are not assumed to be applicable to individual ridge links but are an average description. The cross-section model is assumed to describe the cross-section averaged for a large number of links with same values H and h_l. These values are thus fixed, while v_l and w_l show statistical variation which is averaged over to give relations $v_l(h_l,H)$ and $w_l(h_l,H)$. The cross-section model need not assume any shape for the link cross-section. However, formations where two keels are in contact will be modeled by assuming some simple shape.

2.2.7. Characterisation of ridge fields by sails

In the present approach a ridge field is characterised by ridge sails. The basic decomposition unit is then a sail segment, called sail link. The approach avoids certain shortcomings of the usual practice where ridge fields are described as collections of ridges with a certain cross-sectional shape. The observed fields differ from this idealised description in many respects. The idealisations are related to the classification of thickness increase processes, to the characterisation of ridging process, to the identification of ridges, and to ridge structure.

Compressed ice pieces or small floes arrange into larger thickness without much breaking. As the floe size increases the floes begin to break into blocks against each other and the process gradually turns into ridging. If there are small and large floes the process is a mixture of rubble compression and ridging. If the rubble is consolidated in its upper layer it may undergo a ridging process while the unconsolidated lower layers behave like compressed rubble. Examples of such ridges were studied in Lensu et al.(1998). Between finger rafting and ridging there are intermediate processes, and it is also possible that the ridge has no sail (Tuhkuri and Lensu 1998). The ridge creating differential movements may be complicated and the ridge may lack linear characteristics and direction. A densely ridged field may not partition unambiguously into decomposition entities like ridge links. Closely arranged ridges may also have keel contact. Such formations will be called ridge clusters and they have an important part in the present study. In a sail field the clusters are described as groups of sails with a common keel. Rubble fields can be understood as very wide ridge clusters.

A sail field can always be characterised in terms of linear surface profiles. The cross-sectional sail maxima are identified from the profiles. The usual identification criterion is to select Rayleigh separated maxima exceeding certain cutoff elevation h_0. Two maxima are Rayleigh separated if the minimum elevation between them is less than half of the shallower maximum. Otherwise the shallower maximum is discarded. The selected maxima are interpreted as cross-sectional sail maxima h_{cs}. The distance between adjacent maxima defines sail spacing x. These quantities are determinable even when no decomposition into elongated sail links is possible.

However, in the present approach the decomposability of a sail field to sail links is assumed. The cross-sectional sail maxima in linear profiles are sampled from the sail links. A sail link may be curvilinear but such that an overall direction can be assigned to it. The sail link length is variable. A sail link that does not belong to a ridge cluster is assumed to be a sail of a ridge link and the link cross-section model applies. For clusters the cross-section models must be adapted. The keel width w_l is ambiguous in clustered ridges as the level ice separating the ridge keels is lacking. The unambiguity can be regained by considering instead spacing cross-sections which are introduced below.

2.2.8. Ridge sail spacings, spacing cross-sections and cross-sectional ridge clusters

Ridge sail spacing x is the distance between adjacent sails along a linear transect. The corresponding line segment is also called spacing, and if this segment has length x, it is called x-spacing. It is assumed that the spacing is defined between adjacent sail links. As the sail links may be curvilinear, it is possible that the transect crosses one and same sail link several times. The short segments created thereby are not considered as spacings.

A spacing between two sail links, which may have different directions, is considered. It meets the links with incidence angles ϕ_1 and ϕ_2 (Figure 7a). To the spacing corresponds a spacing cross-section (Figure 7c) which is the basic structural concept in the spacing evolution theory to be presented. A cross-sectional model gives relationships between parameters pertaining to spacing cross-sections. The model is considered in the next section.

A longer cross-sectional profile with several spacings is considered next (Figure 7b). A group of ridges in keel contact in the profile is called a cross-sectional ridge cluster, while ridges that have no keel contact with other ridges are called detached. In Figure 7a the clustering is illustrated in two horizontal dimensions as the overlap of ridge links. However, such geometry is little known from

measurements. Therefore clustering is described in terms of cross-sectional clusters only. Spacing cross-sections are one possibility to do this. Other descriptions of clustered groups of ridges in cross-sections are discussed in Section 2.2.10.

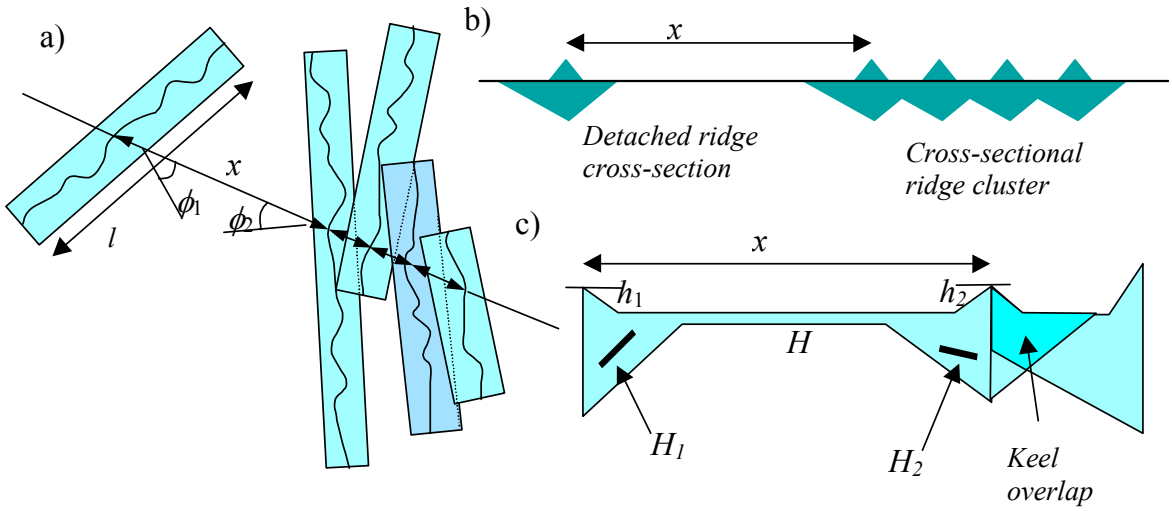

Figure 7. a) Ridge sail spacings along a transect across ridge sail links. The keel contact is illustrated as overlapping of the ridge links. b) The corresponding ice cover cross-section. c) A spacing cross-section model, and an overlap model for ice volume reduction.

2.2.9. A spacing cross-section model

A spacing cross-section model relates the spacing cross-section volume to surface observable ridge parameters and level ice thickness. The two ridges that contribute to the volume are described by link sail height and block thickness as (h_1,h_2,H_1,H_2), and the thickness of level ice between the ridges is H. The spacing cross-section is thus described by

$$\mathbf{x}=(x,H,h_1,h_2,H_1,H_2) \qquad (2)$$

and is called an **x**-spacing for short.

In a sample of **x**-spacings with the same values **x** the cross-sectional volume v, the angles ϕ_1 and ϕ_2, and the width of keel rubble have variation. A spacing cross-section model averages over this variation. For spacings with no keel contact the volume is modeled as

$$v(\mathbf{x}) = \frac{\xi}{2}(v_1 + v_2) + H\left(x - \frac{\xi}{2}(w_1 + w_2)\right) \quad (3)$$

in terms of ridge link models $v_i(h_i,H_i)$, $w_i(h_i,H_i)$, i=1,2. Half of each ridge contributes to the spacing cross-sections. The averaged effect of incidence angles is described by a keel widening factor ξ>1 that affects cross-section volume and cross-section width similarly. In Section 2.5.3 it is shown that for an isotropic ridge field $\xi=\pi/2$. If the keels are in contact, the spacing cross-section volume is

$$v(\mathbf{x}) = \frac{\xi}{2}(v_1 + v_2) - v^*(\mathbf{x}) \quad (4)$$

where v^* is cross-sectional volume reduction due to keel contact. The keel contact also reduces the average keel width from the detached keel value by

$$w^*(\mathbf{x}) = \frac{\xi}{2}(w_1 + w_2) - x \ . \quad (5)$$

The term $v^*(\mathbf{x})$ has not been determined by independent measurements and must be expressed using link cross-section models $v_i(h_i,H_i)$, $w_i(h_i,H_i)$, i=1,2. The simplest possibility is to overlap two triangular keel cross-sections with keel widths $\xi w_1$and ξw_2 (Figure 7 c). The use of the triangular overlap model involves the following assumptions:

1. The fraction of **x**-spacings with keel contact is equal to the fraction of **x**-spacings with $x \le (\xi/2)(w_1+w_2)$.
2. The link cross-section model for detached ridges applies also to clustered ridges.
3. The triangular overlap model is an applicable description of keel contact.
4. The average of keel overlaps equals the overlap of averaged keels.

As measurements of clustered ridges are too few to allow independent parameterisation, these must be assumed.

2.2.10. Description of ridge clusters

Spacing cross-section is one method to describe clustering. However, it does not describe how many successive ridges belong to a cluster and how wide the cluster is. Such parameters are important if, for example, a ship penetrating the cluster is considered. Descriptions for this purpose are introduced.

One method is to use cluster cross-sections as basic features (Figure 8). Detached ridges are clusters with a single sail. Clustering length l_c is the distance between first and last sail in the cluster, and cluster sail number n_c is the number of sails in the cluster. Cluster spacing x_c is the distance between first and last sails of two adjacent clusters. The sails in a cluster are modeled as link sails and their average height is h_c. The average block thickness is H. A cross-sectional model links the values (l_c,n_c,h_c,H) to cluster cross-section volume v_c. A simple model assumes that in a cluster all spacings are equal, all sails have the same height, and that the averaged effect of incidence angle is similar throughout the cluster. The cluster volume is then obtained by the triangular overlap model.

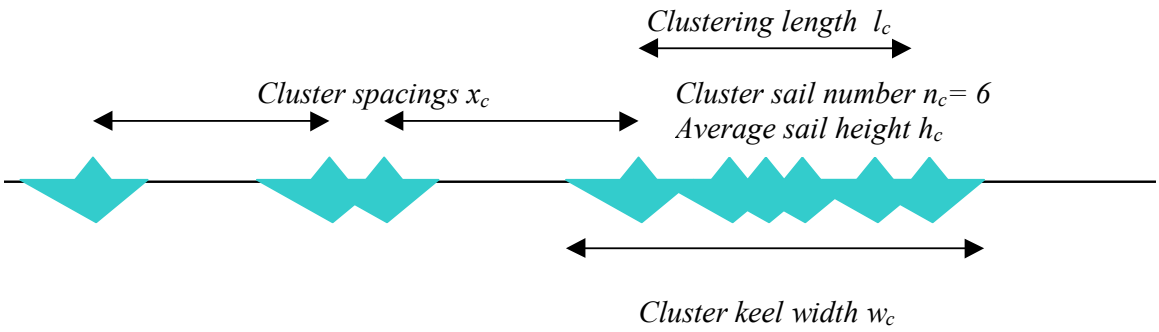

Figure 8. The characterisation of cluster cross-sections.

Another method divides a profile into segments of length L_i (Figure 9). The ridge sail number n_i is the number of sails on a segment. To the segment corresponds segment cross-section which has cross-sectional volume v_i. This is linked to n_i, block thickness H_i and average sail height h_i through a cross-sectional model. A simple approach considers the case n_i>1 as a cluster with average spacing L_i/n_i and uses the cluster volume model outlined above. The use of index i indicates that L_i may be varied.

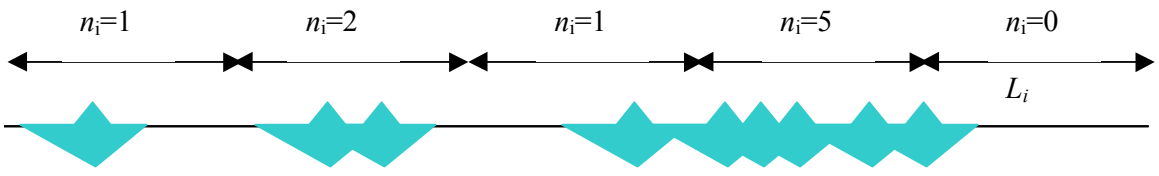

Figure 9. The characterisation of clusters by sail numbers.

2.3. Description of ridge sail fields by distributions

2.3.1. Introduction

The geometry of a ridge sail field is described as horizontal geometry, which is called ridge sail arrangement, and as vertical geometry, or ridge sail height characteristics. This is done in terms of structural parameters for which distributions are defined.

In Section 2.2 several new structural parameters were defined. These describe ridge links, spacing cross-sections, and clusters. If they are used to describe the statistics of ridged ice fields, distributions for them must be defined. This is done in Sections 2.4 and 2.5. The elementary unit of a sail field is a ridge sail link described by height h_l and block thickness H. The proper associated distribution is the bivariate distribution $g(h_l,H)$ even though the extracting of this from the current data is not possible. Spacing cross-sections also require multivariate distributions. Distributions are defined for the cluster parameters as well. The most important of these is the distribution of sail number. Relations of structural parameters can then be averaged over the respective distributions. This is done in Section 2.5.3 for ridge rubble volume and ice consumption.

2.3.2. Basic terminology and notational conventions

Distributions that are continuous with respect to the variable are denoted by f and g, and discrete distributions by k. Distributions need not be of either type in which case the notation for continuous distributions is used. Structural parameters are called variables when they appear as arguments of distributions. Distribution parameters, on the other hand, are statistical parameters like expectation and variance, or parameters functionally dependent on the statistical parameters. Distributions are distinguished from each other by the variables which are separated from distribution parameters by a semicolon, $f(x;p)$. The domain of values is denoted Δ. A continuous distribution is in general a nonnegative function which integrates into unity over Δ. If the domain is positive real axis, $f(x)$ and its cumulative distribution $F(x)$ are related as

$$F(x) = \int_0^x dx\, f(x)\ ,\ \ f(x) = \frac{dF(x)}{dx}\ \ . \tag{6}$$

A discrete distribution is a nonnegative function that sums into unity over a set of values $\Delta=\{x_0,x_1,\ldots.\}$. For conditional distributions the notation $f(x|x')$ is used and

read 'the distribution of x on the condition that x'. The value of x' is then usually fixed and x varies. Expected or mean value of $f(x)$ is $\langle x \rangle$ and $\langle \varphi \rangle$ stands in general for averaging of a function $\varphi(x)$, that is,

$$\langle \varphi \rangle = \int_{\Delta} dx\, \varphi(x) f(x) \ , \ \langle \varphi \rangle = \sum_{\Delta} \varphi(x_i) k(x_i) \tag{7}$$

for the continuous and discrete distributions respectively. The expected value of a distribution is its first moment, moment of order m is $\langle x^m \rangle$, variance is

$$VAR(f) = \langle x^2 \rangle - \langle x \rangle^2 \tag{8}$$

and standard deviation $STD(f)$ is the square root of variance. Bivariate distributions satisfy

$$f(x, x') = f(x') f(x \mid x') \tag{9}$$

from which

$$f(x) = \int_{\Delta} dx'\, f(x') f(x \mid x') \tag{10}$$

and

$$\langle x \rangle = \int_{\Delta} dx'\, f(x') \langle x \mid x' \rangle \tag{11}$$

where $\langle x|x' \rangle$ is the conditional expected value. The distributions $f(x)$ and $f(x')$ are called marginal distributions and they are independent if $f(x)f(x')=f(x,x')$, in which case $f(x|x')=f(x)$ and $\langle x|x' \rangle = \langle x \rangle$. Multivariate variables are denoted by bold type **x**. However, **r** is reserved for field coordinate or horizontal location and **v** for velocity field.

2.4. Distributions describing ridge sail height variation

2.4.1. Distribution of ridge sail height

Ridge sail height distribution is the most common ridge statistics descriptor. In the present approach ridge sail links have linelike crests. The ridge sail height distribution $f(h_{cs})$ gives the probability that a crest point randomly chosen from a

sail field has elevation h_{cs}. If the total length of crest in the field is L, and the length of crest with elevation h_{cs} is $L(h_{cs})$, the distribution is definable in terms of relative length as

$$f(h_{cs}) = \frac{L(h_{cs})}{L} \quad . \tag{12}$$

If a large number N of crest points are randomly sampled, and $N(h_{cs})$ points have elevation h_{cs}, then the ridge sail height can be defined also as relative number

$$f(h_{cs}) = \frac{N(h_{cs})}{N} \quad . \tag{13}$$

2.4.2. Distributions pertaining to ridge sail link height and block thickness

The basic unit of a ridge sail field is a ridge sail link which in this study usually can be identified with its linelike crest. Sail links are described by length l, height h_l and block thickness H. The total length of sail links is equal to the total length L of sail crest. The total length of sail links with height h_l is $L(h_l)$. The link sail height distribution is

$$g(h_l) = \frac{L(h_l)}{L} \quad . \tag{14}$$

The number of sail links in the field is finite. If $g(h_l)$ is idealised as a continuous distribution it describes an infinite sail field which has the same sail height characteristics.

Sail height of an individual sail link has random variation which is assumed not to depend on link length l. The variation is described by distribution $f(h_{cs}|h_l)$ which gives the probability that a crest point chosen randomly from a h_l-link has height h_{cs}. It is defined in terms of relative length

$$f(h_{cs} \mid h_l) = \frac{L(h_{cs} \mid h_l)}{L(h_l)} \tag{15}$$

where $L(h_{cs}| h_l)$ is the total length of crest with elevation h_{cs} in all h_l-links. The three distributions are related as

$$f(h_{cs}) = \int_0^\infty dh_l \, g(h_l) f(h_{cs} \mid h_l) \quad . \tag{16}$$

It is unlikely that all sail links with the same block thickness H would be equally high. Therefore the bivariate distribution

$$g(h_l, H) = g(H) g(h_l \mid H) \tag{17}$$

is introduced. Here $g(H)$ is the probability that link block thickness is H and $g(h_l|H)$ is the probability that the link then has height h_l. As thermally grown ice with thickness H undergoes ridging, this generates $g(h_l|H)$. During the ice season the ridging phases with different parent ice thicknesses $g(H)$ accumulate to generate $g(h_l)$.

2.5. Distributions describing ridge sail arrangement

2.5.1. Length of ridge sail per unit area, ridged ice, and ridge density

Ridge sail arrangement is the horizontal geometry of ridge sail fields. The arrangement in some Lagrangian ice cover region R is considered. It is idealised as the geometry of linelike sail crest on a plane. There is a large number of ways to quantify this irregular geometry. One is to use $\bar{d}$ which is ridge sail length per unit area. Total length of sail crest in R is L. However, there are then several possibilities of definition. If L is divided by the total area A of R the corresponding $\bar{d}$ is affected by all concentration changes. If this is undesirable, L may be divided by the ice area AC in R. Then $\bar{d}$ is not affected by mechanical concentration change if it does not associate with ridging. However, $\bar{d}$ changes if the open water becomes covered by new level ice. If this too is undesirable, the old ice cover may be termed ridged ice which has partial concentration C_{ridged} and

$$\bar{d} = \frac{L}{AC_{ridged}} \quad . \tag{18}$$

It is generally assumed that the descriptors of ridge sail arrangement refer to some subregion S of R that consists of ridged ice only. Without the specification of S such descriptors are not well defined. For ridge height characteristics, on the other hand, this is not required. The defining of S is nontrivial when the ridge field is dynamically changing. The ice outside S is called here level ice. A certain fraction of level ice may turn into ridged ice and become included to S while the

remaining fraction stays outside S. This change in the ridged ice area AC_{ridged} must be specified. A possible solution, for example, is to define as ridged all ice that is closer than 1 km to some ridge sail.

In the present chapter, however, it is assumed that ridged ice subregion S has been defined, and it will be called a ridge sail field. Within the sail field ridge sail density d is the expected number of ridge sails in a randomly chosen unit line segment. It may be determined from a large sample of randomly oriented unit line segments at random locations. The expected number of sails generally depends on segment orientation. If this is not found, the sail field is isotropic with respect to ridge sail density and $d=(2/\pi)\,\bar{d}$ (Mock et al. 1972).

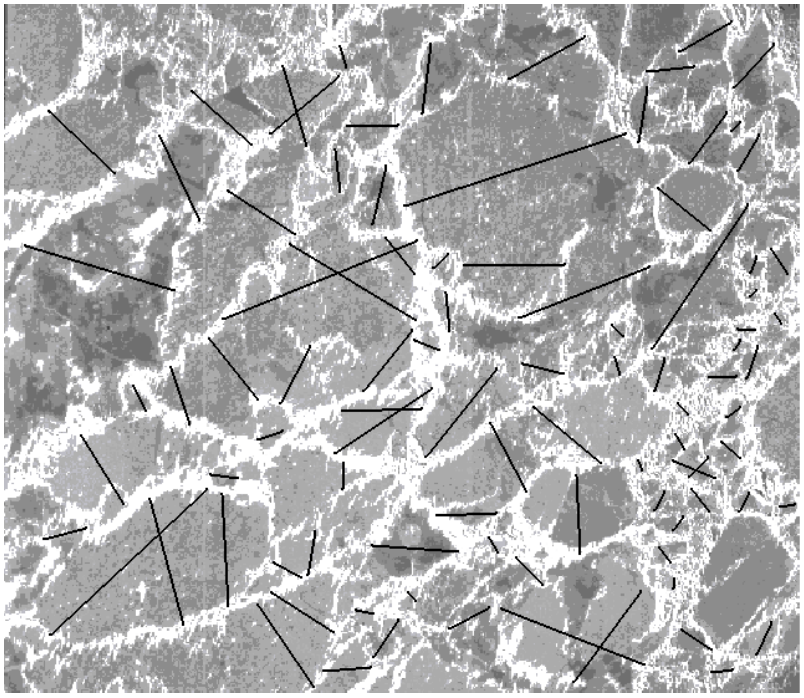

Figure 10. A random sample of spacings (schematic). A 0.8×0.7 km^2 aerial photograph from the Bay of Bothnia, taken in March 1997, has been used.

2.5.2. Sail spacing distribution and distributions for sail spacing cross-sections

Sail spacing distribution $f(x)$ gives the probability that a spacing randomly chosen from a sail field S is an x-spacing. Random sampling is done by choosing randomly a spacing from a transect drawn randomly across S (Figure 10). The

number of x-spacings in a large sample of N spacing is $N(x)$. The sail spacing distribution is then defined in terms of relative number

$$f(x) = \frac{N(x)}{N} \quad . \tag{19}$$

The mean spacing is $\langle x \rangle = 1/d$. Multivariate spacing distribution $f(x_1,x_2,\ldots,x_n)$ is similarly defined for n successive spacings along a linear transect. To a spacing corresponds a spacing cross-section described by (2) and the multivariate distribution $f(\mathbf{x})$ is defined as relative number. The spacing distribution $f(x)$ and the distribution $g(h_l,H)$ are marginal distributions of $f(\mathbf{x})$.

2.5.3. Equivalent thickness of ridge rubble and the clustering effect

In an isotropic field the keel widening factor ξ in (3) has value $\pi/2$. This follows from the ice volume per unit area pertaining to (h_l,H)-links,

$$\overline{d}\, v_l(h_l,H)g(h_l,H) = d\,\frac{\pi}{2} v_l(h_l,H)g(h_l,H) \quad . \tag{20}$$

The left hand side is the volume in terms of sail length per unit area, and the right hand side in terms of ridge density along a transect. The links crossed by the transect are randomly oriented. The average horizontal dimensions of randomly oriented cross-sections are thus link cross-section dimensions multiplied by $\pi/2$.

The convention is adopted that the volume of rubble in a ridge equals the volume cH of the consumed parent ice, (1). On the average the ridge rubble is then thought of as added to a level ice sheet with thickness $\langle H \rangle$. Due to the adopted convention, the partial concentrations of ridged and level ice are not required in relations (23) and (24) below. Taking the keel volume and keel width reduction terms v^* and w^* (Section 2.2.9) into account, the equivalent thickness of ridge rubble is

$$\begin{aligned} H_{eq} &= d\left(\frac{\pi}{2}\langle v_l \rangle - \langle v^* \rangle - \langle H \rangle\left(\frac{\pi}{2}\langle w_l \rangle - \langle w^* \rangle\right)\right) \\ &= d\left(\frac{\pi}{2}\langle v_l \rangle - \langle v^* \rangle\right) - \langle H \rangle C_r = d v_{eq} \end{aligned} \tag{21}$$

Here, v_{eq} is the equivalent cross-sectional volume of ridge rubble, which is defined as equivalent thickness per unit sail density, and C_r is the partial concentration of keel rubble.

To the volume reduction $\langle v^* \rangle$ is associated the reduction $\langle c^* \rangle$ of parent ice consumption so that the total area of ice consumed is

$$A_c = A(S)d\left(\frac{\pi}{2}\langle c \rangle - \langle c^* \rangle\right) = A(S)dc_{eq} \tag{22}$$

where $A(S)$ is sail field area and c_{eq} the equivalent ice consumption, defined as the relative area of consumed ice per unit sail density. The ridge rubble volume V_r can be expressed with the defined quantities as

$$A_c\langle H \rangle = A(S)H_{eq} = V_r \tag{23}$$

and from the given relations follows

$$v_{eq} = \langle H \rangle c_{eq} \quad . \tag{24}$$

The terms v_{eq} and c_{eq} depend on the sail arrangement. Their reduction due to keel contact, and the resulting reduction in A_c ,V_r and H_{eq}, is called clustering effect.

2.5.4. Distributions of sail spacing concatenations and ridge clusters

Sail spacing concatenations can be used to characterise ridge clusters (Figure 11). If n successive sail spacings are chosen they define an n-concatenation with total length y_n and the distribution is $f(y_n)$. The average length of component spacings is y_n/n and is a measure of the degree of clustering.

Threshold concatenations are defined by a spacing threshold x_0. An x_0^--concatenation is a maximal concatenation with all spacings shorter than x_0. The concatenation length is y^-, the number of component spacings is n^-, and the distribution is $f(y^-,n^-;x_0)$. The length measures the extension of the cluster, while y^-/n^- is a measure for the degree of clustering. An x_0^+-concatenation is a maximal concatenation with all spacings longer or equal than x_0 and the distribution is $f(y^+,n^+;x_0)$. A simple cluster model may set $x_0=(\pi/2)\langle w_l \rangle$ and represent clusters as x_0^--concatenations.

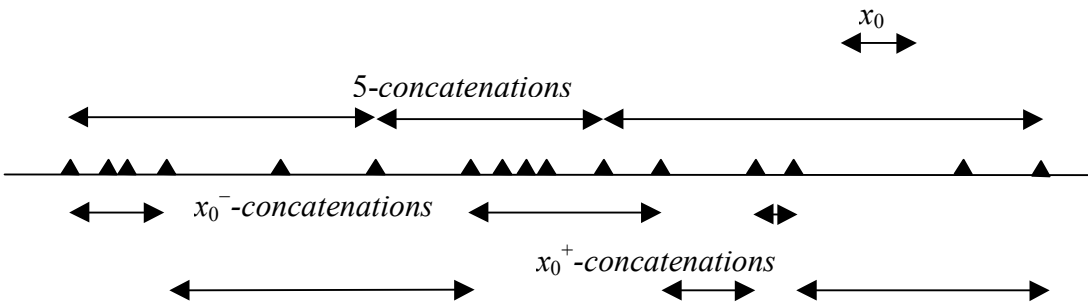

Figure 11. Sail spacing concatenations.

2.5.5. Ridge sail number distribution

Ridge sail number n_i is the number of ridge sails on a line segment of length L_i (Figure 12). The sail number distribution $k(n_i;L_i)$ is the probability that a L_i-segment chosen randomly from the ridge sail field contains n_i sails. If $N(n_i)$ such segments are found in a large sample of N segments

$$k(n_i;L_i) = \frac{N(n_i)}{N} \quad . \tag{25}$$

The segment length is a parameter of the distribution, and the mean value is $\langle n_i \rangle = d/L_i$. The local ridge density $d_i = n_i/L_i$ is a measure of the degree of clustering. The segment length can be varied. Lengths $\ldots > L_i > L_j > L_k > \ldots$ are considered. An L_i-segment containing n_i sails is selected. If an L_j-subsegement is then chosen randomly, then $k(n_j|n_i)$ is the probability that it contains n_j sails. For the next level of subsegments $k(n_k|n_j)$ is defined, as well as $k(n_k|n_i)$. Such collection of conditional distributions is called a scale system.

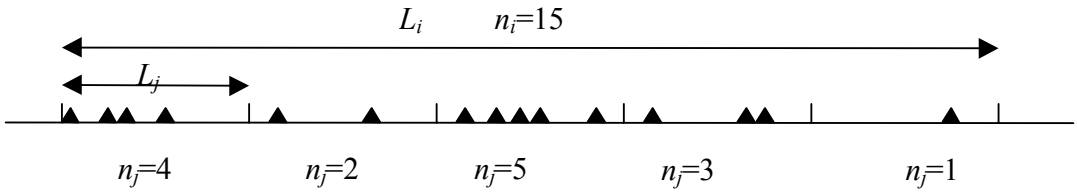

Figure 12. Description by ridge sail numbers along a transect.

3. MORPHOLOGICAL EVOLUTION

3.1. Introduction

Distributions pertaining to ridge sail height characteristics and to ridge sail arrangement were defined in Chapter 2. As the ice cover undergoes ridging the distributions change and a certain area of parent ice is used up. The main focus is in the ridge sail spacing distribution. The objective is to describe its time change and link it to the ice area decrease. An equation governing the spacing distribution evolution is formulated in the theoretical context of discontinuous Markov processes. The equation is a specific version of the general Kolmogorov-Feller equation (Kolmogorov 1931, Feller 1936). The spacing equation parameters are observable quantities and determine the distribution that is the solution of the equation. Thus the task of explaining observed distributions reduces to the task of relating the equation parameters to ice cover characteristics and ice cover dynamical processes.

Although the ridging process is fundamentally governed by deterministic equations a statistical approach is appropriate. This is due to the variability of ice cover geometry, ice properties and driving forces. The spacing equation is derived from assumptions on the stochastic nature of the ridging process. That a deterministic description is in principle possible is shown by present computer simulations of particle systems. They can produce a close replica of the observed behaviour if the initial configuration is known and the interactions between particles can be deterministically described, for example as elastic collisions. The complexity of ice cover, however, is far greater and a similar agreement between simulations and observations is not in sight. On the other hand, a stochastic evolution process has several possible end results, called realisations. The evolution equation predicts probabilities for the realisations, and what is observed is one possible realisation of the process. The probability for its occurrence is interpreted as its relative frequency in an ensemble, which is a large collection of realisations. Ensembles are used to interpret the predicted probabilities in the present approach.

The spacing equations are formulated in four phases. In present chapter the equation is derived in a general form. The equation components are not yet interpreted physically or morphologically. In Chapter 4 Lagrangian spacing evolution equations are obtained through a more detailed formulation of these components. In Chapters 5 and 6 solution methods for the spacing equations are developed and the solutions are compared to observations. Finally, in Chapter 7 Eulerian conservation equations are formulated and parameterised with the Lagrangian results. Alternative ways to describe ridge arrangement and clustering are developed besides this main line of work.

The parameterisation of the spacing equations depends on the present stage of knowledge on ridging process and ridge structure. This lacks in many respects sufficient detail for conclusive results. It will be pointed out where more research is required, and how the new results can be assimilated to the general framework. The framework itself, on the other hand, will not change unless the general assumptions specified in Section 3.4 are replaced. This is much less likely as the assumptions apply to most ice morphological evolution processes. Specifically, the thickness equation of Thorndike et. al (1975) is of Kolmogorov-Feller type and thus mathematically similar to the spacing equation. This is also the case for equations governing floe size distribution. For this reason a generally applicable approach is presented. The motivation is to connect the ice morphological studies to the main body of research around Kolmogorov-Feller type equations.

As the general theory has not been presented before in ice research context, morphological distributions are first defined and discussed in Section 3.2. Morphological features, variables and distributions are defined. The theoretically predicted distributions are interpreted in terms of ensembles of realisations, which concept is discussed. In Section 3.4 the evolution process is characterised and the general assumptions of the approach formulated. In Section 3.5 the evolution equation is derived in a general form and extended to a system of conservation equations for morphological variables. These equations can be included to dynamic ice models. Prompted by the ridge sail number distributions, the event number approach is introduced in Section 3.5.3. Mechanisms of energy dissipation are summarised in Section 3.5.4. Finally, the remaining sections discuss aspects of parameterisation and application.

3.2. Morphological distributions

In the present approach ice cover morphology is described in terms of morphological features. The features are quantified by morphological variables for which distributions are defined. Morphological evolution is described by distributions that change in time. A morphological evolution theory derives equations that govern the time change of the distributions.

Complex ice cover geometry can be described only approximately. It is convenient to use morphological features which are geometrically definable entities in the ice cover. They select out relevant scales and relevant processes, and take into account that certain patterns repeat in the ice cover. The features are quantified by morphological variables. The random variable notation is adopted so that the values of a morphological variable X are denoted x. The domain of values of X is denoted Δ_X. Adapting the style of Rothrock (1986), a feature for which X has value

x is called an x-feature. Time change of X is called an X-process and is here a stochastic process.

There are two basic ways to define the distribution of X: as a relative amount distribution, or as a probability distribution. These may be understood as observed and predicted distribution respectively. A relative amount distribution is specific to some measure μ of the amount of ice features. The common measures are number, length, area or volume of features. Cumulative distributions in a region R are considered and a measure μ is chosen. The amount of features smaller than x is $\mu(x,t)$ and the amount of all features is $\mu_X(t)$. The cumulative distribution is the relative amount of features smaller than x,

$$F(x,t) = \frac{\mu(x,t)}{\mu_X(t)} \ . \tag{26}$$

In the following discussion it is assumed that X is continuous and that the measure is the number of features. Usually the total number is finite and the observed $F(x,t)$ is an approximation of a continuous distribution model $F^*(x,t)$. A stochastic theory of the X-process derives another continuous $F^{**}(x,t)$. However, it need not be close to the model $F^*(x,t)$ that fits the observations. What is observed is one realisation of the stochastic X-process. If the process were repeated many times the realisations would be different. If the realisations were put together, then the predicted $F^{**}(x,t)$ would describe this collection. When applied to an single realisation it gives the predictive probability that $X \le x$ holds for a feature randomly picked at time t. A heuristic analogue is the tossing of one hundred coins. Although the number of heads (observed distribution) is usually different from 50 it is proper to say 'if I toss the coins and pick one it will be heads with 50 % probability' (predicted probability). If the tossing is repeated many times, the average number of heads approaches 50.

In most developments to follow the distributions may be assumed to be continuous. Therefore, from this point onward, the presentation uses distributions $f(x,t)$ rather than their cumulative distributions. Thus $\mu_X(t)f(x,t)$ is the amount of x-features at t. It can be defined for some region R but as well for any subregion of R which contains all X-features. One such subregion $S_X(t)$, which may also be R, is selected. It is called an X-field and said to consists of X-icetype. In certain cases $\mu_X(t)f(x,t)$ depends on how S_X is selected.

An X-field depending on continuous horizontal coordinate $\mathbf{r}$ is considered next. The $\mathbf{r}$-integral of this field both over the region R and over the X-field S_X must be $\mu_X(t)f(x,t)$. The partial concentration of X-icetype is

$$C_X(t) = \frac{A(S_X(t))}{A(R(t))} \tag{27}$$

where A is for area. The density of X-features in the X-field is

$$\rho_X(t) = \frac{\mu_X(t)}{A(S_X(t))} \quad . \tag{28}$$

The required continuous field is $C_X(\mathbf{r},t)\rho_X(\mathbf{r},t)f(x,\mathbf{r},t)$. If μ is volume, area or number, then ρ is equivalent thickness, partial concentration, or number density respectively. If C_X equals total ice concentration C and changes in the X-process only, the conservation equations in an ice velocity field $\mathbf{v}$ are

$$\begin{aligned} \frac{\partial}{\partial t}\left(C\rho_X f(x)\right) &= -\nabla\cdot\left(\mathbf{v}C\rho_X f(x)\right) + CS_1(x) \\ \frac{\partial C}{\partial t} &= -\nabla\cdot(\mathbf{v}C) + CS_2 \end{aligned} \tag{29}$$

where the terms S_1 and S_2 describe the effect of the X-process.

3.3. Morphological distribution as an ensemble average

A consistent way to reconcile the continuum description with the discontinuity of the ice cover is to consider it as a random field. Its evolution at each location $\mathbf{r}$ is then a stochastic process. The spatially continuous probability distributions are defined as ensemble averages. Similar approach is applied in the statistical theory of turbulent flow fields (Landahl and Mollo-Christensen 1992).

A distribution observed in a region R is also a realisation. If the evolution is repeated a large collection, or ensemble, of realisations $[\mu_X f]_i$ with average $\langle[\mu_X f]_i\rangle$ is generated. The limit of $\langle[\mu_X f]_i\rangle$ when the number of realisations goes to infinity is $\mu_X(t)f(x,t)$ and is called ensemble average. A stochastic theory of the X-process derives an equation for $\mu_X(t)f(x,t)$. If it is not too different from the realisations it can be used to predict the evolution. Likewise, an observed time series $x_i(\mathbf{r},t)$ at a location is a realisation. If the evolution is repeated an ensemble of realisations $[C_X\rho_X f]_i$ is generated. These are defined as functions which have value 1 if there is an x-feature at $\mathbf{r}$ at t, and otherwise 0. Now $C_X(\mathbf{r},t)\rho_X(\mathbf{r},t)f(x,\mathbf{r},t)$ is defined as ensemble average of $[C_X\rho_X f]_i$. In other words, it is the relative frequency of x-feature occurrences in the ensemble.

The time series $x_i(\mathbf{r},t)$ depends on the stochastic ice velocity field $\mathbf{V}(\mathbf{r},t)$. During a time interval a feature at $\mathbf{r}$ drifts to $\mathbf{r}'$ with a certain probability related to $\mathbf{V}(\mathbf{r},t)$. This description requires pairs $(\mathbf{r},\mathbf{r}')$. Such theory is considered as a proper theory of $X(\mathbf{r},t)$. An approximate theory may refer to regular grid cells. The grid cell areal average of $C_X(\mathbf{r},t)\rho_X(\mathbf{r},t)f(x,\mathbf{r},t)$ is idealised as a descriptor of grid cell center. Only the expected velocity field $\mathbf{v}(\mathbf{r},t)$ is assumed to count and the effect of advection over cell boundaries is described approximately by $-\nabla\cdot(\mathbf{v}C_X\rho_X f)$.

The general view is adopted that continuum equations describing ice cover refer to ensemble averages. The problem between the theory and observations does not then concern the applicability of continuum theory to a granular medium (Overland et al. 1988) but the relationship of the ensemble averages to individual realisations. If the theory does not fit observations this may be due to the status of the observed distribution as a realisation, or due to theory assumptions. It will be argued throughout this work that the comparison of theory and observation should be made rather for the process parameters than for the resulting distributions. The parameters are expected to show less spatial variation and be more easily determinable as continuum fields. The discrete element simulating of large pack ice areas, in the style of Hopkins (1996, 1999), could be also used to derive the ensemble averages. Such approach would clarify the obscure relationship between the spatially continuous theory and the observed ice cover.

3.4. Morphological processes as discontinuous Markov processes

3.4.1. Morphological feature processes

Time change of X is called an X-process. The objective is to characterise the X-process so that an equation can be formulated for $\mu_X(t)f(x,t)$, or for $C_X(\mathbf{r},t)$ and $\rho_X(\mathbf{r},t)f(x,\mathbf{r},t)$. The variable X quantifies features, and the X-process quantifies a feature process. In a mechanical process ice is mechanically deformed, while thermal processes involve thermal ice creation or ice melting. The overall process is described in terms of such component processes. For example, possible processes for ice floes are floe fragmentation, floe aggregation, and lateral melting. Fragmentation process is a mechanical process and the other two are thermal processes. These are thus feature processes, and the change of floe area X is a quantifying X-process.

The X-processes are either continuous or discontinuous. In a continuous process the value x changes continuously with time, for example as in lateral melting of floes. A discontinuous X-process, or event process, may consist of events of three types. In a transition event the variable experiences an instantaneous transition $x'\rightarrow x$. A progeny x-feature is produced from a parent x'-feature. The other two

types are emergence and destruction events. The discontinuous *X*-process quantifies a feature process consisting of feature events. In the floe example fragmentation and aggregation events are mechanical and thermal feature events respectively. Floes may emerge from fast ice, and become destroyed through shattering to debris. Emergence and destruction events may also occur as the variable value evolves into the domain Δ_X or out of it.

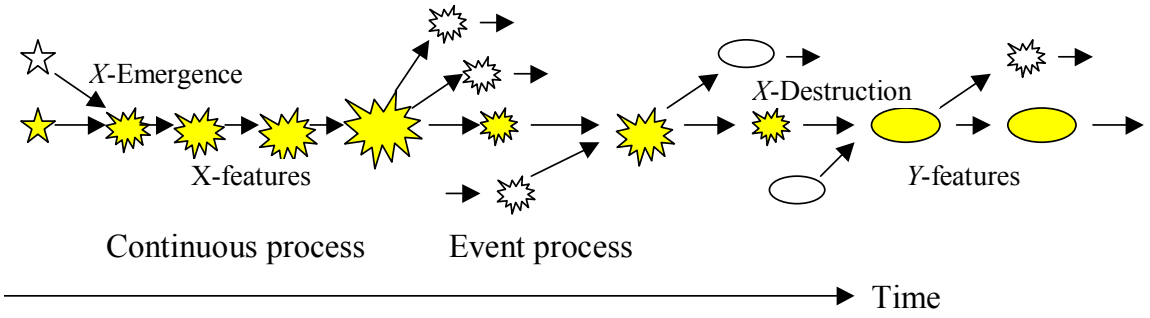

Figure 13. A morphological feature process. The process is quantified as an *X*-process and is traced by following a small volume element carried by the shaded features.

The identity of a feature does not necessarily persist in events, for example if two progeny features are produced from one parent. However, the event process can be traced by following a small volume element. Figure 13 gives an example of traced evolution. An *X*-feature emerges from features of other type, undergoes a continuous evolution and a sequence of transition events, and is finally destroyed. The *X*-destruction event is at the same time a *Y*-creation event. The overall *X*-process is an interlaced totality of such traced evolution histories. A paradigmatic example is a floe fragmentation process. If a parent floe fragments into two progeny floes, this is a binary transition event $x' \rightarrow x$ for floe area *X*. A binary transition process is illustrated in Figure 14.

An *X*-process is characterised by specifying the continuous and discontinuous component processes. Each component corresponds to a term in the evolution equation. There are three basic ways to approach the evolution: to follow an individual feature, to follow a Lagrangian region, or to follow some geographical location. These are considered in the following sections.

3.4.2. Morphological Markov process for a traced feature

A traced *X*-feature is followed (Figure 14). The evolution process is repeated and an ensemble of realisations is generated. These can be realised simultaneously by starting from a large collection of identical *X*-features. The probability $f(x,t|x',t')$ is

defined as an ensemble average. It gives the probability that a feature that was an x'-feature at t' is an x-feature at a later time t. The basic assumption is the Markov property

$$f(x,t \mid x',t' \wedge x'',t'') = f(x,t \mid x',t') \tag{30}$$

where $t>t'>t''$ and $\wedge$ is a symbol for 'and'. The probability $f(x,t|x',t)$ does not depend on the prehistory before t'. If this is not the case, new variables can be included so that the prehistory is expressed by present values of the new variables. Thus it is assumed that Markovian formulation is always possible. For a Markov process the $f(x,t|x',t)$ are called transition probabilities and satisfy the Chapman-Kolmogorov equation

$$f(x,t \mid x'',t'') = \int dx' f(x,t \mid x',t') f(x',t' \mid x'',t'') \tag{31}$$

where $t>t'>t''$ (Prabhu 1965).

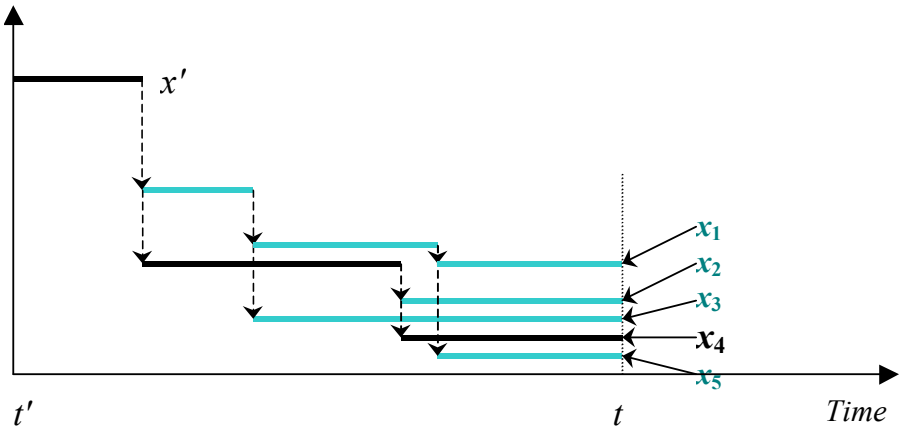

Figure 14. A binary transition process, proceeding from a single x-feature at time t'. The traced feature is marked with darker shade and is at time t an x_4-feature.

3.4.3. Markovian transition flux process

A Lagrangian region R is followed. The evolution process is repeated for the ensemble of realisations so that transition probabilities can be defined as ensemble averages. A binary process where $R(t')$ contains a single x'-feature at time t', is considered first (Figure 14). The number of features at a later time t is also a random variable. The associated transition probability is written $k(n,t|x',t')$ and gives the probability that n features are generated from a single initial x'-feature.

The probability that a random choice from the n features gives an x-feature is another transition probability $f_n(x,t|x',t')$. The summing of $f_n(x,t|x',t')$ over $k(n,t)$ gives $f(x,t|x',t)$ which is the transition probability that a feature created from x'-feature is an x-feature. The mean $\langle n|x',t'\rangle$ of $k(n,t|x',t')$ is the expected number of features, and $\langle n|x',t'\rangle f(x,t|x',t)= N(x,t|x',t')$ is the expected number of x-features created from the single x'-feature.

Generally, $\mu(x,t|x',t)$ is defined to be the expected amount of x-features created from a unit amount of x'-features. It is called here transition flux. If the initial amount $\mu_X(t')f(x',t')$ is large, then $\mu(x,t|x',t')\mu_X(t')f(x',t')$ is the observed amount of x-features created from x'-features. Then the total observed amount of x-features is

$$\mu_X(t)f(x,t) = \int dx'\,\mu(x,t\,|\,x',t')\mu_X(t')f(x',t') \quad . \tag{32}$$

This is a Chapman-Kolmogorov equation for transition fluxes. It holds if X-features are not destroyed or emerged.

3.4.4. Morphological process with continuous spatial variation

In the third approach a location $\mathbf{r}$ is followed. The components $C_X(\mathbf{r},t)$, $\rho(\mathbf{r},t)$ and $f(x,\mathbf{r},t)$ and the transition probabilities $f(x,\mathbf{r},t|x',\mathbf{r},t')$ are defined as ensemble averages. They include the effect of ice drift and are related to transition probabilities $f(x,\mathbf{r},t;\mathbf{i}|x',\mathbf{r}',t';\mathbf{i})$ that an x'-feature, identified by marker $\mathbf{i}$ and found at $\mathbf{r}'$ at time t', will be an x-feature at $\mathbf{r}$ at time t. The ice drift includes a stochastic component. This is not considered further here but it is remarked that it is the way to proper spatially continuous theory. Instead, the evolution is described for regions $R(\mathbf{r})$ centered at $\mathbf{r}$ as outlined in Section 3.3. The continuum description is then obtained from the relative amount description of Lagrangian regions by adding the advection term. The evolution in $R(\mathbf{r})$ is then approximately described by conservation equations of the type (29), where S_1 is obtained from the Lagrangian description.

3.4.5. Discontinuous transition process

The evolution equation for $\mu_X(t)f(x,t)$ will be derived first for a process with discontinuous transitions $x'\rightarrow x$. Continuous X-processes, emergence and destruction terms, and advection term are then included. The derivation is based on transition fluxes $\mu(x,t+dt|x',t)$ for short time periods dt. It is a basic assumption that the transitions $x'\rightarrow x$ have duration of the order of dt and are separated from

each other by much longer stationary periods. Such process constitutes a discontinuous Markov processes and the transition flux can be written

$$\mu(x,t+dt|x',t) = \kappa(x'\rightarrow x,t)\,\alpha(x'\rightarrow x,t)dt \qquad (33)$$

where $\alpha(x'\rightarrow x,t)$ is the rate of transitions, and $\kappa(x'\rightarrow x,t)$ the amount of x-features produced from unit amount of x'-features. The relation (33) holds because multiple transitions, that is $x'\rightarrow x''$ followed by $x''\rightarrow x$, do not occur during dt as the stationary periods between the transitions are much longer than dt.

The continuous stochastic processes are not considered in the present work. Such processes are described, for example, by Fokker-Planck equations (Prabhu 1965). The drift of ice particles, and perhaps the deformation of ice rubble bed under compression, are of this type. However, insofar the ice cover is locally characterised by discrete features and steplike gradients, the discontinuous theory is expected to apply. The simplest example is the spatial Poisson process where pointlike features are placed at random locations on a line. The feature spacing X experiences then discontinuous transitions. More general processes are described by the Kolmogorov-Feller equation (Kolmogorov 1931, Feller 1936) which will be applied in the present approach. In many cases the transition processes are generalised Poisson processes, where the assumption of random placement is replaced by another condition of placement. To this the ridge spacing evolution adds the feature that each placement induces a certain local deformation of the line. General presentation of stochastic processes to the extent relevant here can be found for example in Prabhu (1965). Books on applicable stochastic theory are numerous, for example Bendat and Piersol (1986) or Ochi (1990).

3.5. The evolution equation for morphological distributions

3.5.1. Discontinuous evolution

The equation for $\mu_X(t)f(x,t)$ is in the present section derived for a discontinuous Markov process of transitions $x'\rightarrow x$. The derivation is presented so that it can be applied also to more general transitions $(x_1',x_2',\ldots,x_i')\rightarrow(x_1,x_2,\ldots,x_j)$. The continuous processes, emergence and destruction terms, and advection term are included to the equation in Section 3.5.2. The changes of amount and especially the transition fluxes during dt are ensemble averages and thereby well defined.

The amount of x'-features transiting to x-features during dt is $Ann(x',t|x'\rightarrow x)dt$. This amount is thus annihilated through transitions $x'\rightarrow x$. The rate of transitions $x'\rightarrow x$ is then defined as

$\alpha(x' \to x,t)dt = Ann(x',t|x' \to x)/\mu_X f(x',t)dt$. (34)

It is the relative amount of x'-features transiting to x-features during dt. The x'-feature transition event rate is

$$\alpha(x',t) = \int_{\Delta_{Ann(x')}} dx\, \alpha(x' \to x,t) \tag{35}$$

where $\Delta_{Ann(x')}$ is the domain of values x for which $x' \to x$ is possible. The probability of transition $x' \to x$ in an x'-feature transition event is

$$B(x' \to x,t) = \frac{\alpha(x' \to x,t)}{\alpha(x',t)} \quad . \tag{36}$$

A time instant t from a period $[t_1,t_2]$ is considered. The amount $\mu_{orig}(x',t)$ of x'-features that have suffered no transition after t_1 but remained inert decreases as

$$d\mu_{orig}(x',t) = -\alpha(x',t)\mu_{orig}(x,t)dt\ ,\ \ \mu_{orig}(x',\, t_1) = \mu(x',\, t_1). \tag{37}$$

From this differential equation it follows that from a unit amount of original x'-features is left at time t_2 the amount

$$p_s(x';t_1,t_2) = \exp\left\{ -\int_{t_1}^{t_2} d\tau\, \alpha(x',\tau) \right\} \quad . \tag{38}$$

This is the probability for a x'-feature to survive the period $[t_1,t_2]$. If $\alpha(x')$ does not depend on time, $1/\alpha(x')$ is the expected survival time for x'-features. If the x'-feature does not survive it transits following $B(x' \to x)$.

The overall balance of $\mu_X f(x,t)$ is

$$\frac{\partial \mu_X f(x)}{\partial t} = Cr(x) - Ann(x) \tag{39}$$

where $Cr(x)$ and $Ann(x)$ are creation and annihilation fluxes of x-features. In an event process the fluxes are due to creation and annihilation events. A simultaneous annihilation and creation event is a transition event. Annihilation and creation events that are not transitions are destruction and emergence events respectively. Presently only the transition events are considered. During dt,

$Cr(x,t|x' \to x)dt$ is the amount of x-features created from x'-features and $Ann(x,t|x \to x'')dt$ is the amount of x-features annihilated when creating x''-features. Thus

$$\frac{\partial \mu_X f(x)}{\partial t} = \int_{\Delta_{Cr(x)}} dx' Cr(x \mid x' \to x) \quad - \quad \int_{\Delta_{Ann(x)}} dx'' Ann(x \mid x \to x'') \tag{40}$$

where $\Delta_{Cr(x)}$ contains all x' such that transition $x' \to x$ is possible, and $\Delta_{Ann(x)}$ all x'' such that the transition $x \to x''$ is possible. Continuity of x is not required, and the integrals are to be interpreted in a generalised sense.

Equation (40) is now transformed into an applicable form. The transitions $x' \to x$ produce from a unit amount of x'-features the amount

$$\kappa(x' \to x) = \frac{Cr(x \mid x' \to x)}{Ann(x' \mid x' \to x)} \tag{41}$$

of x-features. This is called progeny production. With (34,41) the equation (40) is changed to

$$\frac{\partial \mu_X f(x)}{\partial t} = \mu_X \int_{\Delta_{Cr(x)}} dx' \kappa(x' \to x)\alpha(x' \to x) f(x') - \mu_X f(x) \int_{\Delta_{Ann(x)}} dx'' \alpha(x \to x'') \tag{42}$$

and using (35,36) it takes the form

$$\frac{\partial \mu_X f(x)}{\partial t} = \mu_X \int_{\Delta_{Cr(x)}} dx' \kappa(x' \to x)\alpha(x') B(x' \to x) f(x') - \mu_X \alpha(x) f(x) = \mu_X \Psi_X \ . \tag{43}$$

The term Ψ_X is called discontinuous evolution term. The components κ, α and B can be time dependent, either explicitly or through dependence on f. In the latter case the equation is nonlinear. If $\kappa(x' \to x) = 1$, μ_X vanishes from the equation. If the measure is number, then the equation for traced feature distribution $f(x,t)$ (Section 3.4.2) is obtained from (43) by putting $\kappa(x' \to x) = 1$.

The most well-know case of (43) is the fragmentation equation for which a large number of applications can be found in other fields. These include dispersion, turbulent mixing, polymer chemistry, crushing and grinding of minerals, mineral

processing, combustion, aerosol behaviour, fluid turbulence, nuclear physics, and astronomy. The results from other fields are as such applicable to ice floe fragmentation process or to ice fragmentation processes in smaller scales. Survey articles with bibliographies are Ramkrishna (1985) and Redner (1990).

3.5.2. Conservation equations for the morphological state

The equation (43) is now formulated for spatially continuous distribution fields and generalised to multivariate distributions $f(x_1,x_2,\ldots,x_n)=f(\mathbf{x})$. Continuous deterministic processes and emergence and destruction terms are also included. In a spatially continuous formulation the instantaneous velocity of an ice particle is

$$v_i = \frac{dr_i}{dt},\ i = 1,2 \tag{44}$$

where $\mathbf{r} = \langle r_1, r_2 \rangle$. The continuous deterministic processes for **X**-features have usually thermal origin and are described by rate equations for the X_i,

$$\frac{dx_i}{dt} = \theta_i(x_i,t),\ \ i=1,\ldots,n\ . \tag{45}$$

It is assumed that the measure is conserved in the continuous processes. On the basis of mathematical similarity of (44) and (45) divergence operators for both **r** and **x** are defined (Ramkrishna 1985). Then, as a further development of (29,43), the conservation equation for $C_{\mathbf{X}}\rho_{\mathbf{X}}f(\mathbf{x})$ is

$$\frac{\partial C_{\mathbf{X}}\rho_{\mathbf{X}}f(\mathbf{x})}{\partial t} = -\nabla_{\mathbf{r}}\cdot(\mathbf{v}C_{\mathbf{X}}\rho_{\mathbf{X}}f(\mathbf{x})) - \nabla_{\mathbf{x}}\cdot(\Theta C_{\mathbf{X}}\rho_{\mathbf{X}}f(\mathbf{x})) + C_{\mathbf{X}}\rho_{\mathbf{X}}\Psi_{\mathbf{X}} + \gamma^e_{\mathbf{X}} + \gamma^d_{\mathbf{X}} \tag{46}$$

where $\Theta=\langle \theta_1,\theta_2,\ldots,\theta_n \rangle$. The conservation equation for $C_{\mathbf{X}}\rho_{\mathbf{X}}$, obtained by integrating over **x**, generally depends on the **X**-process. The emergence and destruction terms γ^e and γ^d have also been added.

A general recipe for constructing equation systems based on (46) is finally outlined. The ice cover is described by distributions $f(\mathbf{x}), f(\mathbf{y}), f(\mathbf{z})\ldots$. The ice cover is in addition partitioned into mutually exclusive classes k, for example with respect to the age of ice. Each of the classes is described by a state $(\mathbf{X}^k,\mathbf{Y}^k,\mathbf{Z}^k,\ldots)$. A closed system of equations (46) for the $C_{\mathbf{X}^k}\rho_{\mathbf{X}^k}f(\mathbf{x}^k)$, $C_{\mathbf{Y}^k}\rho_{\mathbf{Y}^k}f(\mathbf{y}^k),\ldots$ is defined. For each $\rho_{\mathbf{X}^k}$ that is not partial concentration a conservation equation for

$C_{\mathbf{X}^k}$ must be included. In some cases this is derived from the equation for $C_{\mathbf{X}^k}\rho_{\mathbf{X}^k}f(\mathbf{x}^k)$ but independent formulation may be needed. The fluxes between the classes are described as emergence and destruction terms $\gamma^e_{\mathbf{X}^k}, \gamma^d_{\mathbf{X}^k}, \gamma^e_{\mathbf{Y}^k}, \gamma^d_{\mathbf{Y}^k}, \ldots$. Certain amount of ice is destroyed from a class to emerge in another class.

In other fields, which have usually a particulate process context, examples of (46) are frequently called population balance equations. They are widely applied, especially to model processes where a particle size distribution must be controlled in terms of environmental parameters. For overviews, see Ramkrishna (1985) or Alvarez et al. (1994). The only generally known sea ice application is the thickness equation of Thorndike et al. (1975). The connection of the thickness equation to the general theory and the main body of research has not been conceived and the notation and terminology of Thorndike et al. (1975) have been adopted by all subsequent developments in the ice geophysical context. The present study, on the other hand, seeks to conform more to the terminology and notation that is common in the research around Kolmogorov-Feller type equations and their applications. For the thickness equation and its ridging terminology the correspondence is as follows

Present study		*Thorndike et al* (1975)	
Ψ	mechanical evolution	Ψ	redistribution function
Ψ'	(essentially, Sec.7.2.2)	$w(x,f)$	ridging mode
$B(x'\to x)\kappa(x'\to x)=B(x'\to x)(x'/x)$		$\gamma(y,x)$	redistribution process, redistributor
$B(x'\to x)$	transition probability		
$\kappa(x'\to x)$	progeny production		
$\alpha(x,t)$	transition event rate	$b(x)$	weighting function
$\alpha(x)f(x)$		$a(x)$	distribution of ice participating to ridging
$\int dx'\,\alpha(x')f(x')(x'/x)B(x'\to x)$		$n(x)$	distribution of newly ridged ice

Timokhov (1998) has suggested the use of the present formalism to the construction of sea ice conservation equations. Formulations for common morphological variables are given in Lensu (1999 c,d). Marchenko (1999) suggested a bivariate thickness equation where the other variable described the degree of damage in the ice.

The equation (43,46) is a specific and simple formulation of discontinuous evolution $\Psi_{\mathbf{X}}$, applicable to processes which are analogical to fragmentation. Equations for other kinds of processes can be derived by a procedure similar to Section 3.5.1 whenever the transition events $(x_1',x_2',\ldots,x_i')\to(x_1,x_2,\ldots,x_j)$ can be figured out. Multivariate formulation may be required. Most well-known of these

is Smoluchowski coagulation equation for $(x_1', x_2') \to x_1$ (Smoluchowski 1916, Norris 1998). Adding it to (43), a fragmentation-coagulation equation is obtained (Dubowskii and Stewart 1996, Ball and Carr 1990). It is applicable, for example, to floe size distributions when the floes, in addition to fragmentation, may thermally bond together.

3.5.3. Event number equation

The discontinuous Markov evolution proceeds as a sequence of transition events. Thus it is possible to include a discrete variable n counting the number of events undergone. The evolution is described by the joint distribution $f(n,\mathbf{x},t)$, where n is event number (Lensu 1998a). The transitions are $(n\text{-}1,\mathbf{x}') \to (n,\mathbf{x})$. The equation is a generalisation of (43),

$$\frac{\partial \mu_{\mathbf{X}} f(n,\mathbf{x})}{\partial t} = \mu_{\mathbf{X}} \int_{\Delta_{Cr(\mathbf{x})}} d\mathbf{x}' \, \kappa(n-1,\mathbf{x}' \to \mathbf{x}) \alpha(n-1,\mathbf{x}') B(n-1,\mathbf{x}' \to \mathbf{x}) f(n-1,\mathbf{x}') - \mu_{\mathbf{X}} \alpha(n,\mathbf{x}) f(n,\mathbf{x}) \,. \tag{47}$$

This approach is prompted by the ridge sail number approach, where n is the number of sails on a segment and $\mathbf{x}$ includes other variables describing the segment. The joint distribution can be decomposed as

$$f(n,\mathbf{x},t) = k(n,t) f(\mathbf{x},t \mid n) = k(n,t \mid \mathbf{x}) f(\mathbf{x},t) \tag{48}$$

where $k(n,t)$ is the distribution of event number, $f(\mathbf{x},t|n)$ is the distribution of $\mathbf{X}$-features that have event number n, and $k(n,t|\mathbf{x})$ the event number distribution for $\mathbf{x}$-features. From the solution of (47) the distribution $f(\mathbf{x},t)$ is obtained by summing over n, and the event number distribution by integrating over $\mathbf{x}$. After this the conditional probabilities $f(\mathbf{x},t|n)$ and $k(n,t|\mathbf{x})$ are obtained from (48).

Equation (47) is solvable by iteration. The solution for any finite n can in principle be obtained through a sequence of integrations. The event numbers are not expected to be high for ice processes. For decreasing processes, like floe fragmentation, $\mathbf{x}$ typically changes with n in a geometric procession. In a binary fragmentation process event number 10 corresponds to size reduction by three magnitudes on the average. On the other hand, for increasing processes like mechanical thickness increase the ice tends to grow with n more resistant to further deformation. For a first-year ice particle the number of mechanical thickness increase events in which it participates is probably 0-3, for example thermal creation (n=0), rafting (n=1), ridging (n=2), and secondary ridging (n=3). Thus the event number version is particularly applicable to mechanical ice thickness increase.

If the components α and B of (47) do not depend on n, summation over all n gives the equation (43). If α and κ do not depend on $\mathbf{x}$, integration gives the event number equation

$$\frac{\partial \mu_{\mathbf{X}} k(n)}{\partial t} = \mu_{\mathbf{X}} \kappa(n-1)\alpha(n-1)k(n-1) - \mu_{\mathbf{X}} \alpha(n)k(n) \tag{49}$$

in which case, provided that $B(n,\mathbf{x}' \rightarrow \mathbf{x})$ are time-independent, $f(\mathbf{x}|n)$ are given by

$$f(\mathbf{x} \mid 0) = f_0(\mathbf{x}),\ f(\mathbf{x} \mid n) = \int_{\Delta_{\mathbf{x}}} d\mathbf{x}'\, B(n-1, \mathbf{x}' \rightarrow \mathbf{x}) f(\mathbf{x}' \mid n-1)\,. \tag{50}$$

The distribution $f(\mathbf{x},t)$ for $\mathbf{x}$-features can then be constructed by (48). The equation (49) is applied to the sail number distributions in the present study.

3.5.4. Energetics of mechanical evolution

The mechanical evolution of a morphological distribution $f(x)$ is a sink of energy. The energy is either stored to the ice cover as internal energy or dissipated. The dissipation mechanism often depends on the changing distribution $f(x)$. The energy balance is a link from morphological evolution to larger scale deformation characteristics. If the constitutive equations of a dynamical ice model include a relation between the stress or strain tensors and the parameters α and B, it can be assumed that the model dissipation rate, defined as the tensor product $\dot{\varepsilon} : \sigma$, equals that associated with $f(x)$ and its evolution. This allows the fixing of one parameter in the constitutive equation, usually the aggregate strength (Rothrock 1975). In relation to $f(x)$ the following main components in the energy balance can be identified.

Internal energy is some function $p(x)$ and the dissipation of energy due to the increase of total internal energy P is

$$\dot{P} = \int_{\Delta} dx\, p(x) \frac{\partial \mu_X f(x)}{\partial t} \quad . \tag{51}$$

The example is the change in potential energy due to thickness increase changing the thickness distribution $f(x)$. The external rate of dissipation is

$$\dot{E}_{ext} = \mu_X \int_{\Delta x} dx\, \dot{\eta}(x) f(x) \tag{52}$$

where $\dot{\eta}(x)$ is the rate of dissipation for x-features. The example is dissipation due to ice-water drag which depends on the ice underside geometry described by the keel spacing distribution $f(x)$. The rate of dissipation due to binary interactions is

$$\dot{E}_{bin} = \mu_X \int_{\Delta} dxdy\, \alpha(x,y)\eta(x,y) f(x) f(y) \tag{53}$$

$\alpha(x,y)$ is the rate of interaction events and $\eta(x,y)$ the dissipation per event. Bivariate description $f(x,y)$ may be relevant in this context. The example is dissipation by inelastic ice floe collisions and $f(x,y)$ is the distribution for adjacent floe pairs. Finally, the internal rate of dissipation is

$$\dot{E}_{int} = \mu_X \int_{\Delta} dx \int_{\Delta Cr(x)} dy\, \alpha(y \to x)\eta(y \to x) f(y) \tag{54}$$

where the total dissipation in a transition event is $\eta(y \to x)$. The example is frictional dissipation associated, due to the ridge buildup, to a spacing transition event in which case $f(y)$ is a spacing distribution.

3.6. Parameterisation of the evolution equation

The parameterisation of the evolution equation (43,46) for $f(x)$ comprises the specification of the rate α and the transition probability B. This task can be divided into two parts. First the functional form of α and B must be specified (for example, that α follows a power law $\alpha=ax^{\nu}$ and that B belongs to a certain distribution family). Next the open parameters appearing in α and B must be specified (a and ν for the power law and the parameters pinpointing B within the distribution family). These open parameters are in general dependent on time, on ice dynamical processes, and on ice cover characteristics. The following methods of parameterisation are conceived:

1. Direct determination of α and B from time series data.
2. Realistic discrete element simulating of the evolution process.
3. Construction of B from observed feature structure.
4. Use of general arguments like statistical assumptions, independence, invariance, conservation and scale similarity.
5. Search of α and B reproducing observed distributions.
6. Relating α and B by physical arguments to other random processes, for example in case of floe distributions to wave field statistics through the calculation of bending moments.

7. Relating in Eulerian conservation equations α and B to the partial concentration C_X and to the strain field $\dot{\varepsilon}$.
8. Relating in ice modeling context α and B to the stress field σ.
9. Relating in ice modeling context α and B to the model dissipation $\dot{\varepsilon} : \sigma$.

In a Lagrangian region R the rate α can be estimated by measurements. A subregion consisting of all x-features is monitored for $\alpha(x,t)dt$ which is the probability to suffer transition during dt. Here dt is some finite interval that is short but longer than the transition events. If the rate $\alpha(x,t)$ changes slowly in time, the period can be longer. The rate is expected to depend on the intensity of the atmospheric and oceanic forcing. Thus, as a primary hypothesis, it is sought in the form $\alpha(x,t)=\beta(t)\alpha'(x)$ where the intensity factor $\beta(t)$ and the dependence on x are separated. The forcing can have local length scale, like wave field forcing, or large length scale, like wind forcing. In the latter case the rate depends on how the large scale average stresses are related to the local stresses driving the transition events. However, the stress propagation is presently not understood well.

3.7. Including morphological distributions to dynamic ice models

If the present theory is used to make forecasts in some region, the realisations of the underlying stochastic process should not be very different from their ensemble average. This can be assumed if the events have small length scale in comparison with the region scale. For example, the size distribution for a large number of floes is expected to evolve continuously in time if the floes only fragment. On the other hand, during a short freezing period the floes may consolidate into a single massif. This is a single aggregation event. The massif then fragments but the generated size distribution is hard to relate to that found before the aggregation. Forecasting is in general feasible if the transition events have short length and time scales, thermal processes do not change the horizontal ice cover geometry, the time span is not too long, and persistent features are described. Thus, at least ridge distributions, thickness distribution, and floe size distribution during a melting period are expected to be predictable.

A standard output of an ice model includes partial concentrations and average thicknesses of certain ice categories, strain rate and stress. Two examples of the possible use of distributions in ice models are given. First example is the size distribution of fragmenting floes. Then α is the rate of fragmentation events and B the probability of size decrease. Increasing stress can be assumed to increase α. If this relationship is parameterised the model output stress may drive the floe size evolution. The model output is not otherwise affected. On the other hand, there are models with a collisional rheology. They derive the constitutive equation by

considering the rate and velocity of floe collisions. It then depends on the average floe size (Shen et al. 1987) or floe size distribution (Lu et al. 1989). The floe size distribution may evolve independently of the model, for example if fragmentation is driven by the swell. The distribution is used to parameterise the model. On the other hand, if the fragmentation rate depends on the floe collision rate and collision velocity, the result is a coupled morphological-dynamical model. Stress, strain, concentration and floe parameters determine the collision rate and collisional velocity, and thereby the fragmentation rate. The changing floe size changes the collision rate and velocity.

As another example thickness distribution is considered. The evolution is governed by an equation where α is the rate of thickness increase events and B the probability of increase in such an event. These may depend on the model output under the constraint that average thickness is thickness distribution mean. The thickness distribution evolution is then an external module to the dynamic model. On the other hand, the constitutive equation may depend on thickness distribution in which case a coupled dynamical-morphological model is obtained. This may enhance the prediction of the dynamical fields and thereby also the thickness prediction.

3.8. Morphological homogeneity and spatial continuity in observed ice cover

Another feature related to the status of observed distributions as realisations is that they may be inhomogenous or spatially discontinuous although the ensemble averages are not. Usually $f(x)$ is determined for a region as a distribution model for a histogram. If only a subregion is sampled the histogram should be representative. This is a practical criterion of homogeneity. A histogram bin which has value p in the region and p' in the subregion is considered. If the subregion location is varied, p' shows variance $Var(p')$ which may have several sources. These include correlations, sample size, fluctuation, and inhomogeneity.

The correlations effect in scales shorter than certain correlation length scale L_c. For Arctic ice thickness this scale for the bin $x<1$ m is about 1 km and for the bin $x>5$ m about 10 m (Rothrock 1986). The scale L_c is the characteristic length of profile sections with all values in the bin. This can be taken as a general characterisation of L_c and for the subregion scale L' is required $L'>>L_c$. Then $Var(p')=Var_0+Var'$ where Var_0 is due to sample size and Var' due to inhomogeneity. The coefficient of variation $\delta_i = \sqrt{Var'}/p$ is a measure of homogeneity. However, the inhomogeneity may be accidental, that is, it manifests only in the realisations but not in the ensemble average. It is then called fluctuation instead. The separation of inhomogeneity and fluctuation is not

expected to be simple. However, the fluctuation may occur only in shorter length scales. For example, there is new thin ice formed between thicker floes and the variation of partial concentrations is large in a short length scale L_{fluc} but averages out in the region scale. Then it is required also that $L' >> L_{fluc}$ if δ_i is to be interpreted as a measure of inhomogeneity.

Wadhams (1997) studied 50 km sections of Arctic draft profile determined by submarine sonars. Regions with homogenous appearance where chosen. The values of the coefficient of variation δ^{50km} are reported for section averages of thickness. One of the data sets contained thirty-six sections, criss-crossing an 100 km × 50 km area, and δ^{50km}=0.15. Homogeneity was considered as a good approximation. For more extended areas, sampled during three other submarine cruises, values ranging from 0.07 to 0.14 were found. Larger values were found for thickness histogram bins, especially for thin ice types. For lead density, lead width, and ridge keel density δ^{50km} ranged from 0.22 to 0.24. However, as the fields had homogenous appearance, the results may as well be interpreted as fluctuation in 50 km scale. This is suggested by the smaller value of δ^{50km} for more extended profiles.

Similar problem concerns the extracting of continuum fields from observations. In ice modeling contexts the criterion for the applicability of continuum description requires that the grid cell scale L' satisfies $L' << L_{\nabla v} = v/|\nabla v|$, where the scale $L_{\nabla v}$ measures the steepness of the velocity gradient, and that coherently moving elements are on the average considerably smaller than L' (Leppäranta 1998). The same criterion applies to the extraction of continuum velocity fields. A coherently moving element produces to the velocity field correlations and fluctuation, the latter being due to the stochastic component of its trajectory. The correlations persist in the ensemble average while the fluctuations average out. The morphological histogram bin is again considered and a field $p(\mathbf{r})$ of bin value is determined by sampling $\mathbf{r}$-centered regions with scale L'. Then it should be

$$L_{fluc}, L_c << L' << L_{\nabla p} \tag{56}$$

for the observed gradient ∇p. The above results of Wadhams (1997) were interpreted here as fluctuation in fields with zero gradient. Similar fluctuation is expected when the gradient is nonzero. The gradients can be sought in terms of distribution models which smooth to some extent the fluctuation. The gradients can then be also described by the gradients of the distribution parameters. However, such model may be hard to give as is known in the case of ice thickness distribution.

On the other hand, from an evolution viewpoint the X-homogeneity or continuity is a manifestation of the homogeneity or continuity of α and B. Also, correlations are in part generated by the evolution while fluctuation pertains to realisations only. Homogeneity and spatial continuity may hold for α and B even in case they are not found for observed distributions. The X-process may be homogenous in two regimes with different distributions. This stresses the importance of directing attention from distribution sampling also to the determination of α and B. In Chapter 5 it will be seen that in some cases the regimes evolve towards a common asymptotical distribution and in other cases not. In the first case the evolution homogenises the ice cover while in the other case the regimes retain the difference between their ice characteristics.

4. THE EVOLUTION OF RIDGE SAIL ARRANGEMENT

4.1. Introduction

Ridge sail arrangement is the horizontal geometry of ridge sails in a ridged ice field. Although the bulk of ridged ice volume is in subsurface keels, often only surface measurements and observations are possible. The sail arrangement determines also the signatures of ridges in satellite images. From the images neither information on the keels nor on the sail height can presently be obtained.

Morphological features and variables are selected so that they can be used to formulate evolution equations. The strategy is to use features that experience transitions into features of the same type. The sail arrangement evolution is then a transition event process and equations of the type (43) or (46) are applied. The evolution equation is specific to the variables describing the features. A formulation in terms of surface observable variables is given. Other variables are related to them by ridge structure models.

The principal features are spacing cross-sections. The equations related to them are developed in detail so that the solution methods of Chapter 5 can be applied. Solutions will be constructed also for the sail number equation. Other approaches include spacing concatenations and horizontal segments of different types. The respective equations are related to the sail spacing and sail number equations but not developed further. None of the approaches is unproblematic as the features are always to some extent artificial constructions, designed to make a complex evolution process tractable.

4.2. Evolution of distributions pertaining to sail spacing cross-sections

4.2.1. Distinctive characteristics in ridge spacing evolution

The distribution $f(x,t)$ gives the probability that a spacing randomly chosen at time t is an x-spacing. In a large sample of N spacings $Nf(x,t)$ is the number of x-spacings. The objective is to formulate equations for $Nf(x,t)$. The formulation begins with the choice of features for which transition events are characterised. This is nontrivial as there are differential movements associated to ridge formation. The sail spacing evolution is compared first with simpler crack spacing evolution, for example that driven by thermal stresses in an ice sheet. The crack and ridge sail arrangements have similarities, but this is less so for the evolution process. The crack arrangement changes through the addition of new cracks in instantaneous events. Along a transect this appears as sequential deposition of points that divide the transect into crack spacings. The differential movements

associated with the events are small and can be neglected. The transect retains its linearity and its length. A new crack cuts some spacing x into two shorter spacings x' and x-x'. This transition event does not depend on the ice thickness.

On the other hand, ridge formation events have much longer duration than crack formation events. A local differential movement is associated with the formation. The total magnitude of the differential movement is of the order of hundreds of meters (Section 7.3) and cannot be neglected. It depends on the local thickness characteristics and the volume of the formed ridge. If thickness increases by ridging only, then in a region with C=1 these differential movements determine the strain field in 100 m length scale. On the other hand, the strain field characteristics in, say, 10 km length scale set constraints to the sail arrangement evolution. For example, if a 10x10 km^2 rectangular region with C=1 is compressed uniaxially it must fail across its whole width. This creates across the region a failure zone which is a connected chain of compressive and shearing local deformations. The deformation cannot be constrained to one ridge formation site at a time. This is dissimilar to crack arrangement evolution where the cracks can appear locally one at a time.

The local differential movements associated to ridge buildup may have any direction, although certain directions are certainly preferred by the global strain. A linear transect across R, fixed to ice, distorts into a discontinuous sequence of line segments (Figure 15). The total length of these segments is less than the length of the original transect. Simple description of the process as a deposition of objects on a line is not possible. The transitions cannot be described as dividing of line segments into two shorter segments.

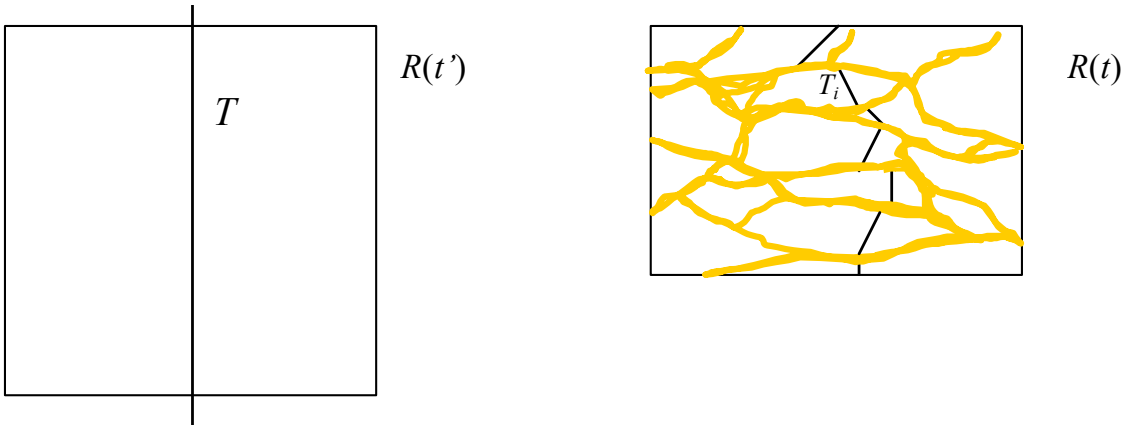

Figure 15. Ridging of a uniaxially compressed level ice region (schematic). A linear transect T is fixed to ice and becomes partitioned to segments T_i.

4.2.2. Transition events of spacing cross-sections

In a spacing transition event two progeny spacings are created from one parent *x*-spacing. The transition event starts by a ridge buildup initialisation on the parent spacing and is completed as the buildup ceases. The buildup consumes a certain fraction of the parent spacing. A progeny spacing is defined by starting from parent spacing endpoint and proceeding in the parent spacing direction to the new sail (Figure 16). The progeny spacings *x*' and *x*'' are separated by the differential movement if it is not aligned with the parent spacing.

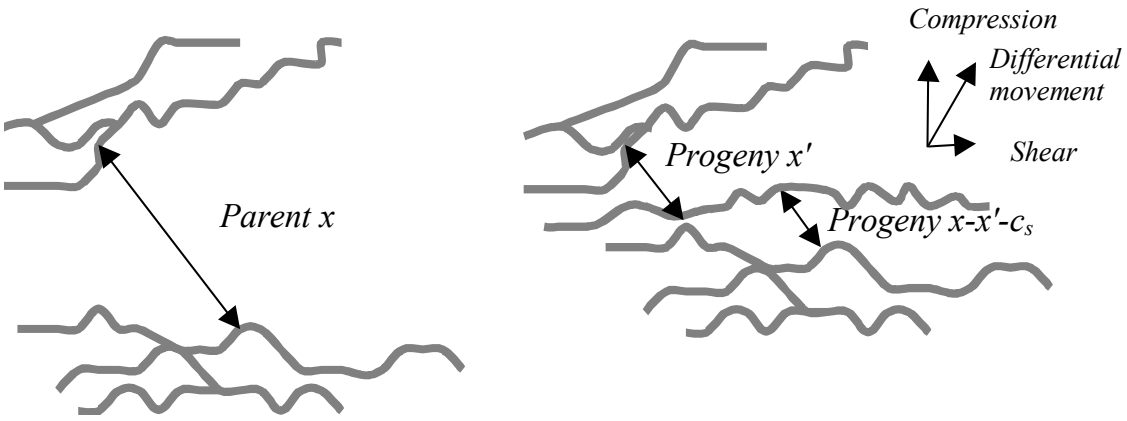

Figure 16. A transition event for a spacing.

Spacing is one variable describing spacing cross-sections. Spacing transitions corresponds to physical feature transitions of the spacing cross-sections which are thus the features of the approach. Additional cross-sectional variables are required to quantify the spacing transition. The selected cross-section variables are $\mathbf{x} = (x, H, h_1, h_2, H_1, H_2)$ if the keels are detached and $\mathbf{x} = (x, h_1, h_2, H_1, H_2)$ if the keels have contact (Section 2.2.9). The parent **x**-cross-section produces progeny **x**'- and **x**''-cross-sections (Figure 17). This transition event is described by properties averaged over all actual physical transitions with same values of **x**, **x**' and **x**''. This averages over the spacing/sail incidence angles and over the angle that the parent spacing makes with the differential movement. The cross-section of the new ridge is similar for both progenies and has height *h*'. Isotropicity is assumed and the spacing cross-section models of Section 2.2.9 are applicable.

The progeny spacings of a parent *x*-spacing are *x*' and *x*''=*x*-*x*'-c_s. They add thus to *x*-c_s where c_s is called parent spacing consumption (Figure 17). If there is no keel contact, the parent spacing consumption

$$c_s = \frac{\pi}{2}\left(\frac{v_l(h', H)}{H} - w_l(h', H)\right) \tag{55}$$

is obtained by a ridge link cross-section model (Section 2.2.6). If the transition results into a keel contact, or if the parent spacing already has keel contact, the clustering effect reduces c_s. This is not simply expressed even when using the keel overlap model (Section 2.2.9). This is discussed more in Section 4.2.4. A binary transition has two progenies. Transitions may also be due to simultaneous buildup of several ridges so that the number of progeny is higher. Pure shear, finger rafting and ridge keel formation without sail formation are transitions with single progeny. However, here the spacing transition process is assumed to be binary.

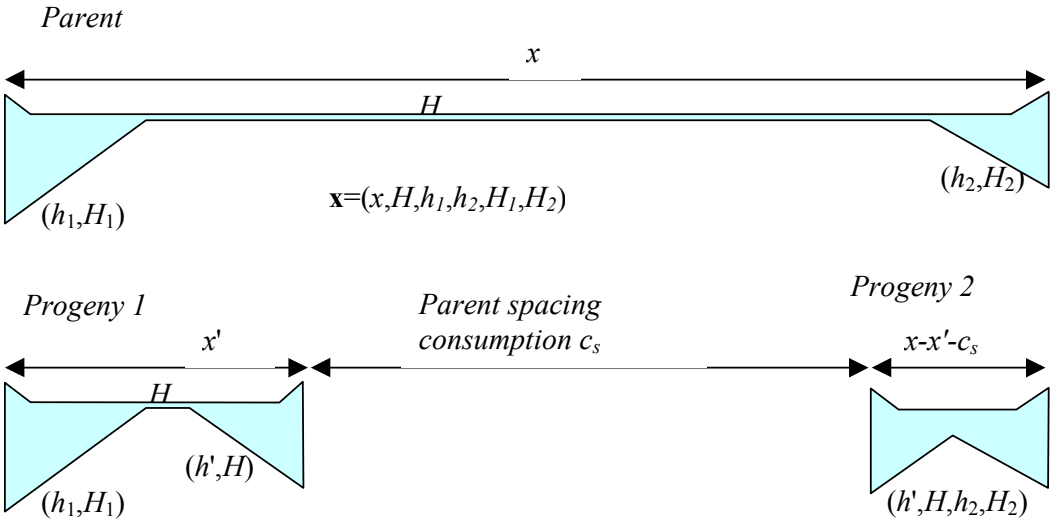

Figure 17. Transition event for a spacing cross-section.

4.2.3. Spacing cross-section evolution as a discontinuous Markov process

A discontinuous Markov process consists of identifiable transition events of short duration *dt*. This is not obvious as ridge formation may take an hour or more. It may also be intermittent, continuing after forcing has attained higher level (Lensu and Green 1995). Other ridges may be also forming nearby. Problems arise if a progeny transits into second generation progenies before the parent transition is complete. Up to a certain limit this is a transition with three or more progenies. In the extreme case all ridges in a ridge field grow simultaneously and the discontinuous theory does not apply.

How a ridging event proceeds in a ridge field scale is not known in detail. The parent spacing consumption is about 300 m (Section 7.3). A typical strain rate due to ridging is 1% per hour (e.g. Leppäranta and Hibler 1987). One-dimensional contraction with this rate is assumed. The average rate of ridge formation is then

0.033 ridges per km and per hour. A 24 hour ridging phase attains then ridge density 1 ridge/km and 100 hours the density 6 /km. It is not known what is the typical differential velocity between the opposing sheets during ridge buildup. The maximum is set by the ice drift speed which for compact ice cover is of the order of 0.15 m/s. The buildup time is then half an hour. The growing ridges are on the average 60 km apart if the strain rate is 1% per hour. For differential velocity 0.01 m/s the buildup time is 8 hours and the growing ridges 4 km apart. The typical buildup time is probably between these estimates. However, as was discussed in Section 4.2.1, uniaxial contraction of a compact region creates failure zones that extend across the whole region. It is possible that also in the direction of the contraction the ridge formation is localised to such zones. The basic events may in that case be rather the formation events of ridge clusters. Without further study no conclusive answers to the discussed question can be given.

If the transitions are identifiable the spacing cross-section equation is

$$\frac{\partial N f(\mathbf{x})}{\partial t} = N\kappa \int_{\Delta_{x'}} d\mathbf{x}' \alpha(\mathbf{x}') f(\mathbf{x}') B(\mathbf{x}' \to \mathbf{x}) - N\alpha(\mathbf{x}) f(\mathbf{x}) - \frac{\partial \Theta(H) N f(\mathbf{x})}{\partial H} + \gamma^e(\mathbf{x}) \quad (56)$$

where $\alpha(\mathbf{x},t)$ is the transition rate and $B(\mathbf{x}'\to\mathbf{x})$ transition probability. The thermal change for the level ice thickness and emergence have also been included. The equation may then also describe a longer period with several ridging phases. The emergence may describe the creation of ridges from level ice outside the sail field. The level ice is destroyed and the emerging ridged ice adds to the ridge sail field. In what follows these additional terms are not considered. The number N is an auxiliary variable and $N(0)=1$ is a possible choice. From the solution ridge sail spacing distribution, ridge link height distribution, and level ice thickness distributions are obtained as marginal distributions. If the transitions are not identifiable, the evolution can be formulated in terms of spacing cross-section volume (Section 4.2.5). However, the possibility of including ridge heights and level ice thickness to the characterisation is then lost.

4.2.4. Evolution equations for spacing distribution

The multivariate spacing cross-section equation (56) describes the evolution of sail spacing distribution, ridge link height distribution, and level ice thickness distribution. Another possibility is to use the spacing cross-sections to parameterise a spacing equation

$$\frac{\partial}{\partial t} Nf(x) = N2 \int_{x}^{x_{\max}} dx' \alpha(x') f(x') B(x' \to x) - N\alpha(x) f(x) \tag{57}$$

where α(x,t) is rate of spacing transitions and $B(x' \to x)$ the probability that progeny x is produced from parent x'. It is assumed that the evolution is binary so that κ=2 and the mean value of $B(x' \to x)$ is

$$\langle x' \to x \rangle = (x' - c_s(x'))/2 \tag{58}$$

where $c_s(x')$ is the average consumption of x'-spacings. The following possibilities to derive the spacing distribution evolution are considered:

1. The spacing evolution equation (57) is parameterised using cross-sectional models.
2. The evolution is described by the multivariate equation (56) and $f(x,t)$ is a marginal distribution of the solution.
3. The equation is formulated for the distribution $f(v,t)$ of spacing cross-section volume (Section 4.2.5) and $f(x,t)$ is obtained by a relationship connecting v to x, constructed by cross-sectional models.

The equation for $f(v,t)$ is simple and often analytically solvable. The multivariate equation for $f(\mathbf{x},t)$ contains much information but is not analytically manageable. The spacing equation has most practical value but is not easily solved either. Its parameterisation is outlined in the following. The rate α(x,t) cannot be constructed from cross-sectional models but requires direct observing or advanced understanding on the process of stress propagation in a ridging ice field. The constructing of $B(x' \to x)$ is considered instead. It is assumed that ice thickness is constant. The parent spacing link heights are (h_1,h_2). The transition produces initial progenies x_0 and x'-x_0 which then contract during the ridge buildup. A ridge is allowed to grow until x_0 is contracted into x. The attained sail height is h. All 4-tuples (x_0,h_1,h_2,h) that can give x constitute a domain $\Delta(x)$. The probability $B(x' \to x)$ is then obtained by integrating $B^*(x' \to x_0)g(h_1)g(h_2)g(h)$ over $\Delta(x)$ where B^* is probability for the initial progenies and the g's link height distributions. However, even with simplifying assumptions (h=h_1=h_2, initialisation at random location or in the middle) the results are not simple. Further pursuing is not motivated as several assumptions on the cross-section geometry and on B^* must be made, none of which is known well.

The transition probability can finally be assumed to be a simple function that displays some characteristics of the spacing transitions. If the spacing

consumption depends only on the parent x', $B(x'\to x)$ is defined on the interval $[0,x'-c_s(x')]$. A simple choice is

$$B(x'\to x)=b\left(\frac{x}{x'-c_s(x')}\right)\frac{1}{x'-c_s(x')} \tag{59}$$

where b is a distribution defined on [0,1], for example a uniform distribution. The parent spacing is first contracted to $x'-c_s(x')$ and then divided following (59). Still the only easily approached case is to assume that $c_s(x')$ is proportional to x' (Section 5.3.1).

4.2.5. Evolution equations for spacing cross-section volume

The cross-section volume is conserved in transitions. The cross-sectional volumes for the progeny spacings add to that of the parent spacing. The volume transition $v\to v'$ is unproblematic as it is defined at the instant of initial failure event. Parent spacing consumption need not be considered. Allowing spacing transitions with one progeny, for example due to rafting, the progeny production κ is between *1* and *2*. There is no additional parameterisation task from such transitions as the cross-section geometry need not be known. Considering the transition process only, the equation for spacing cross-section volume is

$$\frac{\partial Nf(v)}{\partial t}=N\kappa\int_{v}^{v_{\max}}dv'\alpha(v')f(v')B(v'\to v)-N\alpha(v)f(v)\,. \tag{60}$$

Here $B(v'\to v)$ is defined on $[0,v']$ and has mean value v'/κ. The equation is solved for $N(t)f(v,t)$ which then gives $f(v,t)$. The spacing distribution is obtained as

$$f(x)=\int_{v_{\min}}^{v_{\max}}dvf(x,v)=\int_{v_{\min}}^{v_{\max}}dvf(x\,|\,v)f(v) \tag{61}$$

where $f(x|v)$ is the probability that a v-cross-section corresponds to an x-spacing. The direct construction of $f(x|v)$ is outlined in the case of constant H. Sail heights are h_1 and h_2 and cross-sectional ridge link volumes $v_1=v(h_1,H)$ and $v_2=v(h_2,H)$. If $(v_1+v_2)/2<v$, level ice is added between the keels until the spacing cross-section attains volume v, and the resulting spacing x is recorded. On the other hand, if $(v_1+v_2)/2>v$, the keels are let to overlap until v is attained, and x is recorded. Now

all pairs (h_1,h_2) that give x under constraint v determine a domain $\Delta(x)$. The probability $f(x|v)$ is obtained by integrating $g(h_1)g(h_2)$ over $\Delta(x)$.

The volume approach transfers the cross-sectional modelling from the equation to the solutions. Unfortunately triangular keel models give awkward $f(x|v)$. Thus simple ridge cross-section models are not simple when applied in the present context. A better approach would be the direct determination of $f(x|v)$ from joint surface and draft profile. From such data $f(v|x)$, allowing ice volume estimation from observed $f(x)$, can also be determined.

4.2.6. Multivariate equation for spacing cross-section volume

Correlations between adjacent spacing cross-sections are expected. This is considered for the cross-sectional volume only. The origin of the correlations is that the progeny volumes v and v'-v are deterministically related. The volume distribution for n successive cross-sections is governed by

$$\begin{aligned}
\frac{\partial}{\partial t} N f_n(v_1, v_2, ..., v_n) &= N \int_{v_1}^{v_{\max}} dv' \alpha(v') f_n(v', v_2, ..., v_n) B(v' \to v_1) \\
&+ N \int_{v_n}^{v_{\max}} dv' \alpha(v') f_n(v_1, v_2, ..., v_{n-1}, v') B(v' \to v_n) \\
&+ N \sum_{i=1}^{n-1} \alpha(v_i + v_{i+1}) f_{n-1}(v_1, ..., v_{i-1}, v_i + v_{i+1}, v_{i+2}, ..., v_n) B(v_i + v_{i+1} \to v_i) \\
&- N \left(\sum_{i=1}^{n} \alpha(v_i) \right) f_n(v_1, v_2, ..., v_n)
\end{aligned} \tag{62}$$

which is adapted from Lensu (1997). It is a mathematical transcription of the following creation and annihilation fluxes for n-tuples of cross-sections, illustrated in Figure 18 for pairs of cross-sections:

- The first or last component cross-section in an n-tuple transits; these transition events gives the two integral creation terms.
- An n-tuple is created by emergence events from an (n-1)-tuple. This gives the next term which depends on the distribution of (n-1)-tuples.
- An n-tuple is annihilated if one of the component cross-sections does; this gives the last term.

The equation is solved iteratively, starting from $f(v)$ and proceeding to n-tuples. Due to differential movements, (62) can be assumed to apply only approximately to linear segments containing n spacings.

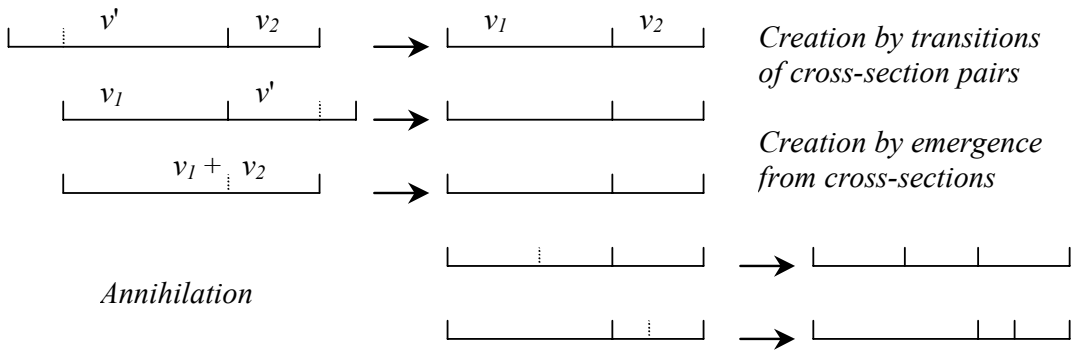

Figure 18. Creation and annihilation events in the evolution of pairs (v_1,v_2) of spacing cross-section volumes.

4.2.7. Evolution of spacing concatenations

Spacing concatenations can describe ridge clusters. The evolution processes are outlined without details. An n-concatenation of length y_n has n component spacings. It transits if one of the component spacings does. At the same time one spacing is discarded from either end to keep n constant. The transition probability $B(y_n' \rightarrow y_n)$ describes the combined effect of parent spacing consumption and component spacing discarding. The evolution equation is similar to (57).

In an x_0^--concatenation of length y^- all component spacings are shorter than x_0^-. Four kinds of events are possible (Figure 19). Their characterisation gives a construction recipe for the evolution equation. It is not written down as the characterisation can be used to relate the properties of solutions to those of spacing equation (Section 6.3.6). The events for x_0^--concatenations are as follows:

- A concatenation emerges from a spacing exceeding x_0^-.
- A concatenation transits when one component spacing does.
- A spacing exceeding x_0^- and adjacent to a concatenation transits, and one or both progenies join the concatenation.
- Two concatenations join together through a spacing transition.

The evolution equation for $f(y^-;x_0)$ is thus of the fragmentation-coagulation type (Section 3.5.2) with an emergence term.

An x_0^+-concatenation of length y^+ with all spacings exceeding x_0 is finally considered. It transits when one of the component spacings does. It then either contracts, produces two progeny concatenations, or is destroyed. The evolution equation for $f(y^+;x_0)$ is thus of the fragmentation type with $\kappa<2$ and with a destruction term.

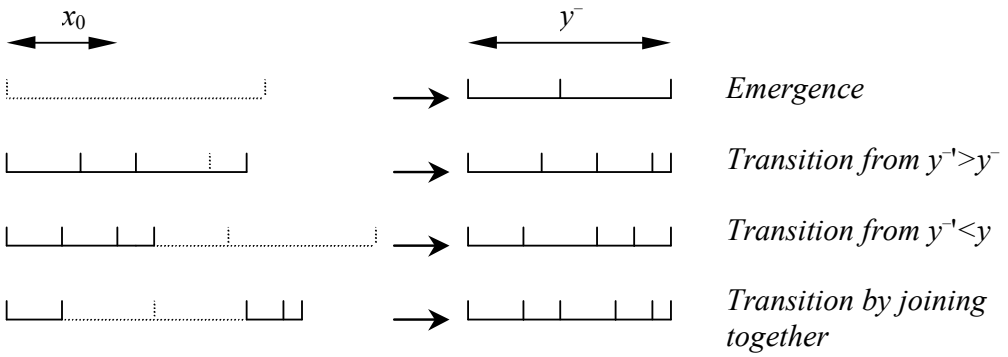

Figure 19. Creation events of x_0^--concatenations described by $f(y^-;x_0)$. The annihilation events are also due to transitions of the three types.

4.3. Alternative characterisations of sail arrangement evolution

4.3.1. Evolution of ridge sail number distributions

Ridge sail number distribution $k(n_i,t)$ gives the probability that there are n_i sails on a line segment of length L_i. To the line segment corresponds a segment cross-section. The underlying feature process consists of transitions of segment cross-sections. However, the evolution is described here in terms of ridge sail number only. First a comparison with crack arrangement evolution is made. Crack number is the number of crack intersections on a line segment. The transition is an addition $n_i \rightarrow n_i+1$ of one crack intersection. The differential movements can be neglected in the transitions. For ridge sails the transitions are due to ridge formation events and the differential movements count (Figure 20). Transitions $n_i \rightarrow n_i'$, $n_i'>n_i+1$, are possible.

However, it is argumented that simple transitions $n_i \rightarrow n_i+1$ can be applied. The component of the differential movement perpendicular to the segment does not, on the average, change the sail number, while the aligned component increases it.

Thus it is assumed that the ridge sail numbers increase monotonously. Further, the time scale *dt* is assumed to be short so that the differential movements are small during *dt.* The transition events $n_i \rightarrow n_i+1$ are either ridge buildup initialisations, or sail influx events due to differential movements. The evolution is governed by the simple equation

$$\frac{\partial k(n_i)}{\partial t} = \alpha(n_i - 1)k(n_i - 1) - \alpha(n_i)k(n_i) \tag{63}$$

which is a version of the event number equation (49).

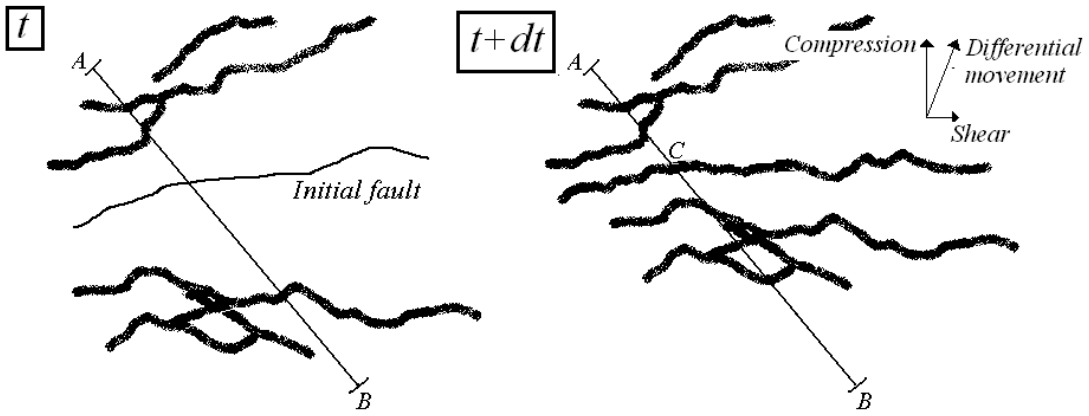

Figure 20. Transition event for a line segment. End point *A* is fixed to ice and *dt* equals ridge buildup time. A ridge *C* is created and the sail number transition is $3 \rightarrow 6$. If *dt* is very short instead, only the buildup event effects and the transition is $3 \rightarrow 4$. The differential movement induces subsequent transitions $4 \rightarrow 5$ and $5 \rightarrow 6$.

4.3.2. Sail arrangement evolution described in two horizontal dimensions

Sail spacings and sail numbers are one-dimensional descriptions of the horizontally two-dimensional ridge sail arrangement. Some possible two-dimensional descriptions are shortly investigated. Floe size can be quantified by floe area, and by floe chords along linear transects. Similar alternatives are conceived for sail arrangement. If the ridge density is high the sails join into a continuous network. It partitions the ice cover into floelike features, or quasifloes (for example as in Figure 10). The sail spacings are chords of the quasifloes. The quasifloes transit into smaller quasifloes as a new ridge sail crosses them (Figure 21a). The equation is similar to spacing equation where parent spacing consumption is replaced by area reduction.

Another choice takes ice floes as basic features. The simplest description uses floe area and the length of ridge sail within the floe. The floes may fragment and coalesce, and ridges may form to floe interiors and to floe contact interfaces (Figure 21b).

As a third alternative square segments with side length L_i are considered (Figure 21c). The length of ridge sail on a segment is l_i. This is a two-dimensional correspondent of the ridge sail number. To characterise transition events the segment center point is fixed to the ice. Sail length is increased by ridging in the segment and by sail length influx.

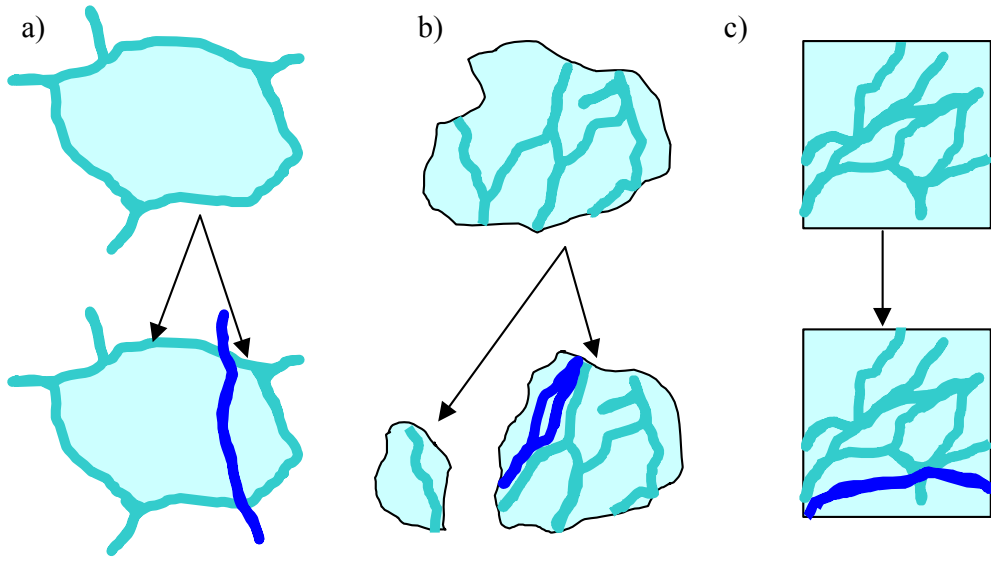

Figure 21. Possible feature transitions in the two-dimensional description of ridge arrangement evolution. a) Partitioning of a quasifloe, or a sail-fringed level ice area. b) A fragmentation and ridging event for a floe. c) Ridging event in a square segment.

5. SOLUTIONS OF EVOLUTION EQUATIONS

5.1. Introduction

Linear Lagrangian evolution equations can in principle be solved analytically. In practice, the range of analytical methods has a limit beyond which their further pressing on results to great complexity. This is meaningful if the equation is a good description of the process. This requires that the transitions are instantaneous and identifiable, the number of transitions during dt is large, and the transition rate and transition probability are well known. If the description or parameterisation is approximate, complex specificity of the solutions is not motivated. This is the case for distributions pertaining to ridge sail arrangement. Therefore, the objective is to derive simple solutions that can be related to the distribution models applied to observed distributions. The focus is on the ridge sail spacing and ridge sail number distributions as these are determinable from profile data. The properties of sail spacing distributions are inferred from the solutions of spacing volume distribution. On the other hand, sail number distributions are directly approached.

The dominant parameter in the asymptotic behaviour of the evolution equation is the transition event rate. The solutions can often be asymptotically characterised without specific knowledge on the transition probabilities. For ridging processes the transition rates are expected to be related to the propagation of stresses in the ice cover. The details of this process are not well known, and thus direct arguments for certain functional form of the rates are hard to give. Rather, if certain assumptions on the rates produce the observed distributions as solutions of the evolution equation, this gives insight to the mutual feedback process of stress propagation and local deformation.

The methods applied here include integral transforms and iterative constructions. Due to the mathematical similarity of equations, the results are applicable to other ice morphological processes as well. The main output of the analytical developments is simple and accessible from the nontechnical sections of the present chapter. Figuratively, the spacing distributions reside on a continuum where the end points are exponential and lognormal distributions respectively. This continuum is expressible in terms of sail number distributions as well and the corresponding continuum of solutions is also found.

5.2. Spacing volume distribution

5.2.1. Preliminaries

The spacing consumption complicates the spacing equation and is not known well enough either. The equation (60) for spacing cross-section volume is considered instead. Spacing consumption does not appear and the transition probabilities $B(v'\to v)$ can be simple functions.

The finite maximum volume $v_{\max}$ is a parameter in the solutions $N(t;v_{\max})f(v,t;v_{\max})$. These are called here proper solutions. It is enough to find $N_b(t;v_0)f_b(v,t;v_0)$ for the initial condition of one v_0-spacing; these are called here basic solutions. For the general initial condition $N_0f_0(v_0)=N(0;v_{\max})f(v_0,0;v_{\max})$ the proper solution is

$$N(t)f(v,t) = N_0 \int_v^{v_{\max}} dv_0 f_0(v_0) N_b(t;v_0) f_b(v,t;v_0) \ . \tag{65}$$

For example, $f_0(v_0)$ is what is observed and $f(v,t)$ is the prediction.

The proper solutions of (60) are complicated and difficult to relate to empirical models applied to spacing data. As these models have no upper bound they are not proper solutions but at most asymptotical solutions. There are no time series data or general arguments that could pinpoint the transition rate. The adopted approach is therefore to make simple assumptions on the rate and transition probability and derive asymptotic solutions. These comprise a space with respect to parameters appearing in the rate and transition probability. The empirical models can be located within this solution space, after which explanations to the parameters this comparison suggests are sought. For spacing processes the focus is on the commonly suggested negative exponential and lognormal distribution models.

It is assumed that time appears in the rate as an intensity factor, $\alpha(v,t)=\beta(t)\alpha'(v)$. It can be assumed further that $\beta(t)=1$, as otherwise this is achieved by a variable change. The simplest assumptions on transition probabilities are $B(v'\to v)=1/v'$ and $B(v'\to v)=\delta(v-v'/2)$. The first is random volume division where the progeny volume is uniformly distributed on $[0,v']$. The other halves the volume to equal parts $v'/2$. However, to proceed more generally, it is assumed

$$B(v'\to v)dv \equiv b(v/v')(dv/v') \tag{66}$$

where $b(\eta)d\eta$ is a distribution defined on [0,1]. As (66) depends only on the scale independent ratio v'/v it is scale similar. The two simple assumptions on B above correspond then to $b(\eta)=1$ and $b(\eta)=\delta(\eta-1/2)$. For (66) the equation (60) reads

$$\frac{\partial N f(v)}{\partial t} = N\kappa \int_0^1 dv' \alpha(v') f(v') b(v/v')(1/v') - N\alpha(v) f(v) \qquad (67)$$

where the variable v has been scaled so that the upper bound is 1.

5.2.2. Integral transform technique

The solutions of (67) are approached using the transform

$$F(s) = \int_0^1 dv\, v^{cs} f(v) \qquad (68)$$

where c is a suitably chosen constant. The technique is to derive an differential-difference equation for $NF(s)$, solve it, and obtain $Nf(v)$ as the inverse. This technique was developed in Lensu (1993 a) and it is more convenient than the use of power series (McGrady and Ziff 1987). It is based on the fact that the transform of a convolution

$$(f_1 * f_2)(v) = \int_v^1 dv' f_1(v') f_2(v/v')(1/v') \qquad (69)$$

is the product $F_1(s)F_2(s)$. If $\alpha(v) = v^\rho \sum a_n v^n$ and $c=\rho$ the right hand side of (67) transforms into a sum of terms proportional to $F(s+n)$. It is assumed that the rate has the simple form $\alpha(v)=v^\rho$. Only the basic solution $N_b(t;1)f_b(v,t;1)$ is then required as the other basic solutions are

$$N_b(t;v_0)f_b(v,t;v_0) = N_b(v_0^\rho t;1)f_b(v/v_0, v_0^\rho t;1)(1/v_0) \quad . \qquad (70)$$

Thus the solving of (67) for the initial condition of one spacing with unit volume is sufficient to generate solutions for arbitrary initial conditions.

5.2.3. Gamma distribution solutions

If the rate has the form $\alpha(v)= v^\rho$, $\rho>0$, then (68) with $c=\rho$ transforms (67) into the differential-difference equation

$$\frac{\partial NF(s)}{\partial t} = N\left(\kappa K(s) + \kappa - 1\right)F(s+1) \tag{71}$$

where

$$K(s) = -1 + \int_0^1 d\eta\, \eta^{\rho s} b(\eta) \ . \tag{72}$$

After solving $F(s,t)$ for $F_0(s)$=1 the inverse transform provides the basic solutions $f_b(x,t;1)$ for simple functions $b(\eta)$ in terms of hypergeometric functions (Lensu 1993a). These can be also obtained by power series methods (McGrady and Ziff 1987). Asymptotic analysis can then be done. However, it is simpler to use an asymptotic equation directly. This is derived by a scaling transformation (Cheng and Redner 1988, 1990, Treat 1997 a,b) which amounts to the substitution $\xi = vt^{1/\rho}$, $N = Ct^{1/\rho}$ where C fixes the number of spacings at certain t=t_0. Applying directly to the transform gives

$$F(s,t) = \int_0^1 dv\, v^{\rho s} f(v,t) = t^{-s} \int_0^{t^{1/\rho}} d\xi\, (\xi t^{1/\rho})^{\rho s} \phi(\xi,t) = t^{-s}\Phi(s,t) \tag{73}$$

where $\phi(\xi,t)$ normalises to unity. Substituting to (71), and assuming that in the limit of large t the $\Phi(s)$ does not depend on time, an asymptotic difference equation

$$\Phi_{as}(s+1) = \frac{(1/\rho) - s}{\kappa K(s) + \kappa - 1}\Phi_{as}(s) \tag{74}$$

is obtained. Solutions $f_{as}(v,t)$ in terms of generalised hypergeometric functions are derivable when $b(\eta)$ is a polynomial (Treat 1997 a). Here only the simplest case $b(\eta)$=$\delta\eta^{\delta-1}$, κ=(δ+1)/δ is considered for which

$$\Phi_{as}(s) = \frac{\Gamma(s + \delta/\rho)}{\Gamma(\delta/\rho)} \ . \tag{75}$$

Asymptotically $\Phi_{as}(s)$ is the Mellin transform of $\phi_{as}(\xi)$. By taking the inverse Mellin transform, and by returning to the original variable, it is found that the asymptotic solution is powered Gamma distribution

$$f_{as}(v,t) = \frac{\rho v^{\delta-1} e^{-v^{\rho} t} t^{\delta/\rho}}{\Gamma(\delta/\rho)} \quad . \tag{76}$$

This result does not depend on the initial distribution (Lensu 1993a). Thus the evolution seeks to homogenise the ice field.

5.2.4. Univariate lognormal solutions

For $\rho<0$ in $\alpha(v)= v^{\rho}$ asymptotic solutions of (67) are not found and the proper solutions have singularity character (McGrady and Ziff 1987). This case is unlikely for ridge spacings and is not considered further.

For the remaining case $\rho=0$ the asymptotics depends on the initial distribution. The transform (68), where c=1, gives from (67)

$$\frac{\partial NF(s)}{\partial t} = N\big(\kappa K(s) + \kappa - 1\big)F(s) \;\; , \;\; K(s) = -1 + \int_0^1 d\eta\, \eta^s b(\eta) \;\; . \tag{77}$$

The general solution is

$$F(s,t) = F_0(s) \exp\{\kappa K(s) t\}, \; N(t) = N_0 e^{(\kappa-1)t} \tag{78}$$

where $F_0(s)$ is the transform of the initial distribution, and $\exp\{\kappa K(s)t\}$ the transform of $f_b(v,t;1)$. Solutions f_b for simple $b(\eta)$ in terms of modified Bessel functions are obtained by inverting $F(s,t)$ (Lensu 1993a), and are also derivable by series methods (McGrady and Ziff 1987). For large t the solution is asymptotically lognormal for any $b(\eta)$

$$f_{as}(v,t) = \Lambda(v;\mu,\sigma) = \frac{1}{\ln\sigma\sqrt{2\pi}} \frac{1}{v} \exp\left\{ -\frac{1}{2} \left(\frac{\ln(v/\mu)}{\ln\sigma} \right)^2 \right\} \tag{79}$$

(Lensu 1993a, 1997). The parameters are geometric mean and geometric standard deviation

$$\mu = \exp\{\langle \ln v \rangle\} \tag{80}$$

$$\sigma = \exp\{(\langle \ln^2 v \rangle - \langle \ln v \rangle^2)^{1/2}\} \;\; . \tag{81}$$

The geometric mean equals median. The expectation and moment of order n are

$$\langle v \rangle = M_1(V) = \mu \exp\left\{\tfrac{1}{2}\ln^2\sigma\right\}, \quad M_n(V) = \mu^n \exp\left\{\tfrac{1}{2}n^2\ln^2\sigma\right\} \tag{82}$$

(Aitchison and Brown 1957). The geometric parameters are obtained as

$$\ln\mu = \ln\mu_0 + \kappa t L_1\,, \quad \ln^2\sigma = \ln^2\sigma_0 + \kappa t L_2\ . \tag{83}$$

Here μ_0 and σ_0 are the parameters of the initial distribution and

$$L_1 = \left.\frac{\partial K(s)}{\partial s}\right|_{s=0}, \; L_2 = \left.\frac{\partial^2 K(s)}{\partial s^2}\right|_{s=0} \tag{84}$$

where $K(s)$ is from (77).

5.2.5. Multivariate lognormal solutions and spacing correlations

The multivariate solutions of equation (62) for ρ=0 and κ=2 are approached by the transform

$$F_n(s_1, s_2, ..., s_n) = \int_0^1 dv_1 dv_2 .... dv_n \, v_1^{s_1} v_2^{s_2} ... v_n^{s_n} f_n(v_1, v_2, ..., v_n) \tag{85}$$

which produces from (62) with $\alpha(x)$=1, $v_{\max}$=1, and for any $b(\eta)$

$$\begin{aligned} &\frac{\partial}{\partial t} N F_n(s_1, s_2, ..., s_n) = N F_n(s_1, s_2, ..., s_n)(K(s_1) + K(s_n) - n + 2) \\ &+ N \sum_{j=1}^{n-1} F_{n-1}(s_1, ..., s_{i-1}, s_i + s_{i+1}, s_{i+2}, ..., s_n) E(s_i, s_{i+1}) \end{aligned} \tag{86}$$

where

$$E(s_i, s_j) = \int_0^1 d\eta \, \eta^{s_i} (1-\eta)^{s_j} b(\eta)\,. \tag{87}$$

(Lensu 1997). The solutions are built iteratively starting from univariate equation. The univariate solution (78) with F_0=1 is inserted into the bivariate form of (86), which is solved, and so on. The transform of the proper bivariate solution is

$$F(s_1,s_2)=F_0(s_1,s_2)\frac{E(s_1,s_2)\exp\{2K(s_1+s_2)t\}}{2K(s_1+s_2)-K(s_1)-K(s_2)+1}\quad . \tag{88}$$

The corresponding asymptotic solution is bivariate lognormal distribution

$$f_{as}(v_1,v_2)=\frac{1}{2\pi\ln^2\sigma\sqrt{1-\rho_1^{\,2}}}\frac{1}{v_1v_2}\exp\left\{-\frac{1}{2\ln^2\sigma\sqrt{1-\rho_1^{\,2}}}\left(\ln^2\frac{v_1}{\mu}-2\rho_1\ln\frac{v_1}{\mu}\ln\frac{v_2}{\mu}+\ln^2\frac{v_2}{\mu}\right)\right\} \tag{89}$$

(Lensu 1997). Here, ρ_1 is the correlation of the normally distributed random vector $(\ln V_1,\ln V_2)$. For the initial condition of unit volume

$$\rho_1=\frac{\varepsilon+2L_2(t-1)}{2L_2t}\quad ,\qquad \varepsilon=\int_0^1 d\eta\,\ln(\eta)\ln(1-\eta)b(\eta) \tag{90}$$

in terms of (84). The conditional distribution is lognormal

$$f_{as}(v_2|V_1=v_1)=\Lambda\left(v_2;v_1^{\rho_1}\mu^{1-\rho_1},\sigma^{\sqrt{1-\rho_1^2}}\right)\qquad . \tag{91}$$

The correlation ρ_n for $(\ln V_1,\ln V_{n+1})$, pertaining to pairs of spacings separated by *n-1* intermediate spacings, is

$$\rho_n=1+\frac{\varepsilon}{2L_2t}-\frac{1}{t}\sum_{j=1}^{n}\frac{1}{j}\quad . \tag{92}$$

These determine the asymptotic *n*-variate lognormal solutions of (62). The ρ_n approach unity with increasing *t*. The asymptotical correlation of the lognormally distributed random vector (V_1,V_{n+1}), on the other hand, has the limit value

$$\rho(V_1,V_{n+1})\xrightarrow{t\to\infty}\frac{E(1,1)}{2+2K(2)}\prod_{j=3}^{n+1}\frac{j-2}{j+2K(2)}\quad . \tag{93}$$

For the $b(\eta)=1$ (random volume division) and $b(\eta)=\delta(\eta-½)$ (volume halving) the first limit values of $\rho(V_1,V_2)$, $\rho(V_1,V_3)$,.. are 1/4, 3/20, 9/80, 81/880,.. and 1/2, 1/3, 4/15, 8/35,.. respectively.

5.3. Exponentiality and lognormality

5.3.1. Exponentiality and lognormality of spacing distributions

The motivation to use spacing cross-section volume was the fact that volume conservation simplifies the equation. The spacing distribution $f(x)$ is then obtained by $f(x|v)$ as in (61). However, functional dependencies $v=v(x)$ are applied in the present section. The objective is to explain the main features of observed spacing distributions. The two usual spacing distribution models are negative exponential and lognormal distributions, while other models have rarely been applied.

The asymptotic solutions for $\alpha(v)=v^{\rho}$, $\rho>0$, and $b(\eta)=\delta\eta^{\delta-1}$ were found to be powered gamma distributions. If $\delta=1$ they are proportional to $\exp\{-v^{\rho}t\}$ and exponential distribution is found for $\rho=\delta=1$. However, whenever $\alpha(v)=v^{\rho}$ the asymptotical tail distribution has approximately ρ-powered negative exponential slope (Redner 1990).

Asymptotic lognormality of $f(v)$ was found for $\rho=0$ whenever the transition probability is expressed in a scale similar form by $b(\eta)$, (66). A family of powered gamma distributions mediates between the lognormal and exponential distributions. However, the limit distribution of the gamma family does not exist when ρ goes to zero. Also, the parameters of proper solutions equal those of asymptotic solutions for $\rho=0$ but not for $\rho>0$. The limit property and a ρ-continuum of solutions is found for the proper solutions only (Lensu 1993a).

If $f(x|v)$ is constructed with overlapping triangular cross-sectional models the result is complicated if the keel size variation is taken into account. The simplest model assumes that all triangular keels have the same width w, depth d, and volume $\frac{1}{2}dw$, neglects the sail volume, and assumes constant level ice thickness H. Then, for short spacings $x<w$, $v=xd-\frac{1}{2}dx^2/w$, and for longer spacings $x\geq w$, $v=\frac{1}{2}dw+H(x-w)$. For very short spacings, $v=xd$ applies approximately. The general features of this model can be assumed to be present in more detailed approaches. For very short spacings the keels join into a rubble bed and v increases linearly with x. On the other hand, for longer spacings with no keel contact the v increases likewise linearly with x, only much slower. An intermediate sublinear range joins the two linear ranges.

Thus, changing the point of view to spacing distribution, ρ-powered exponential slope is expected for longer spacings whenever $\alpha(x)\sim x^{\rho}$ or $\alpha(v)\sim v^{\rho}$, $\rho>0$. The solution $f(x)$ is asymptotically negative exponential if $\alpha(x)\sim x$ and $b(\eta)=1/(1-c)$, where c is constant. The spacing consumption cx is then proportional to the spacing. This may be acceptable for shorter spacings with keel contact, but does

not apply to longer spacings. Thus the negative exponentiality is likely to be at most approximate for spacings, or found for longer spacings only.

On the other hand, the lognormal asymptotics applies for any $b(\eta)$. Spacing distribution is asymptotically lognormal if $\alpha(x)\sim 1$ and the transitions are scale similar. The same applies if $f(v)$ is lognormal and $v\sim x^{\lambda}$. Also, the distribution $f(y_n)$ of n-concatenation length follows an equation which is similar to the spacing equation (Section 4.2.7). If $\alpha(x)\sim 1$, then also $\alpha(y_n)\sim 1$. The concatenation shortening in transitions can be assumed to be proportional to y_n/n and be thus scale similar. If spacing evolution is a lognormal process, then lognormality is expected to hold even better for n-concatenation length.

The cases $\rho=0$ and $\rho=1$ have a special status in the spacing evolution. If $\alpha(x)\sim 1$ or $\alpha(x)\sim x$ for spacing rates, then $\alpha(y_n)\sim n$ and $\alpha(y_n)\sim y_n$ for the respective concatenation rates. Any linear combination of these rates satisfies $\alpha(y_{n+m})=\alpha(y_n,)+\alpha(y_m)$. This is a very natural requirement which the other cases $\rho>0$ do not satisfy. It is thus a natural starting assumption that $\alpha(x)\sim 1+ax$. The evolution can be then considered as a superposition of two processes, exponential and lognormal. The parameter a governs the relative intensity of the processes. A negative exponential tail is found for long spacings which have $1<<ax$. On the other hand, in the regime $1>>ax$ the lognormal features dominate. Therefore the principal hypothesis will be that

$$\alpha(x)\sim 1+ax\ . \tag{94}$$

This hypothesis is related to the ridge sail number evolution in Section 5.5 below.

5.3.2. Lognormality and the Central Limit Theorem

Asymptotical lognormality is likely even without the assumption of scale similarity for transition probabilities. This can be argumented with the Central Limit Theorem (CLT) which, since Kolmogorov (1941), has been the usual qualitative explanation of lognormality for fragmentation processes. The CLT argument is now related to the present theory. The spacing volume after n transition events is a random variable

$$V_n= V_0 b_1 b_2 \ldots b_n \tag{95}$$

where n is the event number. The b_i are random variables for volume reduction, defined on [0,1]. They are identical if the transitions are scale similar. As $\ln V_n$ is a sum of random variables, it is according to CLT approximately normally

distributed for large n if certain quite general conditions are fulfilled. Then V_n is approximately lognormally distributed. The conditions do not require that the b_i are identical or independent. For identical b_i with geometric mean μ_b and geometric standard deviation σ_b the approximating lognormal distribution for V_0=1 is

$$f_n(v) = \Lambda(v; \mu_b^n, \sigma_b^{\sqrt{n}}) \,. \tag{96}$$

Here n has deterministic value, that is, it is not distributed. This, however, is not the case for solution (79). A general proper solution of (67) for ρ=0 is obtained with the event number approach. Expanding the transform (78) and inverting the terms in the series the solution is

$$f(v,t) = f_0(v) * \sum_{n=0}^{\infty} \left(\overset{n}{\underset{k=0}{*}} b(v) \right) \frac{e^{-\kappa t}(\kappa t)^n}{n!} = \sum_{n=0}^{\infty} \frac{e^{-\kappa t}(\kappa t)^n}{n!} f(v \mid n) = \sum_{n=0}^{\infty} k(n,t) f(v \mid n) \tag{97}$$

(Lensu 1998). Here $k(n,t)$ is the event number distribution, and $f(v|n)$ the volume distribution for cross-sections that have experienced n transitions (Section 3.5.3). The star operation is an n-fold iteration of the convolution (69). Here $k(n,t)$ is a Poisson distribution, which is asymptotically normal. If the transitions are divisions into equal halves, then n is proportional to ln$v$. Substituting this to the normal $k(n,t)$ it follows that $f(v,t)$ is asymptotically lognormal.

Thus the asymptotic normality of the event number distribution $k(n,t)$ is decisive in the lognormality of (79). This can be put into CLT form by considering forcing events which may or may not result into a transition. They are described by random variables R_i with value 1 if the forcing results into a transition and 0 otherwise. The total number of forcing events N is deterministic. The product

$$V_N = V_0 b_1^{R_1} b_2^{R_2} \ldots b_N^{R_N} \tag{98}$$

is asymptotically lognormal if the conditions of CLT are fulfilled (Epstein 1947). In the case the b_i are not random variables but deterministic and equal, b_i=b, then

$$V_N = V_0 b^{R_1 + R_2 \ldots + R_N} \,. \tag{99}$$

If the R_i satisfy the conditions of CLT, then their sum, which is the event number, has approximately normal distribution, and V_N has lognormal distribution.

To conclude, there are two limit cases of CLT. In the first the number of transition events is deterministic, and the transition probability b a random variable. In the other the number of transition events is a random variable, and the transition deterministic. The lognormality (79) can be seen as a continuous rate process version of the CLT argument. On the other hand, (98) can be understood as a process with discrete time. The expectation of R_i is the relative frequency of transitions among all forcing events and is denoted here by α. If α is small, and there is one forcing per unit time, then the probability to survive until time t is $(1-\alpha)^t = \exp\{t\ln(1-\alpha)\} \approx \exp\{-\alpha t\}$ which is the survival probability for the continuous rate process. Thus the process with discrete time approximates the continuous time process. Thus it is probable that asymptotic lognormality is found whenever the transition probabilities $B(v' \to v)$ satisfy the same very general CLT conditions as the b_i in (98). Then $\alpha(x) \sim 1$ is sufficient for the lognormality of $f(x)$ and the details of parent spacing consumption are not relevant.

5.4. Ridge sail number distribution

5.4.1. Solutions of ridge sail number equation

The ridge sail number distribution $k(n_j,t)$ is the probability that a segment of length L_j contains n_j ridge sails. Its evolution is described by equation (63) in which only the rate $\alpha(n_j,t)$ need be specified. The general solution was constructed in Lensu (1998a) and was found to have a manageable form in the case

$$\alpha(n_j,t) = \beta(t)\frac{n_j + aL_i}{bn_j + c} \tag{100}$$

where a, b and c are nonnegative real numbers. By a variable change $\beta(t)=1$ is achieved. The rate $\alpha(n_j)$ is increasing, decreasing or constant depending on whether $c-aL_jb$ is positive, negative or zero; in the third case the Poisson distribution is obtained. For another special case

$$\alpha(n_j) = n_j + aL_j,\ a>0 \tag{101}$$

the solution reduces to a negative binomial distribution

$$k(n_j,t;aL_j) = \binom{aL_j + n_j - 1}{n_j}\left(e^{-t}\right)^a (1-e^{-t})^{n_j} \tag{102}$$

which includes the geometric distribution $k(n_j,t;1)=e^{-t}(1-e^{-t})^{n_j}$. Properties of these distributions are found Johnson and Kotz (1969). The general solution for initial distribution $k_0(m_j)$ is

$$k(n_j,t)=\sum_{m_j=0}^{n_j}k_0(m_j)k(n_j-m_j,t;a_jL_j+m_j) \tag{103}$$

and finally the intensity factor $\beta(t)$ can be brought back.

5.4.2. Finite discrete model for ridge sail number scale system

The solutions $k(n_j)$ of the preceding section are applicable to a large collection of segments. The scale system $k(n_j|n_i)$ was defined as the probability that n_j sails are found in the L_j-segment if there are n_i sails in the longer L_i-segment. If n_i or L_i/L_j is small, the solutions $k(n_j)$ may be bad approximations of $k(n_j|n_i)$ and the following finite model is more appropriate.

An L_i-segment is considered. A sub-L_j-segment is chosen and divided into segments L_k and $L_{k'}$. A sail is assumed to appear into the L_i-segment. It will appear to the L_j-segments with a probability $P(L_j)$, and to the L_k- and $L_{k'}$-segments with probabilities $P(L_k)$ and $P(L_{k'})$. Then it must be $P(L_j)=P(L_k+L_{k'})=P(L_k)+P(L_{k'})$. If $P(L_j)$ depends on n_j and L_j this condition holds if $P(L_j)$ is proportional to n_j+aL_j. This corresponds to the assumption (101) for the sail number equation. Due to the additivity property $P(L_j)=(n_j+aL_j)/(n_i+aL_i)$ and the following recurrence relation

$$k(n_j\,|\,n_i)=k(n_j-1\,|\,n_i-1)\frac{n_j-1+aL_j}{n_i-1+aL_i}+k(n_j\,|\,n_i-1)\left(1-\frac{n_j-1+aL_j}{n_i-1+aL_i}\right)\qquad n_j=0,1,...,n_i \tag{104}$$

ensues. The probabilities $k(n_j|n_i)$ are constructed by iterating (104), starting from empty segments. The result is a negative hypergeometric distribution

$$k(n_j\,|\,n_i)=\frac{\binom{aL_j+n_j-1}{n_j}\binom{aL_i-aL_j-1+n_i-n_j}{n_i-n_j}}{\binom{aL_i+n_i-1}{n_i}} \tag{105}$$

Expectation is $\langle n_j \rangle = n_i L_j / L_i = d_i L_j$ and other properties can be found in Johnson and Kotz (1969). The system is now related to the solutions (102).

i. As $a \to \infty$, $k(n_j|n_i)$ approaches a binomial distribution.
ii. If in addition $L_i/L_j >> 1$, $k(n_j|n_i)$ is approximated by a Poisson distribution. It is defined for all n_j and does not depend on the L_i but only on $\langle n_j \rangle$.
iii. If further $\langle n_j \rangle$ is large, a normal distribution approximates the Poisson distribution.
iv. If a is finite and $L_i/L_j >> 1$, $k(n_j|n_i)$ is approximated by the negative binomial distribution

$$k(n_j) = \binom{aL_j + n_j - 1}{n_j} p^{aL_j} (1-p)^{n_j}, \quad p = \frac{aL_j}{aL_j + \langle n_j \rangle} \tag{106}$$

(Johnson and Kotz 1969). Here the time parameter of (102) is expressed in terms of aL_j and $\langle n_j \rangle$.
v. Geometric distribution is obtained from (106) when $aL_j = 1$,

$$k(n_j) = p(1-p)^{n_j}, \quad p = \frac{1}{1 + \langle n_j \rangle} \ . \tag{107}$$

vi. For small a (106) has approximately power law character, $k(n_j) \sim aL_j / n_j$.
vii. If $\langle n_j \rangle$ is large, the continuous approximation of (106) is Gamma distribution

$$f(n_j) = \frac{1}{\Gamma(\alpha)} \beta^{\alpha} n_j^{\alpha - 1} e^{-\beta n_j}, \ \alpha = aL_j, \ \beta = \frac{aL_j}{\langle n_j \rangle} \ . \tag{108}$$

(Ochi 1990). If L_j is decreased, L_i/L_j increases but $\langle n_j \rangle$ decreases. Thus L_i should be very long or ridge sail density very high for $L_i/L_j >> 1$, $\langle n_j \rangle >> 1$ to hold.

5.5. The evolution hypothesis: Ridging as a combined Poisson and clustering process

Chapter 4 defined various ways to describe the sail arrangement evolution. Their interrelations can be precisely formulated if the evolution is known in detail. On the other hand, if this is not the case, a better understanding of the evolution process can be obtained by studying the observed relations between different

descriptions. The most important relationship is between sail spacing and sail number distributions.

A sail number rate $\alpha(n_j,t) \sim n_j + aL_j$ is considered. Then for the averaged rate $\langle \alpha(n_j,t) \rangle \sim \langle n_j \rangle + aL_j = (d+a)L_j$, where d is ridge sail density. The parameter a is proportional to the average Poisson rate, or the rate of random appearing of sails per unit length. On the other hand, density d is proportional to what is called here average clustering rate. If $1 >> d/a$ or $1 << d/a$, the Poisson or clustering process dominates respectively. If the process starts from zero density the Poisson process dominates first. As the density increases the clustering process gradually takes over. The combined Poisson and clustering process is described by the negative binomial distribution (102,106). If d/a remains small, Poisson distribution approximation applies, and if d/a is large from the outset, the distribution has approximately power law character $k(n_j) \sim 1/n_j$.

The relation between sail spacing and sail number rates is approached by considering first a point process along a transect. The transect is divided into segments L_j. Objects are deposited on the transect. This process can be described either in terms of object spacings x or in terms object numbers n_j on segments. The spacing process rate is $\alpha(x)$ and the segment process rate is $\alpha(n_j)$. An object deposition is a transition for some spacing, and for some segment. For a Poisson process $\alpha(x) \sim x$ and $\alpha(n_j) \sim L_j$ and objects are deposited to a random spacing location. A Poisson distribution $k(n_j)$ and a negative exponential distribution $f(x)$ are generated. The case $\alpha(x) \sim 1$ requires more detailed considerations. An L_j-segment with n_j objects contains n_j-1 complete spacings. If $\alpha(x) \sim 1$ the contribution to $\alpha(n_j)$ from the complete spacings is proportional to n_j-1. Some contribution comes also from the remaining segment outside the complete spacings. On the other hand, each empty segment is contained to some spacing so that $1 > \alpha(n_j=0) > 0$. To compensate this in the total balance of events, the rates $\alpha(n_j>0)$ have on the average a proportionality smaller than n_j. The rate $\alpha(x) \sim 1+ax$ corresponds then for $n_j>0$ to $\alpha(n_j) \sim n_j + aL_j + c_j$ where the term $-1 < c_j < 0$ goes to zero with increasing $\langle n_j \rangle$.

For ridge sail arrangement this result is indicative as it is not known in detail how the differential movements affect the transitions. A spacing rate $\alpha(x) \sim 1+ax$ is assumed. The segment rate has components due to buildup initialisations and due to ridge sail influx events. The initialisation component is proportional to $n_j + aL_j + c_j$. An influx event may occur due to an ongoing buildup in the segment. The corresponding rate component can be assumed to be proportional to $n_j + aL_j + c_j$. However, an influx event may also occur because a ridge immediately adjacent to the segment is building up. If the spacing correlations are weak the rate of such events does not depend on segment variables. Thus it adds a constant term to the

rate. It is assumed that $\langle n_j \rangle$ is large so that $c_j = 0$. The rate $\alpha(x) \sim 1+ax$ corresponds then to the segment process rate

$$\alpha(n_j) \sim n_j + aL_j + c \tag{109}$$

where $c>0$ is a small additional constant. The results are collected to the following hypothesis on the evolution of ridge sail arrangement

- Sail arrangement evolution is a combined Poisson and clustering process
- The sail spacing transition rate has proportionality $\alpha(x) \sim 1+ax$
- The corresponding sail number transition rate has proportionality $\alpha(n_j) \sim n_j + aL_j + c$

The following results are direct consequences of the evolution hypothesis

- If $1>>d/a$ or $1<<d/a$, the Poisson or clustering process dominates and the spacing distribution has an asymptotically negative exponential tail or is asymptotically lognormal respectively.
- In the general case $\alpha(x) \sim 1+ax$ the asymptotic distribution is not known but lognormal features manifest for short spacings and exponential features for long spacings.
- If the spacing distribution has lognormal features, these are enhanced in the distributions for spacing concatenations
- If the spacing distribution has lognormal features, correlations between adjacent spacings are expected to be found and follow a certain pattern.
- The sail number distributions follow the model of Section 5.4.2 where aL_j is replaced by aL_j+c.

These expected results are compared with observations in the next chapter. If they are found this is a strong argument for the validity of the evolution hypothesis. In that case the assumed rates can be used to parameterise evolution equations for Lagrangian regions and corresponding conservation equations for Eulerian continuum fields. What remains in the parameterisation after that is the specification of the intensity factor $\beta(t)$ so that absolute rates $\alpha(x)=\beta(t)(1+ax)$ and $\alpha(n_j)=\beta(t)(n_j+aL_j+c)$ instead of mere proportionalities are obtained. In Lagrangian regions the intensity factor is related to ice area decrease and in the case of Eulerian fields to strain rate and concentration (Chapter 7).

6. COMPARISON WITH OBSERVATIONS

6.1. The data sets

Most ice cover surface profile data is from laser profilometer surveys. A laser profilometer is a pencil beam distance meter with repetition rate up to 2000 Hz. A typical survey consists of vertical distance measurements along linear tracks pursued by a helicopter or an aircraft. To obtain the surface profile from the measured data the vertical platform movement is removed from the distance record. Ridge sails and other features are identified from the profile manually or using some selection procedure. The standard ridge sail selection procedure involves cutoff level and the Rayleigh criterion. Local maxima below the cutoff level are not included to the sail data. The Rayleigh criterion states that the shallower of two adjacent maxima is discarded if it does not have at least twice the elevation of the trough between the maxima. The final sail data consists of locations and heights of pointlike features, the sail cross-section maxima. From this data the statistics of sail heights, sail spacings, and sail spacing numbers can then be calculated.

In the Baltic the laser surveys started by a shipborne installation in 1977-1979 (Leppäranta 1981a, Leppäranta and Palosuo 1981). Table 1 summarises the aerial profilometer surveys to the Bay of Bothnia and the surveyed areas are shown in Figure 22. The survey acronym gives the respective year and the surveys are made in March except B93 in February. On the Baltic pack ice in general see Leppäranta (1981b), and on Baltic ridging characteristics Kankaanpää (1997) and Climatological Ice Atlas (1982). The ice season in the Bay of Botnia is from 3 to 6 months and the maximum thickness of thermally grown ice is 1.2 m. Typical ridges have sail heights from 1 to 3 m and keel depths from 5 to 15 m. The ice season before the B88 survey was mild and the basin contained several regimes with different ice types. The ridge fields had variable ages. The level ice thickness varied from 10 to 60 cm (Lewis et al.1993). The ice season of survey B93 was also mild. In the target area the level ice types were created from multiply layered small floes. The thickness of this ice type was 1.3 m and the ridge sails were formed from its consolidated upper layer (Lensu 1993b, 1994a). The ice season of B94 survey was average. The main ice pack had 0.65 m level ice thickness and was characterised by long regular ridges (Lensu 1994b, 1995a). The ice season of B97 was mild and characterised by frequent storms and the target ice cover contained ridge fields with different ages. The ridge densities were exceptionally high. The level ice thickness was 0.7 m but layered ice type with larger thickness was found (Lensu 1998b, Haapala and Leppäranta 1997). Table 1 provides a good coverage of different ridging conditions and variations due to the severity of ice season and basin geography.

The data that has been available for the analyses of the present work consist of B94 and B97 data of Table 1, and in addition of seven surveys to Kara and Pechora seas (Lensu 1999b, Table 2, Figure 22). The B88 and B93 results are from Lewis et al. (1993) and Lensu (1993b) respectively. The Kara and Pechora Sea data is from April-May 1998 when the ice conditions were more difficult than average. The Western Kara Sea areas start to freeze in mid October and ice free waters are found in September only on the average. The average level ice thickness in April is 1 m and maximum 1.8 m (Lensu et al. 1996). This corresponded well to shipborne observations.

Table 1. Airborne laser profilometer surveys to the Bay of Bothnia. The 0.5 m cutoff data for B88 is calculated using negative exponential sail height distribution.

Survey	Length km	Cutoff height m	Average ridge height m	Ridge density 1/km	Reference for ridge statistical results
B88	662	0.4 (0.5)	0.58 (0.68)	6.4 (3.7)	Lewis et al.(1993)
B93	331	0.5	0.75	4.9	Lensu (1993b)
B94	362	0.5	0.70	3.2	Lensu (1995a)
B97	270	0.5	0.76	18.2	Lensu (1998b,1999a)

Table 2. Airborne laser profilometer surveys to Kara Sea (Lensu 1999b). The cutoff height is 0.5 m.

Survey	Length km	Ridge height m	Ridge density 1/km
K1	123	0.91	12.0
K2	110	0.88	11.8
K3	63	0.71	6.7
K4	113	0.89	28.2
K5	112	0.87	6.6
K6	112	1.01	33.7
K7	73	0.85	6.3

The surveys B93, B94, b97 and K1-K7 have all 100 Hz sampling rate, 0.5 m cutoff, and similar analysis method. In the removal of the vertical platform movement an iterative spline smoothing procedure was used. In this procedure the reference level iteratively approaches the average elevation of the undeformed ice surface, or of the surface of the snow above it. It is based on the fact that in the measured data the ice surface appears as one-sided noise superposed on the

platform movement which is a smooth curve and has a typical wavelength much longer than typical ridge width. Splines fitted to the data in a way that takes into account the wavelength difference can then be used to seek out the platform movement.

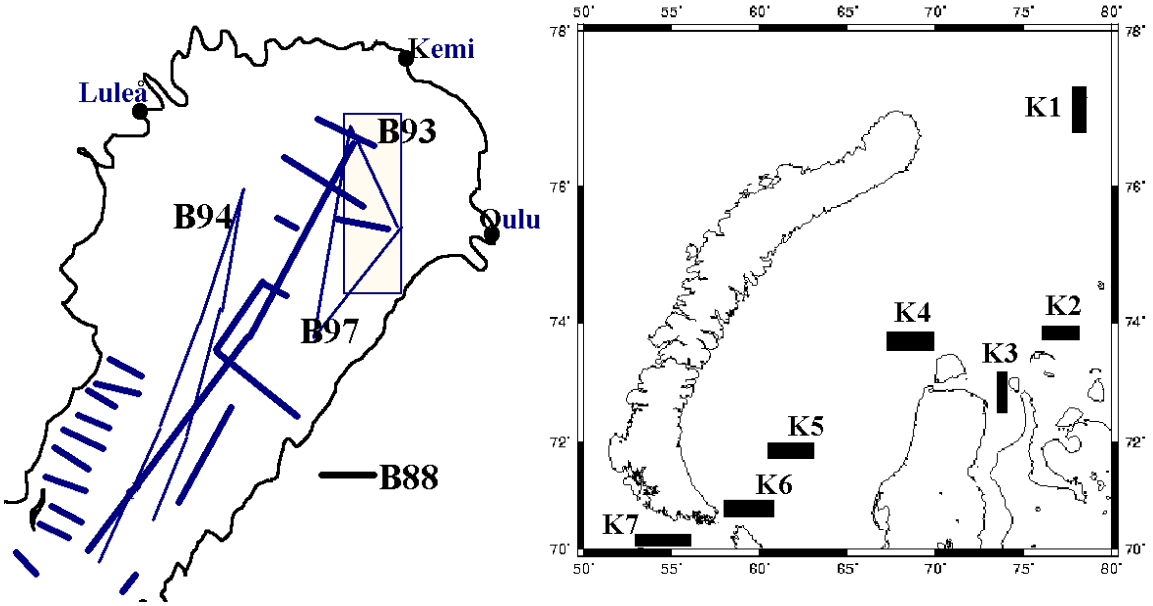

Figure 22. The airborne laser profilometer surveys made to the Bay of Bothnia (Table 1) and to the Kara Sea (Table 2).

For B88, Lewis et al. (1993) used 0.4 m cutoff after removing the vertical movement by the usual low pass filtering procedure of Hibler (1972). The reference level is set by local minima, usually at least 1 km apart. Thus the ridge heights in B88 data are expected to be higher than what would have been obtained with the spline smoothing procedure. Data with different cutoff can be compared using the negative exponential model (143a) for the distribution of cross-sectional ridge height h_{cs}. This model has been well confirmed for laser profilometer data (Section 7.3.1). A change Δh_0 in cutoff h_0 results to the same change in average cross-sectional height, $\langle h_{cs}' \rangle = \langle h_{cs} \rangle + \Delta h_0$, and the ridge density is changed from d to

$$d' = d \exp\left\{ - \Delta h_0 / \left(\langle h_{cs} \rangle - h_0 \right) \right\} . \qquad (110)$$

The 0.5 m cutoff parameters, calculated with the exponential model, are included for B88 data in Table 1.

The average cross-sectional height in Table 1 varies little, within 0.08 m. When grouping their data with respect to five regions, Lewis et al.(1993) found that the

variation between the regions was within 0.07 m. The snow cover thickness on level ice was 0.1-0.3 m for B88 and B94 and almost zero for B93 and B97. The snow is expected to reduce the average height. However, this effect is expected to be smaller than the snow thickness as a snow cover with constant thickness on level ice does not change average ridge height if the ridge tops are bare. On the other hand, the sail densities change then according to (110) where Δh_0 is level ice snow thickness. These results follow from the negative exponential sail height model. In general, all height variation among all profile sections of the four surveys, typically 10-30 km long, is within 0.25 m. Thus, in the first estimate, the average cross-sectional ridge height in the Bay of Bothnia can be assumed to be a constant, about 0.75 m above level ice freeboard. On the other hand, in the Kara Sea the geographical variation in cross-sectional height is significant and the variation for the 10-30 km long profile sections reached 0.6 m. Ridge density shows large regional variation both in the Bay of Bothnia and in the Kara Sea. In the Bay of Bothnia the interannual variation is also large.

6.2. Effect of ridge height cutoff in the statistics

6.2.1. Effect of cutoff in ridge density

Ridge density is sensitive to ridge height cutoff changes. In data set comparisons (110) works well. However, the use of (110) with $\Delta h_0 = -h_0$ to extrapolate the observed ridge sail density $d(h_{cs} \geq h_0)$ down to the true density $d(h_{cs} \geq 0)$ is problematic. This extrapolation, on the other hand, is needed to ensure the intercomparability of ridge densities as the fraction $d(h_{cs} \geq h_0)/d(h_{cs} \geq 0)$ of ridges above the cutoff depends on $\langle h_{cs} \rangle$. If the extrapolation is done by (110) values of $d(h_{cs} \geq 0)$ ranging from 36/km to 124/km are found for Table 1 and values from 25/km to 102/km for Table 2. Only 14% of the ridges are observed for $\langle h_{cs} \rangle$=0.75 m and 37 % for $\langle h_{cs} \rangle$=1.0 m. These values certainly appear too high and thus (110) apparently deviates from exponential as Δh_0 comes close to $-h_0$. It may be assumed that the average cross-sectional height scales with block thickness as $h_{cs} \sim H^{\nu}$. The exponent is not well known but ν =0.5 is the usual assumption (Section 7.3.3). The height below which the deviation from the exponential model is significant scales then likewise with $\sim H^{\nu}$. An approximate extrapolation method basing on this will be given in Section 7.3 where it is estimated that if h_0=0.5 m then 34% of the ridges are recorded for $\langle h_{cs} \rangle$=0.75 m and 91% for $\langle h_{cs} \rangle$=1.0 m. This is done in the context where the volume of ridged ice is estimated. However, in the comparison of the parameters of observed and theoretically predicted distributions more accurate estimate of $d(h_{cs} \geq 0)$ would be required. Therefore the parameter comparisons are in many cases only indicative.

However, it holds generally that for constant $d(h_{cs}\geq 0)$ and h_0 the observed ridge density $d(h_{cs}\geq h_0)$ shows positive correlation with $\langle h_{cs}\rangle$. This probably contributes to the correlations found when comparing regions with different thickness characteristics (Hibler et al. 1972, Wadhams 1981, Lewis et al. 1993, Granberg and Leppäranta 1999). On the other hand, within regions with more uniform ice characteristics no significant correlations are usually found (Tucker et al.1979, Weeks et al. 1989, Lytle and Ackley 1991).

6.2.2. Correlations between sail height and sail spacing

The evolution hypothesis is that the sail spacing and sail number distributions are generated by rates that have the proportionality $\alpha(x)\sim 1+ax$ and $\alpha(n_j)\sim n_j+aL_j+c$ respectively. As a large fraction of ridges is below the cutoff, the spacings determined from cutoff data $h_{cs}\geq h_0$ are concatenations of spacings with $h_{cs}\geq 0$. On the average the number of spacings $h_{cs}\geq 0$ in the concatenation is $d(h_{cs}\geq 0)/d(h_{cs}\geq h_0)$. Sail numbers in the cutoff data are on the average lower by the factor $d(h_{cs}\geq h_0)/d(h_{cs}\geq 0)$. It must be discussed how the cutoff effects the statistics. This depends on spatial correlations. If small and large ridge sails tend to arrange into respective groups the problem is more difficult than in case of independence between ridge sail height and sail arrangement.

Figure 23 shows spacing-height correlation for B94 and B97 as a function of separation. The separation is 1 if the spacing ends to the sail, and is n if there are n-1 sails between the spacing and the sail. The correlations are very small. Similar plots for K1-K7 have maximum value 0.15. Lewis et al.(1993) report the same result for B88 data. In Lensu (1999a) correlations between ridge sail numbers and segment sail height were calculated for B97 and for segments from 12.5 m to 1600 m. The correlations increased from 0.05 to 0.20 having thus more regional than local origin. For the profiles of the same data set, 4-35 km in length, the correlation between ridge density and sail height was 0.09.

On the other hand a weak height correlation is found for nearby sail pairs. In Figure 23 the separation is n if there is n-1 sails between the two sails. These correlations are due to short spacings. For adjacent sails $x<2.5$ m the height correlation was 0.50 and 0.42 for B94 and B97 respectively. This correlation decreases with increasing x until value 0.03 is found between adjacent sails $50<x<100$ m and $20<x<50$ m for B94 and B97 respectively. As a conclusion, closely arranged sails may have height correlation but spacing and ridge sail number are independent on the height properties.

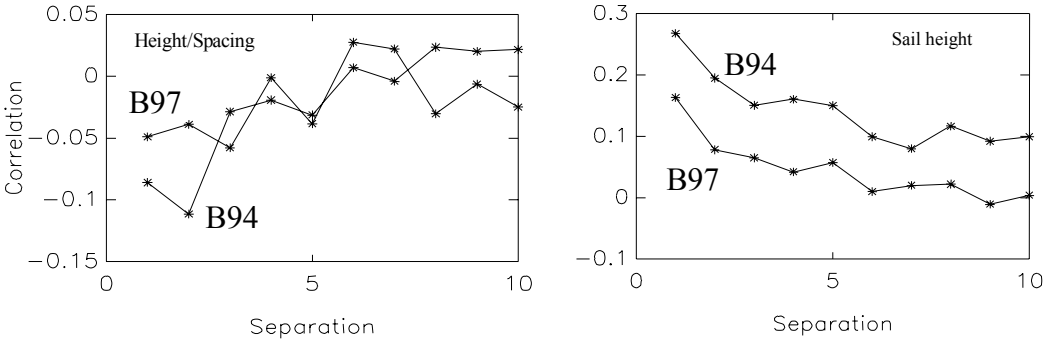

Figure 23. Correlations between spacing length and sail height, and correlations between sails heights (B94 and B97 data). Separation is n if there is n-1 sails between the correlated features.

6.2.3. Effect of cutoff in sail spacing and sail number statistics

In the absence of correlations between sail height and sail spacing it may be assumed that sail heights occur randomly along a profile. Cutoff is increased from h_0 to $h_0'=h_0+\Delta h_0$ and the sail density decreases by $p=d'/d$. Proceeding from a sail exceeding h_0', or h_0'-sail, the probability that the next h_0-sail is also a h_0'-sail is p. The probability that a h_0'-spacing contains n h_0-spacings is thus $p(1\text{-}p)^{n-1}$. Such h_0'-spacing is an n-concatenation of h_0-spacings (Section 2.5.4). The distribution of n-concatenation lengths is denoted here f_n and the h_0'-spacing distribution is

$$f'(x) = p\sum_{n=1}^{\infty}(1-p)^{n-1} f_n(x) \ . \qquad (111)$$

This cannot be presently applied as the f_n are yet unknown. However, to the process $\alpha(x)\sim 1+ax$ a straightforward argument applies. The component $\alpha(x)\sim x$ is the rate of random placement of sails. A random selection of a fraction p of sails is equivalent to a random placement of the same fraction. Thus $\alpha(x)\sim x$ is found for both cutoff values. For the component $\alpha(x)\sim 1$ it holds that the number n of component h_0-spacings is distributed independently on the h_0'-spacing. Thus $\alpha(x)\sim 1$ holds for both cutoff values. Combining the arguments, the spacing distributions for $\alpha(x)\sim 1+ax$ are invariant in cutoff changes. However, the statistical parameters change in a way that is not precisely known until (111) is used. This complicates the comparison of observed and predicted distribution as $p=d(h_{cs}\geq h_0)/d(h_{cs}\geq 0)$ is not well known either.

This result is supported by observations. Cutoff equalling three times profile elevation standard deviation, and thus proportional to the degree of deformation, was applied in Lensu (1993b) to B93 data. The cutoff range was 0.16 to 0.58 m and the overall ridge density increased by a factor 1.6 from 0.5 m universal cutoff data. The relationship $F_1(x)=F_2(1.6x)$ was found between the cumulative distributions, except for the last 10 per cent of the long spacings. Here F_2 is the 0.5 m cutoff distribution. Thus the two distributions were scaled copies of each other for this range.

It must similarly be shown that the cutoff does not effect the assumption $\alpha(n_j)\sim n_j+aL_j+c$. A segment with m sails is considered. If a fraction p of sails is selected randomly, the probability that n from the m sails are selected has binomial distribution. Assuming that the overall sail number distribution belongs to the negative binomial family (102,106) with parameters a and q, the observed distribution is

$$k_{obs}(n)=\sum_{n=m}^{\infty}\binom{m}{n}p^n(1-p)^{m-n}\binom{a+m-1}{m}q^a(1-q)^n=\binom{a+n-1}{n}r^a(1-r)^n,\ r=\frac{q}{p+q-pq} \quad (112)$$

or negative binomial with parameters a and r. Thus the negative binomial distribution is invariant in cutoff changes. The parameter a, or the relative rate of Poisson process, is unchanged and only the statistical parameters like mean and variance change. The distribution models can thus be extended below cutoff if the sail density extrapolation can be done.

6.3. Ridge sail spacing distributions

6.3.1. The evolution hypothesis

In Chapter 5 asymptotic solutions $f_{as}(v)$ for spacing volume equation (60,67) were obtained. The essential properties of the solutions were argumented to hold for spacing distribution $f(x)$ as well. An additivity argument suggested that the spacing transition rate is likely to have proportionality $\alpha(x)\sim 1+ax$. The asymptotic distribution for $\alpha(x)\sim 1+ax$ is not known. If $a=0$, asymptotically lognormal distributions are obtained. It was argumented that this result is not dependent on the formulation of the transition probability. If a is nonzero, the distribution tail is asymptotically negative exponential. If a is small, the lognormality is expected to become enhanced for spacing concatenations. For the lognormal process correlations between adjacent spacings were also derived.

6.3.2. Review of observed spacing distributions

Both negative exponential and lognormal distributions have been applied to sail and keel spacing data. Negative exponential was first proposed by Hibler et al. (1972). Mock et al.(1972) found good agreement for longer spacings quantified from aerial photographs but short spacings were too numerous. Applicability to short spacings was also suspected by Lowry and Wadhams (1979). Good fit for keel spacings was found in Wadhams (1980), for the mid range of the keel spacings in Wadhams and Horne (1980), for sail spacings exceeding 100 m in Wadhams and Horne (1980) and Wadhams (1980), and for sail spacings between 100 and 250 in Wadhams (1981). Leppäranta (1981 a) analysed shipborne profilometer data and for 7 out of 11 profiles negative exponential was accepted with 5 % significance level in chisquare test.

However, Wadhams and Davy (1986) found that the lognormal distribution was generally a better model for keel spacings. The fit was very good for shifted spacing x-x_0 where x_0 varied from 3 m to 15 m for different submarine cruises. The shift x_0 was adduced to the measurement specific effect of keel shadowing (Lowry and Wadhams 1979). This effect was also reproduced by simulated sonar measurements. Key and McLaren (1989) used x_0 ranging from 0 to 18 m for keel data. In a Chisquare test the data did not significantly deviate from lognormality although excess of observed keels was found in the modal 40-80 m range. Dierking (1995) found good fit for sail spacings with x_0=4 m. Good fit was found for Kara Sea sail spacings with unshifted lognormal distribution (Lensu 1999b).

In the Baltic, Lewis and others (1993) found lognormal acceptable for B88 data by a Kolmogorov-Smirnov test while the negative exponential and gamma distributions were rejected. However, the Fisher-Tippet Type I extremal value distribution predicted well the maximum spacing of profiles which indicates exponential tail behavior (Gumbel 1958). In Lensu (1993b) lognormal was also found to be an applicable but not very good model of the pooled data set B93, while for individual profiles it could be much better. The B93 data was also partitioned to 2 km segments which were arranged to 10 classes according to the degree of deformation. Lognormal was found to be a good model for these but several of the tails showed exponential slope. The B94 and B97 data showed similar features: the lognormal was an acceptable model of the pooled data set but the fit was not as good as it was for several individual profiles (Lensu 1995a,1998b). For B94 the pooled data histogram showed a very clear exponential slope.

Lognormal features appear more strongly in the Arctic. This may be partly due to the fact that Arctic keel data and Baltic sail data are compared. The Baltic data sets show also regional variation. In the Bay of Bothnia the ice cover typically consists

of regimes with different ages, and also the basin boundaries have their effect. The scale of the regimes and the basin boundary effect is tens of kilometres, or the same as the length of typical surface profile. If the regimes follow lognormal distributions with different parameters a less good lognormal fit is expected for the pooled distribution.

6.3.3. Agreement with the evolution hypothesis

There is no decisive evidence for either lognormal or negative exponential distribution. The lognormal features are usually more manifest and negative exponential does not apply to short spacings. These observations are in general agreement with the hypothesis $\alpha(x)\sim 1+ax$. However, the equation solutions for this rate are not known so that precise analysis cannot be done. Lognormal is also an asymptotic model valid for large event number $\langle n\rangle$. Average spacing decreases in a geometric series fashion with $\langle n\rangle$. Thus $\langle n\rangle$ scarcely exceeds 10 which corresponds to about 2^{10}- or 1000-fold decrease even when the parent spacing consumption is not counted. Thus the spacing process is not expected to reach the asymptotic regime in observed ridge fields. Due to these facts not much more can be obtained by the analysis of spacings distributions. The evidence for $\alpha(x)\sim 1+ax$ comes rather indirectly from the more effective comparisons presented below, especially from the sail number studies. However, some observations and parameter studies can be made.

A direct approach would determine $\alpha(x)$ from observations. The method applied to floe size distributions in Lensu (1992) can be used. The data consisted of two sets of floe data sampled from the same region on 21 April and 19 May 1982 (Leppäranta 1983). The first set served as an input in a simulated floe fragmentation process with different rates $\alpha(x)\sim x^{\rho}$ and the evolving sample was compared with the latter set. It was found that ρ=0.17 reproduced the observed change in statistics which constituted a demonstration of predictability. Also, ρ=0 was acceptable while ρ=1 and also ρ=0.5 were rejected. As the background process for both floe fragmentation and ridge formation is the generation of cracks this result is expected to have bearing in the ridge context, too.

The comparison of predicted and observed statistical parameters requires time series data. If singular data sets are used an initial distribution must be assumed. The dimensionless geometric standard deviation σ is estimated here by assuming that a lognormal spacing process starts from a single initial 6 km spacing which is the maximum for all Baltic data of Table 1. If the spacing consumption is 1/3 km (Section 7.3) and N=30 spacings are created this consumes 3 km and the remaining 3 km has sail density 10/km. From (78,97) the average event number is

$\langle n \rangle$=7. Spacing volume solutions are used and transition probabilities $b(\eta) = \delta(\eta\text{-}1/2)$ (halving) and $b(\eta)=1$ (random division) are taken as limit cases. Then σ is between 5 and 32. The values for spacing data with height cutoff are difficult to estimate but are probably are not very much different. The observed values in Table 3 are in the lower range.

In a process $\alpha(x)\sim 1$ the parameter σ increases with ridge sail density. However, this is not found in Table 3 where no clear patter can be discerned although the high values of σ are more often associated with low densities. This may have several roots. The transition probability of ($h_{cs}\geq 0.5$)-spacings is more close to $b(\eta) = \delta(\eta\text{-}1/2)$ if the density is high and the number of component ($h_{cs}\geq 0$)-spacings is small. On the other hand, the transition probability is more close to $b(\eta) = 1$ if the density is low and the number of component spacings is large. The Poisson component process may effect. The parameter σ is not known for the combined process $\alpha(x)\sim 1+ax$. However, if the spacings longer than some x_0 have negative exponential distribution, the geometric standard deviation of this tail is constant. It has the value 3.6 for $x_0=0$ and decreases to 1 with increasing x_0. The clustering component seeks to increase σ and the Poisson component to reduce it to a constant value. Thus another possible explanation is that higher d is associated with higher value of a. The results of Section 6.5 also indicate that the ridge sail field S as defined in Section 2.5.1 is a fractal ice cover subregion with dimension increasing with d. For low densities the long spacings that increase σ more often span over level ice outside S. However, no conclusive results can be based on present data.

Table 3. The observed geometric parameters and medians.

Survey	Geom. mean μ	Median	Geom. st.dev. σ	Ridge sail density $d(h_{cs}\geq 0.5$ m) by (156)	Density $d(h_{cs}\geq 0.5$ m)
B93	73	65	4.2	4.9	14.5
B94	58	50	7.4	3.2	15.6
B97	16	13	4.1	18.2	49.8
K1	28	24	4.1	12.0	16.3
K2	31	32	4.1	11.8	17.6
K3	48	45	4.1	6.7	29.0
K4	17	15	3.1	28.2	40.7
K5	46	43	5.1	6.6	15.5
K6	14	13	3.1	33.7	35.9
K7	41	36	5.1	6.3	10.5

In conclusion, due to the lack of time series data a quantitative comparison of the predicted and observed distributions cannot be done. If such data is later collected, the problems of lacking solutions $\alpha(x)\sim 1+ax$, remoteness from asymptotic regime, and the unknown effect of height cutoff in the parameters must be faced. It will be shown later that the sail number approach is a much stronger tool in data analysis. However, the observations generally support the hypothesis $\alpha(x)\sim 1+ax$.

6.3.4. Multivariate lognormality of spacings and spacing correlations

Multivariate spacing distributions $f(x_1,\ldots,x_n)$ describe groups of n successive spacings. Adjacent spacings have separation one. If there are in addition n-2 intermediate spacings the separation is n-1. A multilognormal $f(x_1,\ldots,x_n)$ is determined by the correlations for ln(X) up to separation n-1. The conditional distributions (91) are then also lognormal. These results are generally valid. The present theory adds that the correlations of ln(X) and X have a certain dependence on t and separation. The correlations (92) and (93) are for spacing cross-section volume. However, the associated functional forms are expected to apply to spacings also.

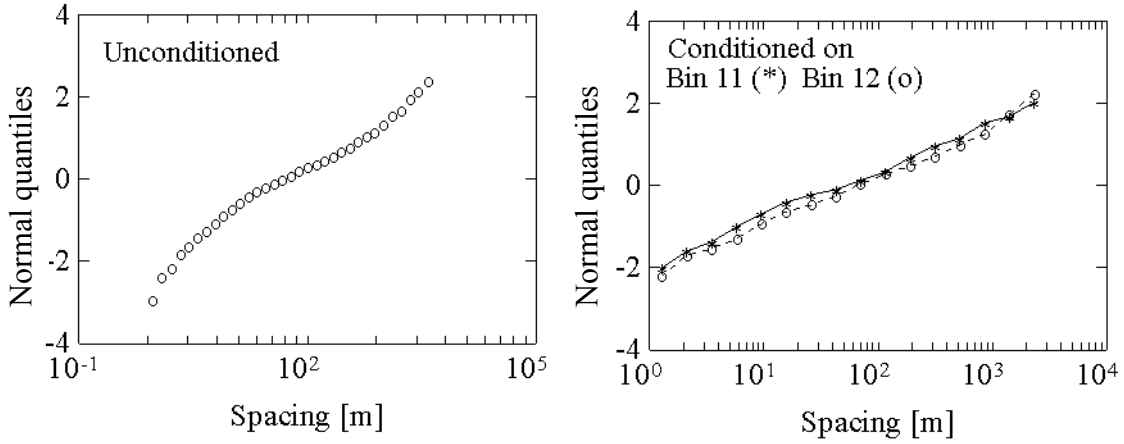

Figure 24. The overall spacing distribution in a probability graph, and distributions conditioned on adjacent bin 11 (148-245 m) and bin 12 (245-403 m) . The percentage corresponding to normal quantile q is the value of cumulative normalised normal distribution for q.

The correlations were calculated for B94 data with overall geometric mean 58 m. The data was arranged with respect to ln(X) to 17 bins of width 0.5 and ranging from 0 (1 m) to 8.5 (4915 m). The number of instances in the bins exceeded 100 for 12 bins and for these conditional distributions $f(x_1|x_2$ *is in the bin*) were calculated for separations 1-17. The agreement with lognormality was good and

for separation one even better than for $f(x)$ (Figure 24). The apparent reason is that the conditioning reduced the relative weight of long spacings that bring exponential features to the distributions. Conditioning by spacings with separation 2-17 produced similar but not as good results. The observed conditional geometric mean was in a very good agreement with (91), Figure 25.

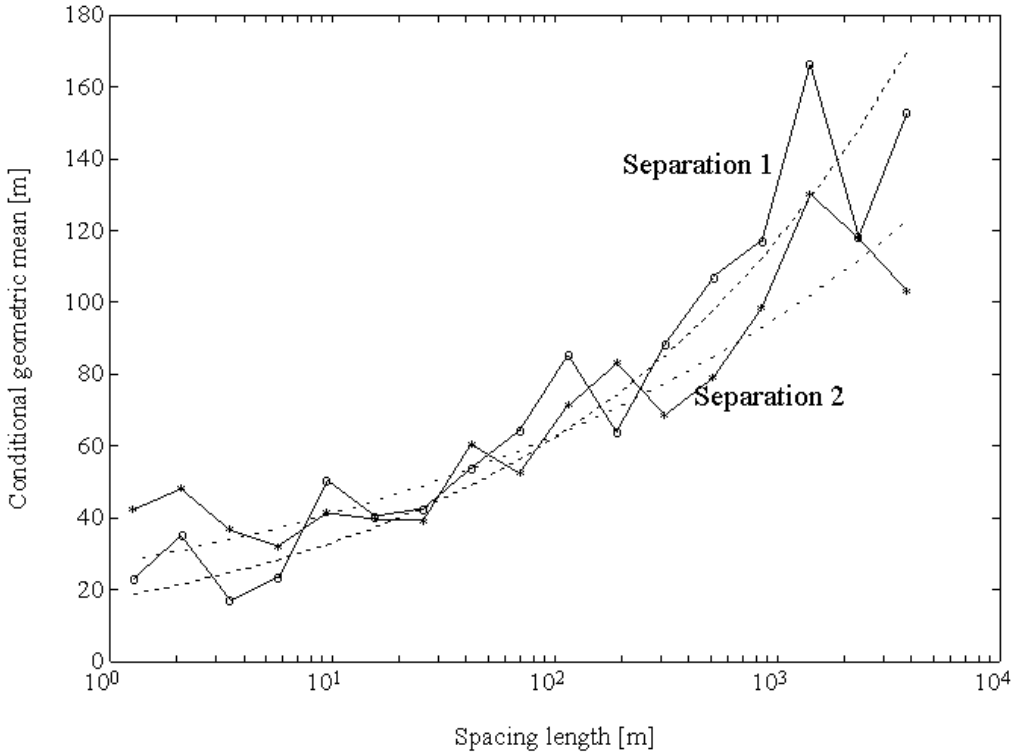

Figure 25. Conditional geometric mean (76) compared with observations. Pairs of adjacent spacings (o) have separation one and pairs separated by one spacing (∗) separation two.

The correlations (92,93) are applied directly as

$$\rho_n(\ln(X)) = \rho_1(\ln(X)) - \frac{1}{t}\sum_{j=2}^{n}\frac{1}{j}\ , \quad \rho_n(X) = \rho_1(X)\prod_{j=2}^{n}\frac{j}{j+2+2K(2)} \qquad (113\ \text{a,b})$$

where n is the separation. The $\rho_n(\ln X)$ have approximately logarithmic decrease. These were fitted to B94 data by varying the parameters t and $K(2)$ respectively. The results for t=11 and $K(2)$=-0.7 are in Figure 26 and a good agreement is found. For spacing volume $K(2)$ is expected to lie between –2/3 (random placement of created crack into spacing) and –3/4 (placement into spacing midpoint, Lensu 1997). For data sets B97 and K1-K7 the correlations had the

same pattern. It was found that correlations tend to decrease with ridge density. The correlations of ln$X$ for pooled data B94, B97,K1-K7 are in Figure 27 and agree well with the logarithmic decrease predicted by the theory. Linear fit to the data gives

$$\rho_n(\ln X) = -0.048\ln(n) + 0.222 \tag{114}$$

which can be used to model correlations in 0.5 m cutoff data.

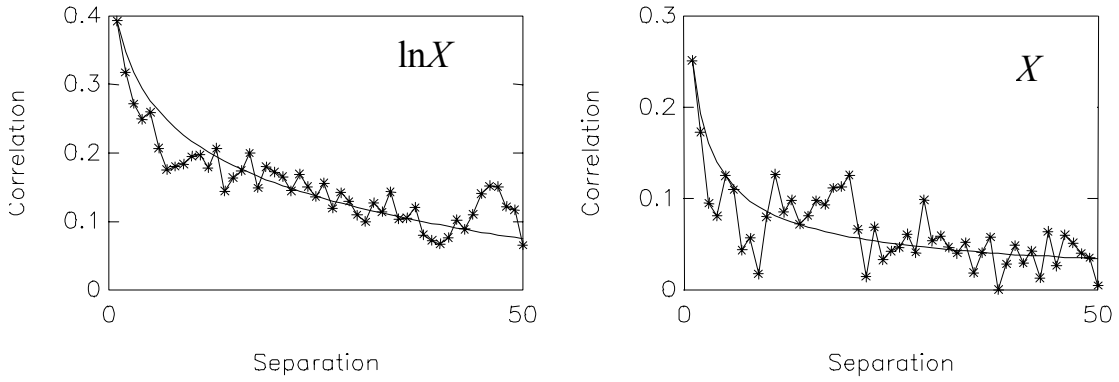

Figure 26. The correlations of ln$X$ and X for B94 data, fitted by the model (106 a,b).

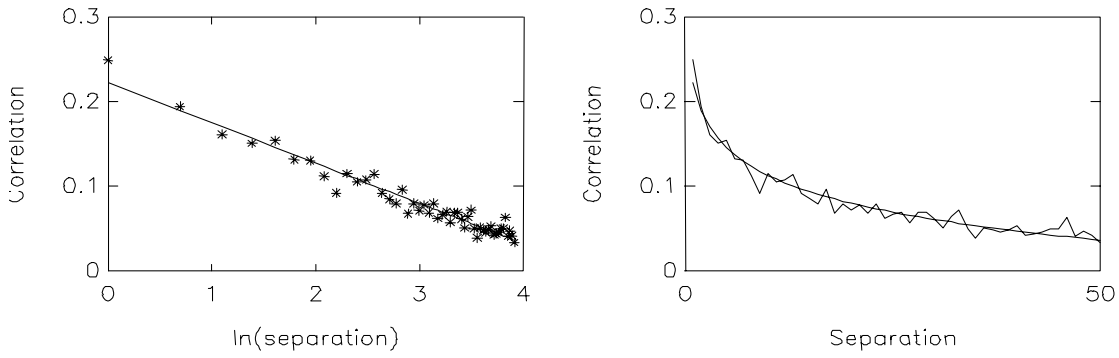

Figure 27. The correlation of ln$X$ for pooled data set B94, B97 and K1-K7. fitted by $-0.048\ln(n) + 0.222$.

These results support the evolution hypothesis $\alpha(x)$~1+ax. Although lognormal is not a perfect model of $f(x)$ it applies better to conditional distributions. The conditioning bins were in the mid range that contains the bulk of the data. The

conditioning spacings are then likely to be due to the lognormal component $\alpha(x)\sim 1$ of the process and this then applies to the adjacent, conditioned spacing as well. The correlations are specific to the evolution theory and followed the predicted pattern. It is likely that the good results are partly due to the fact that the predicted correlations are not restricted to the asymptotic regime, and that the component $\alpha(x)\sim$x produces no correlations. Thus in the multivariate approach the quantitative comparison, not possible for univariate spacing distributions, could be done.

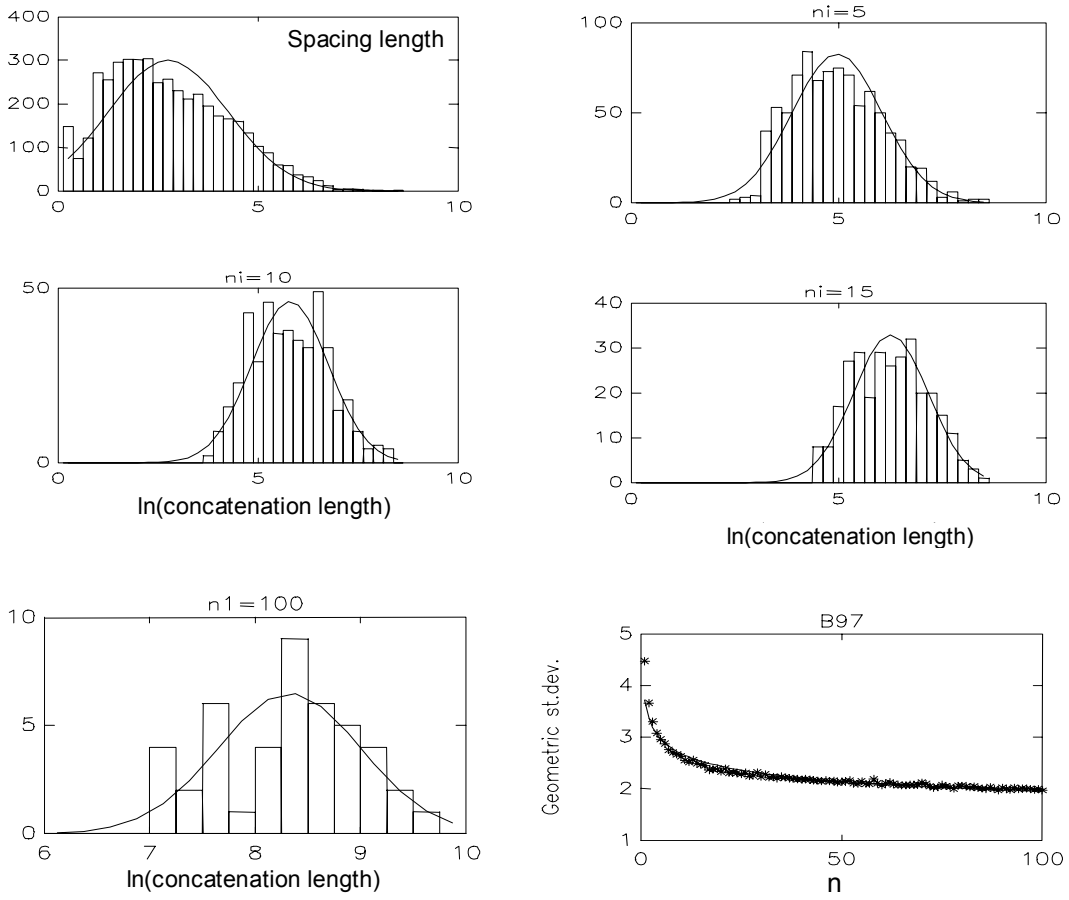

Figure 28. Histograms for the logarithm of length for *n*-concatenations of 1,5,10,15 and 100 spacings (B97 data). A normal distribution with the same mean and variance for each, and the dependence of geometric standard deviation on the number of component spacings are also shown.

6.3.5. Lognormality of n-concatenations of spacings

For n-concatenations $\alpha(y_n)\sim n+ay_n$ whenever $\alpha(x)\sim 1+ax$ (Section 5.3.1). If $\alpha(x)\sim 1$ then for any collection of spacings the evolution is independent on the component spacings. It is only the number of component spacings that counts. If spacing is lognormally distributed the same applies to the length of spacing concatenations. This is peculiar to the process $\alpha(x)\sim 1$ and does not apply to lognormal distributions in general. If n is large the transitions are scale similar. As n increases the difference between parent and progeny decreases. The value of geometric standard deviation decreases, and the probability to find concatenations much longer than the average value decreases. Therefore the tail exponentiality from the process component $\alpha(y_n)\sim ay_n$ is expected to fade out and lognormality become enhanced with increasing n.

In Figure 28 the histograms of $\ln(Y_n)$, where n=1,5,10,15 and 100, are shown for B97. Normal distribution with the same parameters is also shown. The spacing distribution is skewed due to the exponentiality of longer spacings. The skewness disappears rapidly with increasing n and lognormal is a good model for Y_n up to Y_{100} with $\langle y_{100}\rangle$=5.5 km. These results are in a complete agreement with the evolution hypothesis $\alpha(x)\sim 1+ax$. The geometric standard deviation has power law decrease $\sigma_n \sim n^{-0.27}$.

6.3.6. Lognormality of x_0^-*-concatenations of spacings*

An x_0^--concatenation has all component spacings shorter than x_0, and is described by length y^- and spacing number n. Starting from small x_0 the number of the concatenations first increases and then decreases. The concatenation length and process $\alpha(x)\sim 1+ax$ is considered. The effect of a is expected to vanish for concatenations with short x_0. The events changing Y^- were of four types as outlined in Section 4.2.7. For short x_0 the joining together can be neglected. The addition of spacings to either end can be assumed to not depend on Y^-. The dominant event type is decrease of Y^- in the transitions of component spacings. On the average, the rate for these events is proportional to y, $\alpha(y)=by$ for some b, and each event decreases y^- with the same amount c. However, as sequentiality is inessential here, this is equivalent to the rate b for events and decrease cy^-. For short x_0 a lognormal distribution is thus expected.

The statistics for Y^- was calculated for B94 data with x_0 ranging from 5 m 100 m (Table 4). The joining of the concatenations begins to show between threshold values 50 and 100 m where the number of concatenations starts to decrease and the distribution becomes more skewed. For threshold values up to 50 m the

lognormality is a good model for Y (Figure 29). The results are again in an agreement with the rate $\alpha(x)\sim 1+ax$.

Table 4. The statistics for maximal spacing concatenations with all component spacings shorter than x_0, described by length y^- and component spacing number n (B94 data). The average spacing $\langle x_c \rangle$ between the concatenations is also given.

x_0 [m]	N	$\langle n \rangle$	$\langle y^- \rangle$ [m]	*Median*(Y^-) [m]	$\mu(Y^-)$ [m]	$\langle x_c \rangle$ [km]
5	147	1.74	4.6	3.7	3.5	2.58
10	190	2.24	10.0	7.5	7.1	1.97
20	231	2.55	18.3	13.3	12.6	1.63
50	250	3.29	40.9	25.7	23.3	1.65
100	211	4.02	80.0	51.4	40.3	1.73

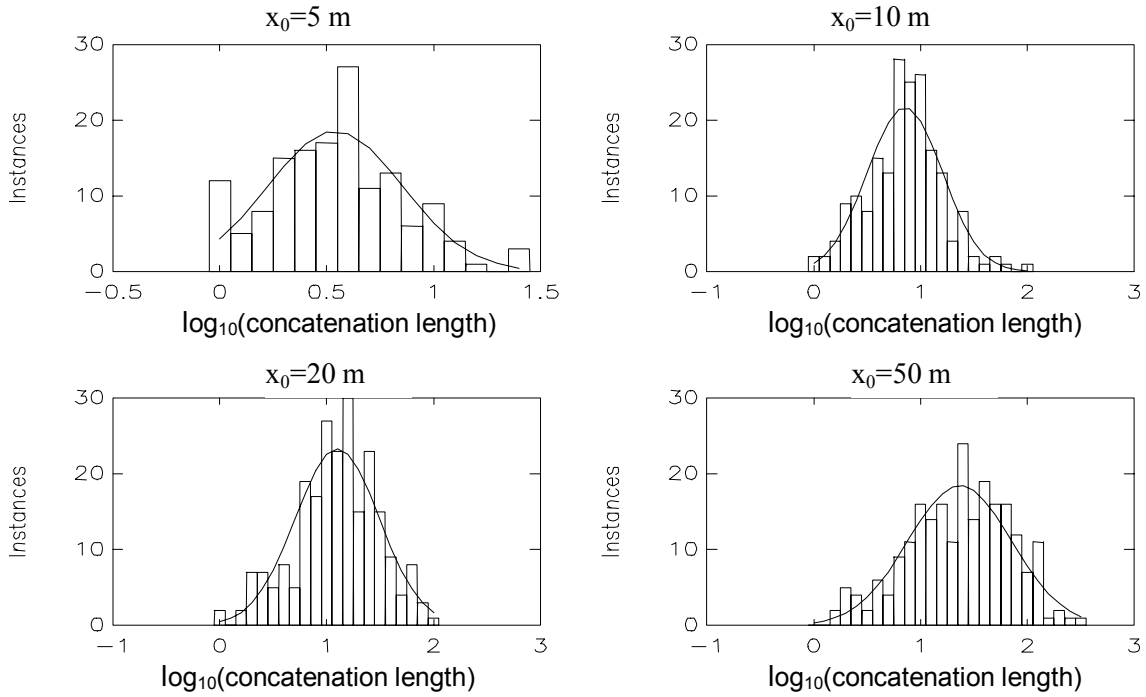

Figure 29. Histograms for the logarithm of length of x_0-concatenations. Normal distribution with the same mean and variance is also shown for each case.

6.4. Ridge sail number distributions

The spacing rate $\alpha(x)\sim 1+ax$ and was found be in agreement with the observed spacing statistics. The effect of a vanished for spacing concatenations for which lognormal was a good model. Also the correlations followed the lognormal model. The corresponding sail number rate is $\alpha(n_j)\sim n_j+aL_j+c$ for large $\langle n_j\rangle$. The clustering rate is proportional to n_j and the Poisson rate to aL_j. As discussed in Section 5.5, the constant c takes approximately into account certain effects due to differential movements. The average rate is $\langle\alpha(n_j)\rangle\sim(d+a)L_j+c$. The average clustering rate is thus proportional to ridge density d and the average Poisson rate to a. This holds irrespective of the segment length.

The sail number statistics was studied for B97 profiles (Table 5). The longer scale L_i is the total profile length (270 km), n_i the total number of sails, and d_i=18.2 the average ridge density. The shorter scale L_j ranged from 12.5 m to 1600 m. The nonempty L_j-segments have coverage C_j. The average sail number is $\langle n_j\rangle=d_iL_j$ and the average sail number of nonempty segments is $\langle n_j>0\rangle=\langle n_j\rangle/C_j$.

Table 5. Statistics for sail spacing numbers n_j (B97 data). The coverage C_j of segments containing at least one sail is also given.

L_j [m]	$\langle n_j \rangle$	Max$\langle n_j\rangle$	$\langle n_j>0\rangle$	C_j
12.5	0.23	5	1.39	0.16
25	0.45	8	1.76	0.26
50	0.91	10	2.34	0.39
100	1.82	17	3.33	0.54
200	3.64	29	5.21	0.70
400	7.28	43	8.65	0.84
800	14.56	78	15.78	0.92
1600	29.12	123	29.77	0.97

The finite negative hypergeometric model (105) where aL_j is replaced by aL_j+c was applied. The negative binomial model (106) differs only insignificantly from it as L_i is much longer than the L_j. The probability of a transition in (105), or the transition rate in (106), was assumed to have the form n_j+aL_j+c. For each L_j of Table 5 the parameter aL_j+c was varied for optimal fit. It was found to be reasonably linearly dependent on L_j and from the linear slope c=0.5 and a=2. The sail number histograms and the fit of the model (105) with these values are shown in Figure 30. The agreement is good for the entire range 12.5-1600 m. The average clustering rate, proportional to ridge density d_i=18.2, is nine times the average Poisson rate, which is proportional to a=2. Thus the latter is negligible for shorter segment lengths.

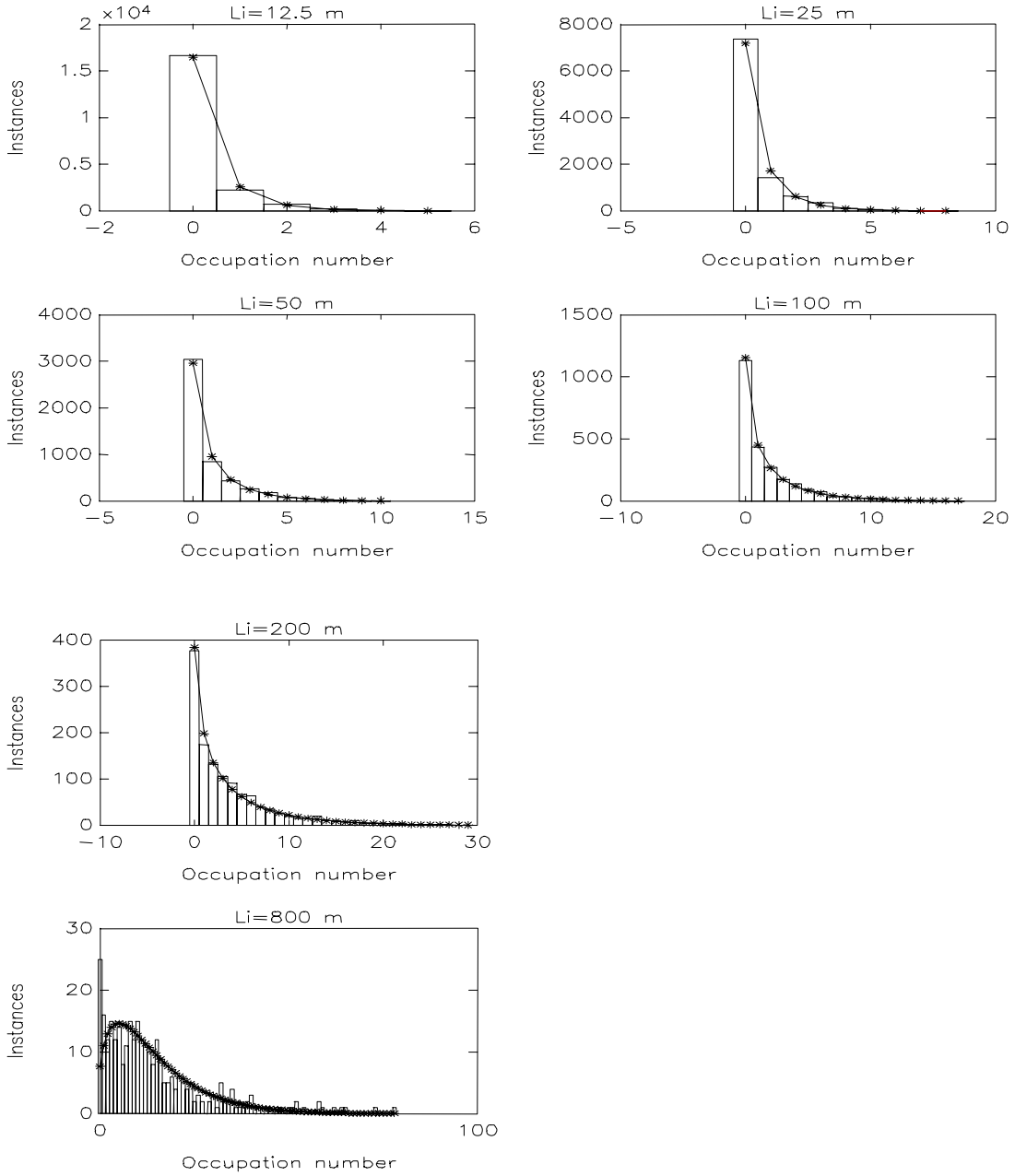

Figure 30. Sail spacing number histograms for B97 data for L_j ranging from 12.5 m to 1600 m. The negative hypergeometric model (105), where aL_j is replaced by aL_j+c, is shown for a=2 and c=0.5

The data B94 and K1-K7 demonstrated likewise the applicability of the negative hypergeometric model. The sail number distributions and the distribution models for c=0.5 are shown in Figure 31 for L_j=200 m. The parameter a ranges from 0.5 to 2.2 and its effect to the distribution shape is clearly seen.

To conclude, the results confirm the hypothesis $\alpha(n_j) \sim n_j + aL_j + c$. As sail number distribution model, as well as the various results for spacing correlations and spacing concatenations, are results of the discontinuous Markov approach to ridge arrangement evolution, it is likely that the approach is valid.

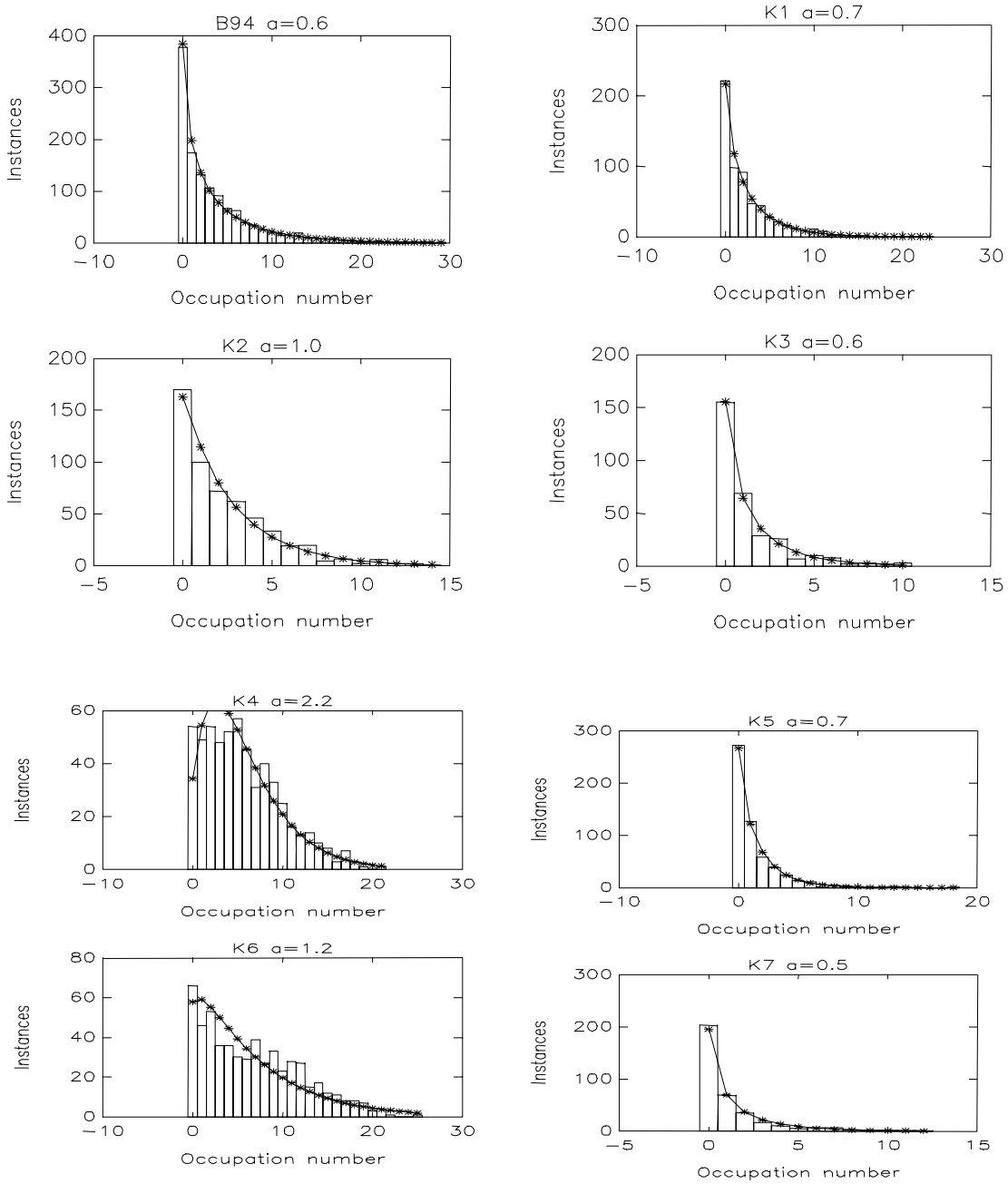

Figure 31. Sail spacing number histograms for B94 and K1-K7 data. Segment length is L_j=200 m. The negative hypergeometric model (105), where aL_j is replaced by aL_j+c, is also shown.

6.5. Spacing and sail number distributions parameterised by sail density

The data analysis has revealed dependencies that can be used to formulate distribution models parameterised by ridge density only. Such models are convenient in applications as ridge density is easily determined. The models apply to cutoff data $d(h_{cs}\geq 0.5)$ and their extension to $h_{cs}\geq 0$ requires further studies not possible here. Partitioning the data of Table 3, excluding B93, to 40 km sections the empirical relationship

$$\sigma = 10.6d^{-0.36} \tag{115}$$

is found (Figure 32). Using (82) to express the geometric mean μ in terms of $\langle x\rangle = 1/d$ the sail spacing distribution can be written

$$f(x) = \Lambda\left(x;\, d^{-1}\exp\left\{-0.065\ln^2 10.6d\right\},\, 10.6d^{-0.36}\right). \tag{116}$$

in terms of notation (79). This can be extended to multivariate distributions with (114).

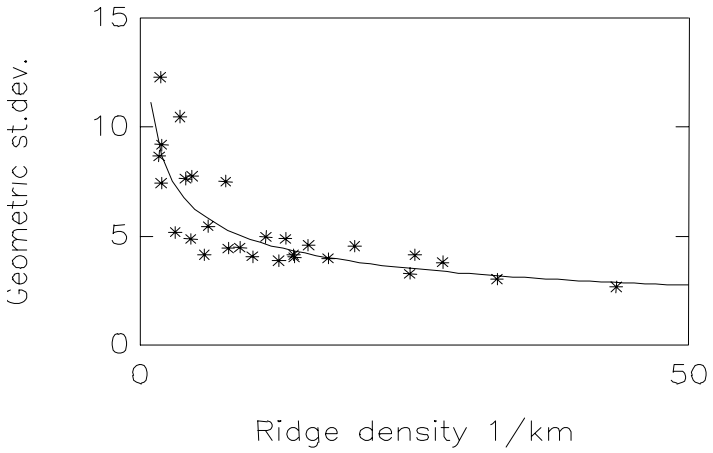

Figure 32. The relation of geometric standard deviation to ridge density, determined from pooled data set divided into 40 km segments.

Figure 28 shows the B97 geometric standard deviation for concatenation length Y_n. The same decreasing power law is found also for B94 and K1-K7. The exponent has a weak dependence $-0.006d+0.276$ on sail density and can be assumed to be constant 0.27. Including (115), a very good fit is found by $\sigma_n = 10.6d^{-0.36}n^{-0.27}$. The mean is $\langle y_n\rangle = n/d$ and the geometric mean is obtained from (82). Thus, an empirical lognormal model can be formulated ,

$$f(y_n) = \Lambda\left(y_n ; \frac{n}{d} \exp\left\{ -\tfrac{1}{2}\left(2.36 - 0.36 \ln d - 0.27 \ln n\right)^2 \right\},\ 10.6 d^{-0.36} n^{-0.27} \right). \quad (117)$$

This describes both spacings (n=1) and spacing concatenations in 0.5 m cutoff data. For small y_n/n the concatenations are expected to belong to ridge clusters.

A model for sail number distributions, parameterised by ridge density, is finally constructed using all data B94, B97 and K1-K7 (Lensu 2002). It is seen that $\langle n_j>0\rangle$-1 has power law dependence with exponent $D(d_i)$ on scale L_j (Figure 33). The density d_i is the overall ridge density of each data set and L_j varies through a ladder of smaller scales. A geometric distribution (107) is found to apply up to segment length 400 m for $n_j>0$. From the properties of geometric distribution, $\langle n_j>0\rangle$-1 is the average when the geometric distribution for $n_j>0$ is extrapolated to $n_j=0$. This extrapolation defines the coverage

$$\hat{C}_j = \frac{d_i L_j}{\left\langle n_j > 0 \right\rangle - 1} \quad (118)$$

which has power law dependence with exponent 1-$D(d_i)$ on L_j. This can be interpreted that the coverage has fractal dimension D for which the tentative relationship

$$D(d)_i = e^{-1.8/d_i} \quad (119)$$

is given (Figure 33). To fix the model $\hat{C}_j$ should be known for some L_j. As L_j decreases $\langle n_j>0\rangle$ approaches unity. Variation of $\langle n_{12.5\mathrm{m}}>0\rangle$ between the data sets is small and is assumed to be a constant 1.3. Then $\hat{C}_{12.5\mathrm{m}}=0.042 d_i$ and

$$\hat{C}_j(d_i) = 0.042 d_i \left(\frac{L_j}{12.5} \right)^{1-D(d_i)} . \quad (120)$$

The distribution model is

$$k(n_j) = (1-\hat{C}_j)\delta_{n_j 0} + \hat{C}_j p (1-p)^{n_j} \ , \ p = \frac{\hat{C}_j}{d_i L_j + \hat{C}_j} \quad (121)$$

where the first term refers the ice outside the coverage $\hat{C}_j$ and the latter term is the geometric distribution within the coverage.

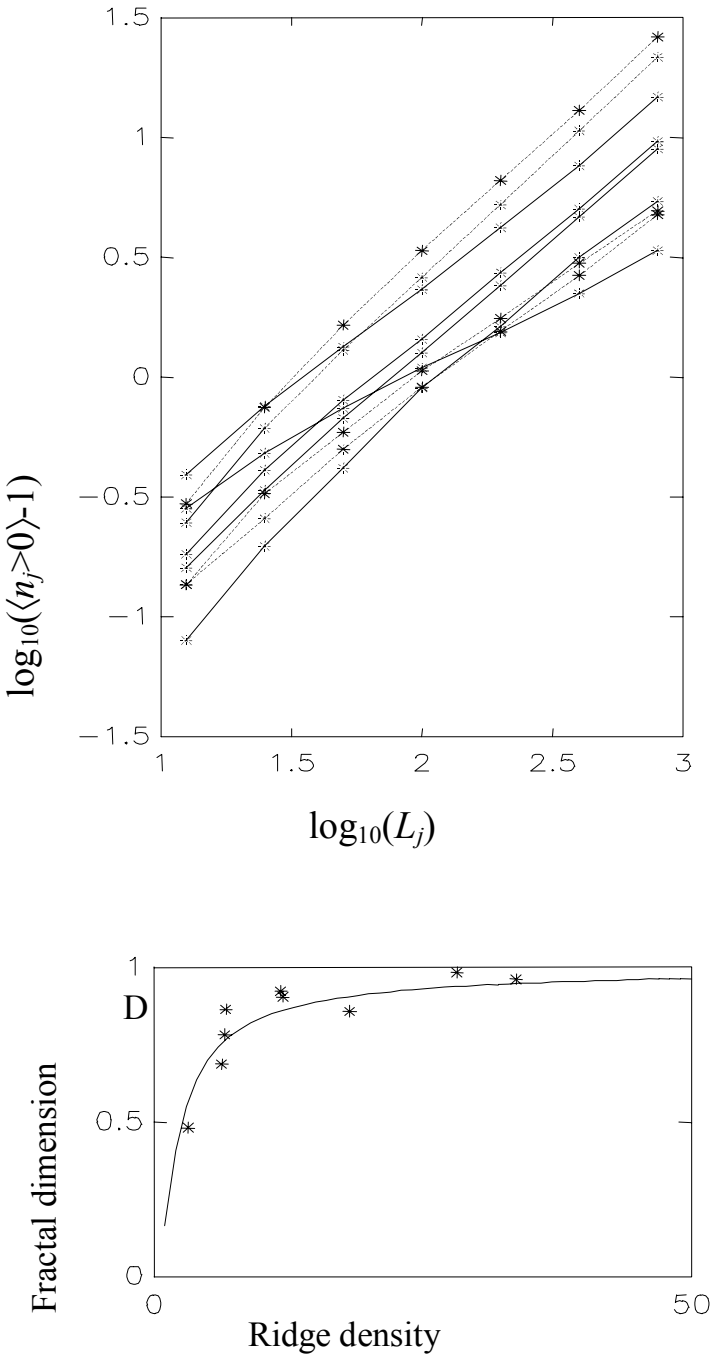

Figure 33. Power law dependence of $\langle n_j>0\rangle$-1 on segment length L_j, and the fractal dimension, determined from the slopes, as a function of ridge density.

7. RIDGE ARRANGEMENT EVOLUTION AND ICE THICKNESS CHANGE

7.1. Introduction

Two approaches to the evolution of continuously spatially varying sail spacing distribution $f(x,\mathbf{r},t)$ are considered. In the first Eulerian conservation equations are formulated for sail spacing distribution. In the other approach the equations are formulated for ridge sail density. The density field $d(\mathbf{r},t)$ can then be used to parameterise sail spacing and sail number distributions. The equation for $f(x,\mathbf{r},t)$ involves the parent spacing consumption which links the spacing evolution to ice concentration change. In the case of sail density evolution the linking is attained by a function $\varphi(d)$ which is the relative change in ice area per unit change in ridge sail density. It is constructed from volume conservation and expressed in terms of average thickness $\langle H \rangle$ and the equivalent cross-sectional volume $v_{eq}(d)$, which is equivalent thickness of ridge rubble divided by ridge density.

Due to ridge clustering $v_{eq}(d)$ decreases with ridge density. It is parameterised by considering first a ridge link cross-section model in the case of no keel contact. After a discussion on cluster morphology the clustering effect is taken into account with a simple overlap model. The parameterised v_{eq} gives estimates of the equivalent thickness of ridged ice. For the Baltic the estimates are larger than those previously published but are a supported by profile data. The parameterisation is given in terms of the average cross-sectional height $\langle h_{cs} \geq h_0 \rangle$ which is a quantity obtainable from profiling measurements with cutoff h_0. The parameterisation involves scaling of the published cross-sectional data. This is required as the field measurements do not refer to randomly selected sail heights h_{cs}.

7.2.Conservation equations for ridge arrangement evolution

7.2.1. Conservation equations for ridge sail spacing distribution

It is assumed that the partial concentration of ridged ice equals ice concentration C. Ice thickness increase is due to ridging only and thermal processes are not considered. The conservation equation for sail spacing distribution is obtained from the Lagrangian equation (57) by replacing the number N of spacings with the measure density Cd, and by adding the advection term $-\nabla\cdot(\mathbf{v}Cdf)$ where $\mathbf{v}$ is ice velocity field. The equation for $C(\mathbf{r},t)d(\mathbf{r},t)f(x,\mathbf{r},t)$ is then

$$\frac{\partial}{\partial t} Cdf = -\nabla \cdot (\mathbf{v} Cdf) + Cd\Psi \tag{122}$$

where

$$\Psi = 2 \int_{x}^{x_{\max}} dx' \alpha(x') f(x') B(x' \to x) - \alpha(x) f(x) \quad . \tag{123}$$

The equation for the measure density Cd is obtained by integration as

$$\frac{\partial}{\partial t} Cd = -\nabla \cdot (\mathbf{v} Cd) + Cd \int_{0}^{x_{\max}} dx \, \Psi \quad . \tag{124}$$

As $d\langle x \rangle = 1$ the concentration equation is obtained by multiplying (122) by x and integrating,

$$\frac{\partial C}{\partial t} = -\nabla \cdot (\mathbf{v} C) + Cd \int_{0}^{x_{\max}} dx \, x \, \Psi \quad . \tag{125}$$

The sign of the last term in (125) is negative as ridging seeks to reduce ice concentration. The equation for ridge density is solved from (124) and (125) as

$$\frac{\partial d}{\partial t} = -\mathbf{v} \cdot \nabla d - d \int_{0}^{x_{\max}} dx \, \Psi + d^2 \int_{0}^{x_{\max}} dx \, x \, \Psi \quad . \tag{126}$$

These equations for C and d are direct consequences of the spacing evolution equation.

7.2.2. Dependence of spacing evolution parameters on ice concentration and kinematics

If the transition rate α and transition probability B are known the concentration equation (125) follows. On the other hand, if the concentration equation has a certain form it can be used to parameterise α and transition probability B. It is assumed that B is not dependent on ice concentration and kinematics. Thus the relation of α to C and $\dot{\varepsilon}$ is in concern.

Ridging sets on when a certain limit concentration is reached in a converging ice field. If the concentration is below unity, part of the convergence increases concentration while the remainder manifests as ridging. At another concentration limit the two processes counterbalance and the concentration does not increase any more. This limit may be below unit concentration, especially if the kinematic state is not pure convergence. The dependency on concentration can be described in a simple way as function $r(C)$, increasing from $r(0)=0$ to $r(1)=1$ and defining the fractions $r(C)$ and $1-r(C)$ that from the convergence are used to ridging and to concentration increase respectively (Shinohara 1990, Gray and Morland 1994, Gray and Killworth 1996, Schulkes 1995).

Ridge formation is observed also during pure shear. As then $\nabla\cdot\mathbf{v}=0$, ridging is accompanied with simultaenous concentration decrease. The problem is generally to relate the rate α to the kinematic state $\dot{\varepsilon}$. This can be done by a function $\gamma(\theta)|\dot{\varepsilon}|$ where

$$|\dot{\varepsilon}| = \sqrt{\dot{\varepsilon}_{\mathrm{I}}^2 + \dot{\varepsilon}_{\mathrm{II}}^2} \quad , \quad \theta = \arctan(\dot{\varepsilon}_{\mathrm{II}} / \dot{\varepsilon}_{\mathrm{I}}) \tag{127}$$

in terms of the strain rate invariants $\dot{\varepsilon}_{\mathrm{I}}$ and $\dot{\varepsilon}_{\mathrm{II}}$ which correspond to divergence and twice the maximum rate of shear respectively. This formulation was suggested by Thorndike et al. (1975) while other approaches to the same problem include Hibler (1984), Shinohara (1990) and Gray and Killworth (1996). The magnitude of horizontal global deformation is $|\dot{\varepsilon}|$, while the angle $0\le\theta\le\pi$ parameterises the contributions of divergence and shear. Pure divergence corresponds to $\theta=0$, pure shear to $\theta=\pi/2$ and pure convergence to $\theta=\pi$, while $\theta=\pi/4$ and $\theta=3\pi/4$ are uniaxial divergence and convergence. It is demanded that γ increases from $\gamma(0)=0$ to $\gamma(\pi)=1$. If $\gamma(\pi/2)>0$ both ridging and opening are operative during pure shear. Expressions for γ have been derived in Rothrock (1975), Fily and Rothrock (1990), and Stern et al. (1995) in the context of plastic rheology.

It is assumed that the kinematic state and concentration affect only the intensity factor $\beta(C,\dot{\varepsilon})\beta(t)$ of the spacing transition event rate. The rate is thus assumed to be

$$\alpha(x,t) = \beta'(C,\dot{\varepsilon})\beta(t)\alpha'(x) = |\dot{\varepsilon}|\gamma(\theta)r(C)\beta(t)\alpha'(x) \tag{128}$$

in terms of the functions defined above. Here $\alpha'(x)$ depends only on x. The equation for concentration (125) is then

$$\frac{\partial C}{\partial t} = -\nabla \cdot (\mathbf{v}C) - C\,|\,\dot{\varepsilon}\,|\,\gamma(\theta) r(C) \beta(t) d \left| \int_0^{x_{\max}} dx\, x\, \Psi' \right| \tag{129}$$

where Ψ' is mechanical evolution term (123) for the rate $\alpha'(x)$. For pure convergence and unit concentration, $|\dot{\varepsilon}|\gamma(\pi) = -\nabla \cdot \mathbf{v}$, $r(C)=1$ and $\partial C/\partial t = \nabla C = 0$. It follows

$$\beta(t) = \left| d \int_0^{\infty} dx\, x\, \Psi' \right|^{-1} . \tag{130}$$

The concentration equation reduces to

$$\frac{\partial C}{\partial t} = -\nabla \cdot (\mathbf{v}C) - C\,|\,\dot{\varepsilon}\,|\,\gamma(\theta) r(C) \tag{131}$$

which does not depend on the spacing evolution parameters. If $|\dot{\varepsilon}|\gamma(\theta) r(C)$ in (131) is replaced by some other condition, the spacing transition rate is obtained by making the same replacement in (128).

7.2.3. The inclusion of spacing evolution into dynamic ice models

It is in principle possible to model the rate $\alpha(x, C, \dot{\varepsilon}, t)$ if the dynamics of the ridging process is known in detail. A straightforward option is to assume $\gamma(\theta)$ and $r(C)$ and derive $\alpha(x,t)$ as in the above section. After C and $\dot{\varepsilon}$ are obtained from ice model equations, (122) can be solved. The term $\alpha'(x)$ can be determined by observing the spacing distribution evolution in Lagrangian regions. The present study suggests that $\alpha'(x)=1+ax$ and that $\alpha'(x)=1$ is not a bad approximation. The spacing equation acts then as an external module that interprets ice thickness increase as a change in ridge arrangement. In a more advanced approach the model constitutive equation may also depend on the spacing distribution. For example, the global continuum dissipation $\sigma : \dot{\varepsilon}$ calculated by the model can be equalled with the dissipation determined by the spacing equation. The dissipation in spacing transitions is obtained from ridge formation studies and the total dissipation is given by (54).

Ice thickness evolution can be associated with the spacing evolution by a distribution $f(z|x)$. This is a thickness distribution pertaining to an x-spacing. The overall thickness distribution of ridged ice is

$$f(z,\mathbf{r},t) = \int_0^{x_{\max}} dx \frac{x f(x,\mathbf{r},t)}{\langle x \rangle} f(z \mid x) \tag{132}$$

where the fraction in the integral is the relative length of x-spacings. This approach has benefits in comparison to direct formulation of an equation for $f(z,\mathbf{r},t)$. The parameterisation of spacing evolution refers to tractable transition events related to ridge formation events. Features transit to features of the same kind. It can be precisely stated which kind of measurements are required for a better parameterisation. It is also possible to include other deformation processes to spacing evolution equation. Rafting events, for example, can be described as unary spacing transitions. In numerical modeling context the spacing cross-section equation (56) can also be used and ridge size and level ice thickness distributions are obtained. In this respect the state of matters is better off than for the thickness distribution evolution. For point thickness the features are ice columns with small surface area. They do not transit to similar features in deformation and thus the thickness transition probability must be related to events with larger scale, especially to ridge formation events.

Indeed, the parameterisation of thickness equation has largely been based on simple models of thickness increase in ridging (Thorndike et al. 1975, Hibler 1980, 1986, Thorndike 1992). As far as ridging is considered, these approaches are not expected to give better description of thickness evolution than (132). The modeling of dissipation due to mechanical evolution is also a more feasible project for the sail spacing evolution. The existing knowledge on the energetics of ridge buildup events can be used. The same remark on feasibility applies to anisotropic ice cover characterisation (e.g. Pritchard 1998) which for ridges can be done by direction dependent spacing distributions. In general, the point thickness equation can be understood as a summarising description. It can be parameterised only indirectly, through the reference to physically tractable feature transitions. For large areas containing a multitude of ice types the thickness distribution approach may be more convenient.

7.2.4. Conservation equations for ridge sail density

If the ridge sail density field $d(\mathbf{r},t)$ is known it determines the fields of mean spacing $\langle x \rangle$ and mean sail number $\langle n_j \rangle$. The mean values can be used in the parameterisation of spacing and sail number distributions while the remaining parameters must obtained from some other source. The semiempirical distribution models (116), (117) and (121) are parameterised by sail density but include the 0.5 m sail height cutoff. In applications sail density is often alone sufficient. However, the density equation indirectly involves spacing statistics. Due to ridge

clustering the equivalent thickness of ridge rubble is not expected to increase linearly with d but slower. The parameterisation of the clustering effect makes recourse to the spacing distribution.

It is again assumed that the ice concentration equals ridged ice concentration. The equations for concentration $C(\mathbf{r},t)$ and for the measure density $C(\mathbf{r},t)d(\mathbf{r},t)$ are

$$\frac{\partial C}{\partial t} = -\nabla \cdot (\mathbf{v}C) + C\varphi(d)\alpha(d) \tag{133}$$

$$\frac{\partial Cd}{\partial t} = -\nabla \cdot (\mathbf{v}Cd) + C\alpha(d) \tag{134}$$

where $\alpha(d)=\mathrm{d}d/\mathrm{d}t$ is the rate of appearing of ridge sails per unit linear distance, and $\varphi(d)$ is the relative change in ice area per unit change in ridge density. The function $\varphi(d)$ is constructed in the next section. The equation for ridge density is obtained by substitution of (133) into (134) as

$$\frac{\partial d}{\partial t} = -\mathbf{v} \cdot \nabla d + \alpha(1 - d\varphi) \tag{135}$$

Using cross-sectional models it is always possible to express the conservation equation for ridged ice volume in terms of ridge density and cross-sectional parameters. Such approach was formulated by Leppäranta (1981c) in case where the ridging sets on in converging ice cover with unit concentration. The present formulation adds to this the rate $\alpha(d)$ which can be a function of ridge density, clustering effect, and a more general treatment of concentration and kinematic state.

7.2.5. Relation of area decrease to ridge density increase

With the same assumptions on $\gamma(\theta)$ and $r(C)$ as in Section 7.2.2, the ridge formation rate is

$$\alpha(d) = |\dot{\varepsilon}|\gamma(\theta)r(C)\frac{1}{|\varphi(d)|} \tag{136}$$

and the concentration equation is (131). Similarly as for spacings, the density evolution can be an external ridging module or be linked to constitutive equation through a dissipation model.

The function $\varphi(d)$ is constructed by considering the change in the volume of ridged ice in a Lagrangian region with ice area CA. The average parent ice thickness is $\langle H\rangle$ and is assumed not to change in the ridging process. It was assumed (Section 2.5.3) that in ridging the ridge rubble is heaped below and on a level ice with average thickness $\langle H\rangle$. The actual level ice thickness may be different from $\langle H\rangle$ and need not be considered in the present context. The volume of ridge rubble is

$$V_r = CAdv_{eq} \tag{137}$$

where the v_{eq} is the equivalent cross-sectional volume or equivalent thickness of ridge rubble divided by sail density, (21). The relation (137) is differentiated with respect to d after which the use of the differential relation

$$-\langle H\rangle \mathrm{d}(CA)=\mathrm{d}V_r \tag{138}$$

entails

$$\varphi(d) = \frac{1}{CA}\frac{\mathrm{d}CA}{\mathrm{d}d} = \frac{-1}{dv_{eq}+\langle H\rangle}\frac{\mathrm{d}dv_{eq}}{\mathrm{d}d} \tag{139}$$

This can be also solved for the relations between parent ice thickness, ice area and ridge density,

$$CA = C_0A_0\frac{d_0v_{eq}(d_0)+\langle H\rangle}{dv_{eq}(d)+\langle H\rangle},\ d = \frac{C_0A_0}{CA}\left(d_0\frac{v_{eq}(d_0)}{v_{eq}(d)}+\frac{\langle H\rangle}{v_{eq}(d)}\right)-\frac{\langle H\rangle}{v_{eq}(d)}. \tag{140}$$

These can be used to parameterise the change in sail spacing and ridge sail number distributions in a Lagrangian region. Due to clustering $v_{eq}(d)$ decreases with d. The value when clustering is absent is denoted $v_{eq}(d\to 0)$. The clustering effect is estimated with the spacing distribution $f(x;d)$ so that

$$v_{eq}(d) = v_{eq}(d\to 0)\int_0^{x_{\max}} dx\, p(x)f(x;d) = p(d)v_{eq}(d\to 0) \tag{141}$$

where $p(x)$ is the volume reduction factor for x-spacings, and $p(d)$ the volume reduction factor for ridge density d. From (21)

$$v_{eq}(d \to 0) = \frac{\pi}{2}\left(\langle v_l \rangle - \langle w_l \rangle \langle H \rangle\right) \quad . \tag{142}$$

The link cross-sectional volume v_l and link width w_l in are related to the link sail height h_l and block thickness H by a link cross-sectional model, Section 2.2.6. The averages $\langle v_l \rangle$ and $\langle w_l \rangle$ are then obtained with the joint distribution $g(h_l|H)g(H)$ (Section 2.4.2). However, these averages are not straightforward to obtain for the following reasons:

1. The distribution $g(h_l|H)g(H)$ is not known and only $g(h_l)$ is available.
2. The distribution $g(h_l)$ is not directly determinable from data but must be inferred from observed $f(h_{cs})$ and $f(h_{cs}|h_l)$.
3. The published cross-sectional data cannot as such be interpreted to give $v_l(h_l,H)$ and $w_l(h_l,H)$ but must be scaled.
4. The sail height statistics have cutoff h_0 and thus $\langle h_{cs} \geq h_0 \rangle$ must be related to $\langle h_{cs} \geq 0 \rangle = \langle h_l \rangle$, and $d(h_{cs} \geq 0)$ related to $d(h_{cs} \geq h_0)$.

These problems are addressed in Section 7.3. The parameterised cross-sectional model is then in Section 7.5.1 used to estimate $v_{eq}(d \to 0)$. Before the estimation of clustering effect, Section 7.4 discusses cluster morphology and the plausibility of simple keel overlap models in cluster description. Relevant data from the literature is collected and some Baltic clusters analysed. The magnitude of the volume reduction $p(d)$ factor is then calculated by a simplistic model, after which $\varphi(d)$ is obtained. The results are finally compared with direct observations of equivalent thickness in Section 7.5.2.

7.3. A cross-sectional volume model for surface profile data

7.3.1. A model for sail link height distribution

The sail link height h_l is the average elevation of sail link crest. The distribution $g(h_l)$ is not directly determinable from surface profiles and measurements of individual sail links. From this data, on the other hand, distributions $f(h_{cs} \geq h_0)$ and $f(h_{cs}|h_l)$ can be determined in which case (16) is an integral equation for $g(h_l)$. The following distribution triple was given in Lensu (1995b)

$$f(h_{cs} \geq 0) = \frac{1}{\langle h_{cs} \rangle} \exp\left\{ -\frac{h_{cs}}{\langle h_{cs} \rangle} \right\} \tag{143a}$$

$$f(h_{cs}|h_l) = \frac{\pi h_{cs}}{2h_l^2} \exp\left\{ -\frac{\pi}{4h_l^2} h_{cs}^2 \right\} \tag{143b}$$

$$g(h_l \geq h_{\min}) = \frac{1}{\pi} \frac{2}{\langle h_l \rangle - h_{\min}} \exp\left\{ -\frac{1}{\pi} \left(\frac{h_l - h_{\min}}{\langle h_l \rangle - h_{\min}} \right)^2 \right\} . \tag{143c}$$

Here (143a) is the negative exponential model for $f(h_{cs} \geq h_0)$ extrapolated to zero elevation. The Rayleigh distribution (143b) for link height variation was determined from several ridges in the Baltic, comprising in total 2200 meters of sail measured with average interval 3.3 m (Lensu 1994a,b). Normal distribution has been previously proposed by Hibler and Ackley (1975). The link height distribution (143c) with $h_{\min}=0$ is then obtained from the integral equation (16). It was proposed by Hibler et al. (1972) to describe ridge heights. This result agrees with the observation that pencil-beam instruments like profilometer produce negative exponential distribution (Tucker et al. 1979, Wadhams 1980, 1981, Kreider and Thro 1981,Weeks et al. 1989, Granberg and Leppäranta 1999, Lewis et al. 1993, Lensu 1993b, 1995a, 1998b, 1999b) while (143 c) is obeyed better by data from wider beam measurements, visual observations and stereographic surveys which all observe a certain width of the sail (Hibler et al. 1972, Lytle and Ackley 1991, Sayed and Frederking 1991). For keel draft the results are similarly beam width dependent as suggested first by Wadhams and Horne (1980).

As discussed in Section 6.2.1, the negative exponential $f(h_{cs} \geq 0)$ gives unrealistically high density $d(h \geq 0)$ from the observed $d(h \geq h_0)$. However, as values $h_{cs}=0$ are observed in field measurements of $f(h_{cs}|h_l)$ this must hold for $f(h_{cs})$ as well. On the other hand, $g(h_l \geq h_{\min})$ must have $h_{\min}>0$ as some sail is always found. Then $f(h_{cs})$ deviates from exponential model increasingly when h_{cs} approaches zero. The $f(h_{cs} \geq 0)$ numerically calculated for different $h_{\min}>0$ gives lower densities $d(h \geq 0)$ but changes little $f(h_{cs})$ above $h_{\min}$ (Lensu et al. 1996). Basing on this observation a simplified procedure is adopted here. It is assumed that negative exponentiality holds for $f(h_{cs} \geq h_{\min})$ and that

$$h_{\min} = r\langle h_l \rangle \ , \ \langle h_l \rangle = \langle h_l \geq h_{\min} \rangle = \langle h_{cs} \geq h_{\min} \rangle \tag{144}$$

where r is a parameter to be estimated later in Section 7.3.5. That is, also (143 a,b) are shifted upwards by $h_{\min}$. The negative exponential $f(h_{cs} \geq h_{\min})$ gives the following relations to the average sail height $\langle h_{cs} \geq h_0 \rangle$ of cutoff data. The minimum link height is

$$h_{\min} = \frac{r}{1-r} \left(\langle h_{cs} \geq h_0 \rangle - h_0 \right) \tag{145}$$

the average link height is

$$\langle h_l \rangle = \langle h_{cs} \geq h_{\min} \rangle = \frac{1}{1-r}\left(\langle h_{cs} \geq h_0 \rangle - h_0\right) \tag{146}$$

and the ridge density extrapolation factor is

$$\frac{d(h_{cs} \geq h_{\min})}{d(h_{cs} \geq h_0)} = \exp\left\{-\frac{r}{1-r}\right\}\exp\left\{\frac{h_0}{\langle h_{cs} \geq h_0 \rangle - h_0}\right\} \ . \tag{147}$$

The second moment of (143c) is

$$\langle h_l^2 \rangle = \left(\tfrac{\pi}{2}-1\right)\left(\langle h_l \rangle - h_{\min}\right)^2 + \langle h_l \rangle^2 = \left(\left(\tfrac{\pi}{2}-1\right)(1-r)^2 + 1\right)\langle h_l \rangle^2 \ . \tag{148}$$

This is required in the derivations to follow.

7.3.2. Estimation of link cross-section parameters from published data

As $\langle h_{cs} \rangle = \langle h_l \rangle$ and $\langle v_{cs} \rangle = \langle v_l \rangle$ the relationships between $\langle h_l \rangle$, $\langle H \rangle$ and $\langle v_l \rangle$ would be obtainable from a large sample of (h_{cs},v_{cs},H)-determinations. However, the reported measurements do not usually refer to random cross-sectional heights h_{cs}. Field studies involve the choice of target ridges and cross-section locations. Detached, large ridges are preferred. The cross-section are often selected across the highest point of some sail segment while h_{cs} refers to a random point in the segment and h_l to its average height. Tucker et al. (1984) specify explicitly that the highest sail point within 0.5 km from each helicopter landing site was chosen.

The results usually report linear dimensions of ridge cross-sections, which include sail height, keel draft, keel width, and sail block thickness. Structural dependencies between these are obtained by fitting some assumed functional dependency to the data. The relation of volume to sail height has usually not been determined directly. It must be calculated from other structural relationships after assuming a cross-section geometry. Another shortcoming is the deterministic relationship between block thickness and sail height. This does not fit together with the large height variation found also in ridge fields created from level ice with constant thickness.

A detached ridge sail link with height h_l and length l is considered. It is assumed that only one cross-section across the highest sail point h_{max} has been made. Thus h_l should be related to h_{max} and l. The variation of sail link height is assumed to follow (143b). The random cross-section volume v_{cs} is assumed to vary only little

around the link cross-section volume v_l. This is also supported by observations. Veitch et al. (1991) made six cross-sections every 10 meters across a detached ridge and the cross-sectional volumes varied from 98 m^2 to 126 m^2. No indications of shearing differential movement were present. Lensu et al.(1998) made six cross-sections across a sinuating ridge with an apparent shearing component and the volumes varied from 73 m^2 to 129 m^2. Thus any cross-section is expected to give a keel volume estimate within reasonable error bounds. On the other hand, the sail height variation cannot be neglected as will become apparent below.

The link sail has essential height variation from the vertical arrangement of sail blocks, and inessential variation from the block angles. The sail height h_{cs} at a certain location is now defined as the average elevation of the crest block at the location. Thus the sail is idealised as a step curve where the step length ΔL is the scale of the tilted blocks in a horizontal plane. Block size is assumed to scale with characteristic length (Tucker and Govoni 1981). From the block size and block angle data of Kankaanpää (1997) the relationship $\Delta L=2.4H^{3/4}$ for block thickness H is obtained. This includes also the effect of block angle. The step elevation h_{cs} is assumed to follow (143b) and the expected maximum sail height for a link is

$$E_{\max}(h_{cs}) = \lambda(n)h_l = \frac{1}{\sqrt{\pi \ln n}}(2\ln n + 0.58)h_l, \quad n = l/\Delta L, \quad \Delta L = 2.4H^{3/4} \tag{149}$$

from the extremal statistics of (143b) (Lensu et al. 1996). As $\lambda(10)=1.9$, $\lambda(75)=2.5$, and $\lambda(1000)=3.1$, the value $n=75$ is chosen. This corresponds typically to few tens of meters as ΔL is 0.5 m, 1 m and 1.5 m for block thicknesses 0.12 m, 0.31 m, 0.53 m of respectively. Thus the measured sail height is assumed to be 2.5 times link height h_l on the average.

Therefore, to obtain the structural relationships for the average link cross-section a scaling by factor 2.5 of ridge height in the published data is adopted. That is, the sail height values h are replaced by $h=2.5h_l$. This means a correction factor 6.25 in the relationship between sail height an cross-sectional volume. The lower bound of the height correction factor is assumed to be 2. Thus the volume of ridged ice is expected to become underestimated at least by factor 4 if the unscaled ridge structure models are applied to surface profile data. This error is much larger than that involved to the estimation of link volume from only one cross-section.

7.3.3. A model for link cross-section parameters

Relationships between ridge structure parameters are now extracted from published data and scaled with the assumed correction factor. A double triangular

model link cross-section geometry is used (Figure 5). It is assumed that h_l is proportional to $\sqrt{H}$, and that the relationships between h_l, draft d_l and keel width w_l are linear. It follows from these assumptions that $c+w_l$ is constant. This constant is not affected by the use of the correction factor. The ice consumption c varies then only little as usually $c>>w_l$. This result is supported by the discrete element simulations of Hopkins (1998). As the structural parameters are obtained as functional fits to distributed quantities, the result is to be interpreted rather as an indication of statistical independence of $c+w_l$ or c on the other structure parameters.

The contribution of sail to the average cross-sectional volume v_l is small. For sail volume the ratio 3.4 of sail width to sail height from a well sampled sail link measurement of Manninen (1996) is used. The porosity is assumed to be 0.32 (Veitch et al. 1991, Leppäranta et al. 1995). Measurements made across the highest point of a sail segment are assumed to give the relation $h = b\sqrt{H}$, keel depth to sail height ratio k, and keel width to keel depth ratio l. Including the correction factor 2.5, the structural relationships of the link cross-section model are then

$$
\begin{aligned}
h_l &= 0.4bH^{1/2} \\
d_l &= 2.5kh_l \\
w_l &= ld_l = 2.5klh_l \\
v_l &= (2.1k^2l + 1.2)h_l^2 = \eta h_l^2
\end{aligned}
\qquad \text{(150 a-d)}
$$

where the structure parameters k and l and b are to be estimated from published results.

A range of values can be found for k, l and b. For the keel depth to sail height ratio Timco and Burden (1997) report k=3.95, Kankaanpää (1997) finds k=6.3 for Baltic ridges and the Arctic studies referred by her have k=4.1-5.5. The higher Baltic value may be a consequence of methodology or different ridge buildup characteristics. Bowen and Topham (1996) have k=4.1 determined from 144 profiles across section maxima of a single long ridge. A linear fit by Timco and Burden (1997) gives the keel width to keel depth ratio l=3.91. Kankaanpää (1997) does not have a linear fit for l but an estimate of the same order is obtained from the average keel slope angle. There is a good agreement between the keel slope angles as Kankaanpää (1997) found 29, Timco and Burden (1997) 27, and Kovacs (1972) 33. The parameter ranges are thus k=4...6 and l=3.5...4, so that the range of the factor η is from 123-317. The lower range of k more probably refers to local sail maxima and the value k=4 is adopted. For l the median value 3.75 is taken and thus η=129.

The parameter b is problematic as $g(h_l|H)$ is expected to have considerable variation and a functional dependence is clearly a coarse assumption. The range from 2.8 to 5.24 for b is found in the literature. Here 2.8 is Baltic value from Kankaanpää (1997), while the value 5.24 by Tucker et al. (1984) is the upper envelope of their data as well as that of the pooled published data in Kankaanpää (1997). The value b=3.71, obtained by fitting to data in Tucker et al. (1984), is chosen as the sail height values are reported to refer to sail maxima. The total length of parent ice contained into a ridge link is then 290 m and the ice consumption is of the same order.

The average structural relationships for links with sail height h_l are then summarised as

$$\begin{aligned} h_l &= 1.5H^{1/2} \\ d_l &= 10h_l \\ w_l &= 37.5h_l \\ v_l &= \eta h_l^2 = 129h_l^2 \\ c &= 290 - w_l = 290 - 37.5h_l \end{aligned} \qquad \text{(151 a-e)}$$

7.3.4. Comparison of the link cross-section model with observations

As $\langle h_{cs}\rangle = \langle h_l \rangle$, the ratio 10 in (151b) is comparable to the results of Wadhams (1980) who measured keel draft and sail height along corresponding tracks in the Arctic. The cutoff values were d_0= 9 m and h_0=0.98 m respectively. The ratio of average keel draft to average sail height varied for the ten sections from 8.5 to 10 and was 9.1 for the pooled data set. Wadhams (1981) gave a linear regression result $\langle d_{cs}\rangle = 9.5\langle h_{cs}\rangle - 1.8$ between keel draft and sail height. The ratio 10 is also the upper envelope of cross-sectional sail/keel data both in Kankaanpää (1997) and Timco and Burden (1997).

The value η=129 was estimated from linear dimensions with a simple cross-section geometry. However, there are few cases where sail height and measured cross-sectional volume are reported. Lensu et al. (1998) measured 0.78 m and 0.33 m high ridges, both along seven profiles, finding η=236 and η=875 respectively. Leppäranta et. al (1995) cross-sectioned a gradually weathering ridge thrice along the same profile during the ice season. Sail heights were 1.08, 1, and 0.6 m and η was 106, 126 and 337, and the average is 190. Lensu (1993c) profiled a large detached ridge across highest sail point (3.02 m) and η=24 can be estimated from

the data. Another similar ridge (h_{cs}=1.7 m) had η=29 while a more diffuse ridge with three sails (max h_{cs}=0.87 m) had η=163 or roughly η=54 per sail. Reanalysis of the Veitch et al. (1991) data, where two ridges with equal H were profiled along eight and six equally spaced lines, gives η=(807,355,195,811,176,262,243,228) and η=(55,45,50,25,54,79) respectively. The average values were η=322 and η=71 respectively (sail heights 0.75 m and 1.53 m). Bowen and Topham (1996) report that a 300 m long ridge section contained three times as much ice as calculated by cross-sectional models. These references include cross-sections across sail maximum, as well as and random cross-sections, and η varies within two magnitudes. Leaving the largest value out, their average is η=132, otherwise η=225. Thus it is observed that the variation is very large and that the suggested value η=129 should at least not be an overestimation. Without the suggested correction factor 6.25 for the keel volume, the value η=21 would have been found.

7.3.5. Relations between averaged cross-sectional parameters

The link structure relations (151) are now averaged over link height distribution $g(h_l)$ and, using (144-148), expressed in terms of the observed average $\langle h_{cs} \geq h_0 \rangle$ of cutoff data. The result is

$$\left\langle h_{cs} \geq h_0 \right\rangle - h_0 = (1-r)\left((1-r)(\tfrac{\pi}{2}-1)+1\right)^{-1/2} 1.5 \left\langle H \right\rangle^{1/2} \tag{152a}$$

$$\left\langle d_l \right\rangle = \frac{10}{1-r}\left(\left\langle h_{cs} \geq h_0 \right\rangle - h_0\right) \tag{152b}$$

$$\left\langle w_l \right\rangle = \frac{37.5}{1-r}\left(\left\langle h_{cs} \geq h_0 \right\rangle - h_0\right) \tag{152c}$$

$$\left\langle v_l \right\rangle = \left((1-r)(\tfrac{\pi}{2}-1)+1\right)\frac{1}{(1-r)^2} 129 \left(\left\langle h_{cs} \geq h_0 \right\rangle - h_0\right)^2 \tag{152d}$$

$$\left\langle c \right\rangle = 290 - \frac{37.5}{1-r}\left(\left\langle h_{cs} \geq h_0 \right\rangle - h_0\right) \tag{152e}$$

The equivalent cross-sectional volume $v_{eq}(d \to 0)$ is obtained with (142) and the equivalent thickness of ridge rubble without clustering effect is

$$H_{eq}(h_{cs} \geq h_{\min}) = d(h_{cs} \geq h_0)\frac{d(h_{cs} \geq h_{\min})}{d(h_{cs} \geq h_0)} v_{eq}(d \to 0) \tag{153}$$

where the fraction is the extrapolation factor (147).

The value of r is obtained by estimating a lower envelope $h_{\min}=1.78H^{1/2}=b_{\min}H^{1/2}$ from Tucker et al. (1984) data on sail height and block thickness. The resulting value is $r=b_{\min}/b=0.48$. The parameterised relations (145-147) are then

$$h_{\min} = 0.92\left(\langle h_{cs} \ge h_0 \rangle - h_0\right) \tag{154}$$

$$\langle h_l \rangle = \langle h_{cs} \ge h_{\min} \rangle = 1.92\left(\langle h_{cs} \ge h_0 \rangle - h_0\right) \tag{155}$$

$$\frac{d(h_{cs} \ge h_{\min})}{d(h_{cs} \ge h_0)} = 0.40 \exp\left\{\frac{h_0}{\langle h_{cs} \ge h_0 \rangle - h_0}\right\} \tag{156}$$

and the parameterised relations (152) are

$$\langle h_{cs} \ge h_0 \rangle - h_0 = 0.68\langle H \rangle^{1/2}$$

$$\langle d_l \rangle = 19\left(\langle h_{cs} \ge h_0 \rangle - h_0\right)$$

$$\langle w_l \rangle = 72\left(\langle h_{cs} \ge h_0 \rangle - h_0\right) \tag{157 a-e}$$

$$\langle v_l \rangle = 619\left(\langle h_{cs} \ge h_0 \rangle - h_0\right)^2$$

$$c = 290 - 72\left(\langle h_{cs} \ge h_0 \rangle - h_0\right)$$

The equivalent cross-sectional volume (142) for detached ridges is

$$v_{eq}(d \to 0) = 972\left(\langle h_{cs} \ge h_0 \rangle - h_0\right)^2 - 245\left(\langle h_{cs} \ge h_0 \rangle - h_0\right)^3 \tag{158}$$

and equivalent thickness (153) without clustering effect is

$$H_{eq}(h_{cs} \ge h_{\min}) = 0.40 d(h_{cs} \ge h_0) \exp\left\{\frac{h_0}{\langle h_{cs} \ge h_0 \rangle - h_0}\right\} v_{eq}(d \to 0) \tag{159}$$

The values for 0.5 m cutoff in Table 6 appear reasonable. The parent ice thickness relation is sensitive to the parameter r. The value of H for typical Baltic value $\langle h_{cs} \ge h_0 \rangle$=0.75 m appears somewhat small. On the other hand, the values of H for the Kara sea data of Chapter 6, with $\langle h_{cs} \ge h_0 \rangle$ ranging from 0.85 to 1.01 m, are reasonable. The uncertainty in the estimate for H due to lacking proper statistics is large. On the other hand, it is seen that the equivalent thickness is not very sensitive to present assumptions on r, H and h_{min}. Using r=0 instead would give

H_{eq}=0.147d(h_{cs}≥0.5) for the Baltic standard case $\langle h_{cs} \geq h_0 \rangle$=0.75, while H would decrease to 0.04 m. The parameter η is of decisive importance in the volume estimates.

Table 6. The values for volume model (157-159), parameterised by profile data parameters $\langle h_{cs} \geq h_0 \rangle$ and $d(h_{cs} \geq h_0)$, for h_0=0.5 m. The volume model applies to detached ridges.

Observed ridge height	$\langle h_{cs} \geq 0.5 \rangle$	m	0.65	0.75	0.85	0.95	1.05
Parent ice thickness	$\langle H \rangle$	m	0.05	0.14	0.26	0.44	0.65
Minimum link height	h_{min}	m	0.14	0.23	0.32	0.42	0.51
Extrapolated ridge height	$\langle h_{cs} \geq h_{\min} \rangle$	m	0.29	0.48	0.67	0.86	1.06
Equivalent cross-sectional volume	$v_{eq}(d \to 0)$	m^2	21	57	108	174	253
Ridge density extrapolation factor	$\frac{d(h_{cs} \geq h_{\min})}{d(h_{cs} \geq 0.5)}$		11.14	2.94	1.66	1.21	0.99
Equivalent thickness of ridge rubble for observed unit density	$\frac{H_{eq}(h_{cs} \geq h_{\min})}{d(h_{cs} \geq 0.5)}$	m	0.234	0.168	0.179	0.238	0.250

7.4. Ridge clusters

7.4.1. Observations on ridge clusters

In a cross-sectional ridge cluster several sails correspond to one continuous keel formation. From the profile data it appears likely that such formations are common. The median spacing for B93, B94 and B97 is 65 m, 50 m and 13 m respectively. The extrapolation factor of Table 6 for the Baltic value h_{cs}=0.75 m gives then median spacings 22 m, 17 m and 4 m. From (157c) the average detached keel width $\pi/2\langle w_l \rangle$ along linear transect across an isotropic ridge field is then 28 m. Clusters are thus expected to be common. As systematic data on clustering is lacking, simple structure models in terms of overlapping keels have been suggested. In this section cluster observations reported in literature and indirect indications on them are summarised and discussed. In Section 7.4.2 the morphology of a large Baltic cluster is analysed. These then suggest a preliminary typology and formation hypothesis for clusters in Section 7.4.3.

In Figure 34 a B94 surface profile with spacing mean 132 m and median 17 m is compared with electromagnetic thickness sounding (Multala et al. 1996). The EM reference level is ambiguous but does not affect relative thickness differences. The

EM system gives a weighted average of ice thickness over an area with typical diameter 100 m and does not reproduce shape and depth of keels realistically. However, keel signatures are clearly seen. Narrow keels with a single sail are seen between 3000 m and 3800 m. The keel at 2200 m has no sail and thus a large ridge may be unnoticed in surface profiles. In the majority of cases a 100-300 m wide sail group corresponds to keels separated by less deformed 0.5-1 km long sections. The 250 m wide group at 1000 m contains 27 sails, the average spacing is less than 10 m, and a continuous keel formation is expected to lie beneath. The surface/subsurface correspondence becomes striking when presented by 100 m freeboard/draft averages.

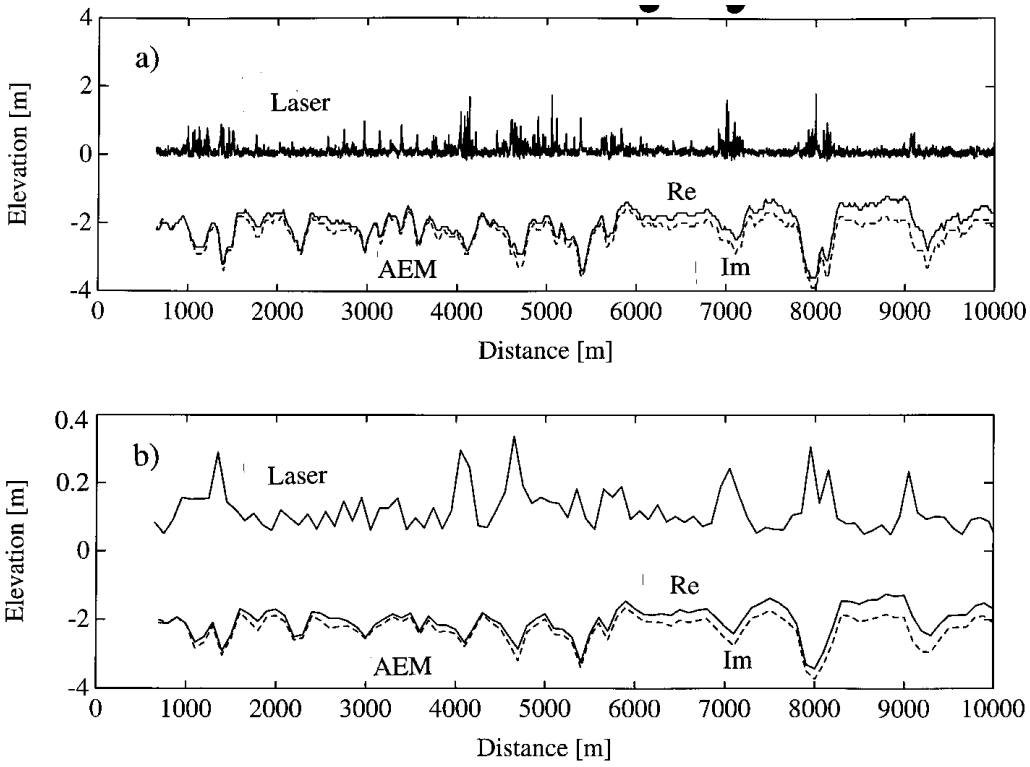

Figure 34. a) Simultaneous laser surface (from B94) and EM draft profile. b) The profiles averaged in 100 m segments. The Re- and Im-components are related to the phase shift of the EM-fields.

Also in the Arctic there is evidence on clusters in profile data. Wadhams (1980) compared laser and submarine sonar data for 10 profile pairs. The mean keel draft and sail height were 14.2 and 1.56 m for 9 m and 0.98 m cutoff values. Keel density varied from 3.0 to 4.4 and sail density from 12.4 to 29.7 and the overall values were 3.7 and 19.8. Thus 5.4 sails corresponded to one keel on the average. Wadhams (1981) gave the relation d_s=4.17d_k –0.71 for keel and sail densities. Connors et al. (1990) studied local ice topography with a sonar along densely

spaced parallel tracks. What was from surface a 400 m wide rubble field consisted of eight keels with drafts from 3 to 10 m. Melling and Riedel (1995) show the profile of a 300 m wide and 25 m deep keel with six minima. They also compared counts of keels exceeding 5 m by the Rayleigh criterion, and by what was called level ice criterion. The latter identified keels as deformed ice sections between level ice sections and does not separate adjacent minima of contacting keels. The level ice criterion identifies thus clusters as basic features. For Rayleigh criterion the keel density was 1.44 times higher than that for level ice criterion. This ratio is thus the average number of Rayleigh separated keels in clusters.

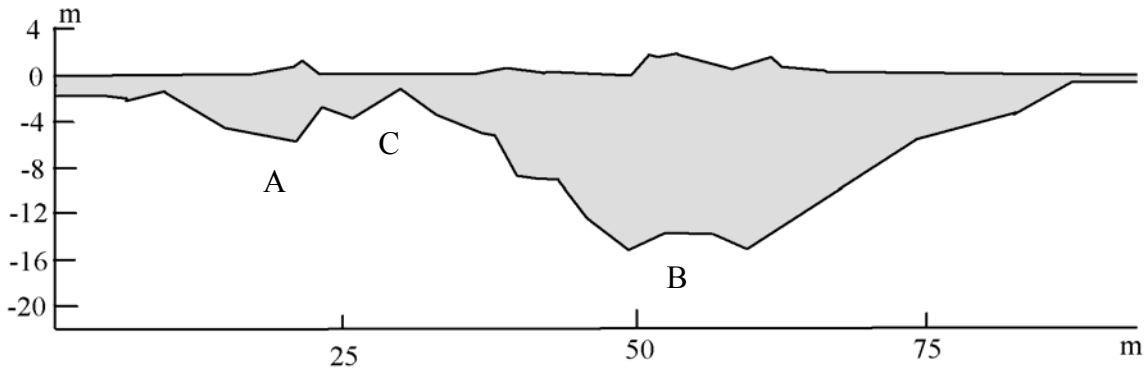

Figure 35. A ridge cluster cross-section from the Bay of Bothnia, drawn after Kankaanpää (1997).

There a few cross-sections from clusters. Kankaanpää (1997) shows three profiles with keel contact. In the first 5 m and 9 m deep ridges have with 1.5 m thick junction. Both ridges have a single sail and their separation is 10 m. The second profile (Figure 35) shows 6 and 15 meter deep ridges *A* and *B* with a 2 m thick junction *C*. The larger ridge has 1.8 and 1.5 m high sails and two equally deep keel minima, both pairs with 10 m separation, while the separation between the sails of the two ridges is 30 m. The keel overlap description applies to the larger ridge well. Another profile from the same site shows 8 and 13 m deep ridges with singular keel minima and 4 m thick junction. The bigger ridge has three sails, two above the keel minimum and separated by 10 m, and one 30 m off above the junction. The smaller ridge has no sail. Some of the detached keels in Kankaanpää (1997) have a shallow side sail near the keel edge. Palosuo (1971) shows adjacent 50 m and 70 m wide clusters with 4 and 5 sails respectively. Reynolds and Lindholm (1992) show a ridge with a 6 and 7 m deep keels and two shallow sails, both pairs separated by a 10 m distance, and a ridge with three sails and three keel minima is found in Lensu (1993c). Melling et al. (1993) show cross-section with 16 and 9 m deep keels joined by a 5 m thick junction, and Bowen and Topham (1996) a keel with three minima corresponding to a 45 m wide multiply peaked group of sails. Weeks et al. (1971) show one two-keel cluster with three sails.

7.4.2. The structure of a large Baltic ridge cluster

Figure 36 shows a large cluster measured by laser profilometry, levelling, and drilling in the Bay of Bothnia 1994. Here, the sail cluster is the formation between 0 and 200 m, consisting of component sails. The keel cluster and component keel are defined likewise. The parent ice thickness was H=0.6 m, typical block size 2x3 m^2, maximum sail height 3.5 m, and maximum keel depth 13.5 m. The average draft over the keel cluster was 8.1, m and average freeboard over the sail cluster 0.82 m. The cross-sectional volume is 1600 m^2 and corresponds to 2600 m or parent ice. The keel cluster keel has four component keels with average keel draft d_l=12.5 m.

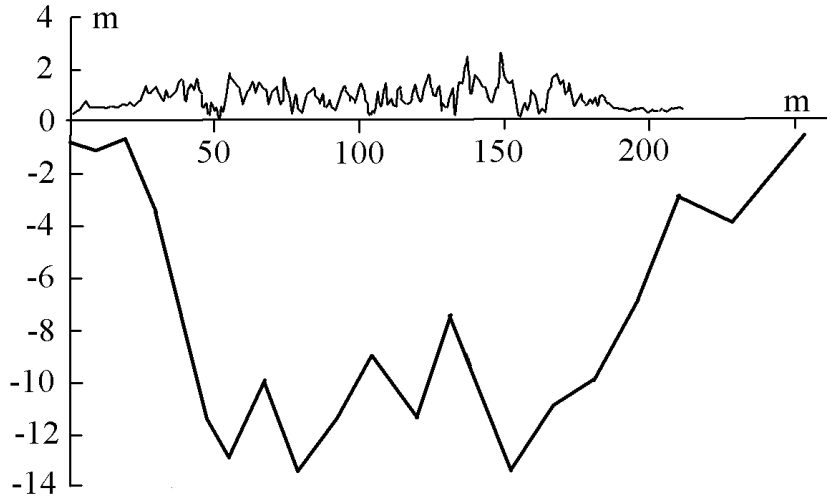

Figure 36. A large ridge cluster from the Bay of Bothnia; a laser profile along the drilled draft profile is shown (Courtesy Aker Finnyards).

In the eight laser profiles crossing the sail cluster its width varied from 150 to 200 m and the average number of Rayleigh separated component sails exceeding 0.5 m was 29. There was no height correlation (ρ=0.03) between adjacent sails, and the overall maxima of the eight profiles were in different locations and did not concentrate to either side. Height and spacing averages for component sails were h_l=1.18 m and $\langle x \rangle$=5.8 m. The distribution of component sail height $f(h_{cs}|h_l)$ followed (143 b). That is, statistically, the sail cluster appears as one sail link rather than a group of several links. The ratios d_l/h_l=10.6 and $h_l/H^{1/2}$ =1.52 agree with (151). The expected maximum of the sail calculated by (149) is 3.3 m which is near the observed maximum 3.5. Thus the suggested volume model applies well. The cluster volume is only 30 % from that obtained by using (151 d) to each component sail, that is, without considering the clustering effect.

7.4.3. Types of ridge clusters and their formation

There is thus enough evidence on the presence of clusters although quantifying structural studies are few. Clusters may contain several tens of sails and the number is apparently not limited. Rubble fields are found to have keel structure and can be interpreted as large clusters. The number of Rayleigh separated component sails may be five times the number of Rayleigh separated component keels. Multiple sails with multiple keel minima may be found in what are interpreted as detached unusually wide ridges.

On the basis of the observations two mechanisms of cluster formation are suggested.

- Type I clusters are created by lateral ridge growth. As the first sail-keel pair is fully grown, a sail growth is initiated at a new location, above the keel or at the keel edge, and is associated with lateral accumulation of the keel.
- Type II clusters a created as all level parent ice between two ridges used up, so that the growing keel becomes into contact with an already existing one.

A simple structural model is obtained by superposing triangular ridge models, one for each sail, and by removing the overlaps. This is not a bad assumption for the profile in Figure 35. If the formation of a new sail is triggered above the existing keel or at the keel edge (Type I), several sails may be located over a single component keel. On the other hand, if the keels are brought into contact by parent ice consumption (Type II), this is unlikely, and only one sail per component keel is expected.

In this typology, the ridge of Figure 35 is a Type II cluster, composed from a singular ridge on the left together with a two-sail Type I cluster on the right. The cluster in Figure 36 is of type I. Assuming triangular overlap model it follows that the Rayleigh criterion tells the component keels of Type II clusters apart, while Type I clusters are interpreted as one keel. In Section 6.3.6 the length of x_0-concatenations was found to have a lognormal distribution. If Type I clusters can be characterised by sail spacing threshold x_0 the width of Rayleigh separated keels should follow lognormal distribution. This was also found by Davis and Wadhams (1995). If forcing and parent ice supply persist, there is no apparent physical limit to the width of Type I clusters. Lineated rubble fields may be considered as extremal cases of Type I clusters. Kovacs (1972) shows an aerial mosaich of a rubble field with sail heights up to 7 m and with a lineation ‘not unlike that of a farmers harrowed field’. Similar lineation can be seen in the rubble field images in Palosuo (1975). Connors et al. (1990) found a clear keel structure in such a field.

The structure of cluster in Figure 36 suggests lateral growth by widening of the keel and by simultaneous sail creation events outside the sail group. Tucker et al. (1984) suggested that wide ridges and rubble fields are created by continued buckling failure. Assuming that the sails have been initiated by buckling failures, the range 1-10 GPa for Young's modulus gives range 5.3-9.4 m for the failure location $(\pi/4)L_c$ in terms of characteristic length L_c (Parmerter and Coon 1973). This corresponds well to the observed $\langle x \rangle$=5.8 m. The observation that the cluster has several keel minima hints to the following formation cycle. New sails are created above the keel until the keel boundary is reached and a phase of keel growth follows. As the keel growth ceases, a new sequence of sail creation events follows. From (151c) the half-keel width $w_l/2$ for a detached ridge with h_l=1.18 m is 22 m, while the average distance of keel minima in Figure 36 is about 25 m. The sails also appear to arrange into groups about 25 m wide. Phenomenologically this formation hypothesis is not much different from the Parmerter and Coon (1973) model where the ridge can extend endlessly laterally through a cyclic repetition of the single keel/sail formation, producing sail and keel rubble beds in isostatic equilibrium.

Continuing lateral keel accumulating associated with a sail group formation was also observed in ice tank tests by Tuhkuri and Lensu (1998), as well as that persistent sail forms only after the keel has attained certain size. The cluster in Figure 36 can be also compared with discrete element simulations by Hopkins (1998). Thin lead ice was pushed against a thick multiyear floe. The first phase of the buildup is thus different. The sail attained maximum height at 200 m ice consumption, after which the feeding of the parent ice was continued. This phase, on the other hand, can be assumed to be comparable with the present considerations A wide keel, growing also constantly deeper was created. For 0.9 m parent ice a 130 m wide and 15 m deep keel formed after 1300 m parent ice consumption. The parent ice was also failing above the keel, feeding the keel from above along its whole width rather than laterally. The shown profile is averaged over many simulations and does not have distinctive keel minima or additional sails. Otherwise the structural similarity with Figure 36 is evident.

7.5.Equivalent thickness of ridge rubble

7.5.1.The effect of ridge clustering

The relations (158,159) apply for detached ridges which have no keel contact with other ridges. The effect of ridge clustering to the volume of ridged ice is now estimated. As the applicability of ridge structure models in a statistical context including clusters is yet uncertain, only a very coarse approach to the volume reduction by ridge clustering is motivated. It is assumed that the relationship

(151c) holds between cross-sectional sail height h_{cs} and cross-sectional keel width w_{cs} which are both exponentially distributed. The x-spacing geometry is described by assigning identical ridges to the spacing ends and by subtracting the overlap. The keels overlap if $(\pi/2)w_{cs}>x$ and the linear dimensions of the triangular overlap follow then negative exponential distribution. The average cross-sectional volume of an overlap, on the condition that overlap occurs on the x-spacing, is then equal to average keel cross-sectional volume. This follows from the properties of negative exponential distribution. Neglecting the sail volume, the effect of clustering can then be estimated by multiplying the ridged ice volume by p, where 1-p is the probability that overlap occurs, or the relative number of spacings with overlap. It is approximated also $h_{\min}=0$ or $r=0$, as this parameter was found to have only a minor effect in the ice volume considerations. With lognormal spacing model and negative exponential keel width model

$$1-p(d)=\int_0^\infty dx\Lambda(x;\mu,\sigma)e^{-x/a}\ ,\ a=\frac{\pi}{2}37.5\left(\left\langle h_{cs}\ge h_0\right\rangle-h_0\right). \tag{160}$$

where $p(d)$ is the volume reduction factor in (141) and a is from (152c) with $r=0$. The integral was calculated numerically for the Baltic standard case $h_0=0.5$ m, $\langle h_{cs}\ge h_0\rangle=0.75$ m which give $a=15$. Two cases were considered: the semiempirical spacing distribution model (105) for $h_0=0.5$ m data, with geometric standard deviation depending on ridge density, and constant value $\sigma=4.1$ (Figure 37). In the first case clustering effect is significant for low ridge densities also, and a linear model of the volume reduction factor applies

$$p(d)=-0.0075d+0.70,\ \ d=d(h_{cs}\ge 0.5). \tag{161}$$

For the constant $\sigma=4.1$ case the fit

$$p(d)=\exp\left\{-0.094(d-1)^{0.67}\right\},\ d=d(h_{cs}\ge 0.5) \tag{162}$$

may be used. From (159) and the linear model (161) the estimate of equivalent thickness for 0.5 m cutoff data is

$$H_{eq}(h_{cs}\ge h_{\min})=0.40d(0.7-0.0075d)\exp\left\{\frac{0.5}{\left\langle h_{cs}\ge 0.5\right\rangle-0.5}\right\}\left(\left\langle h_{cs}\ge 0.5\right\rangle-0.5\right)^2 \tag{163}$$

where $d=d(h_{cs}\ge 0.5)$ is the observed ridge density. The model (161) was derived with the semiempirical spacing distribution (116) for $h_0=0.5$ m data and, on the other hand, used negative exponential distribution for $h_0=0$ to calculate the

overlaps. Thus it underestimates, within the assumptions of the present simple model, the clustering effect. In the Baltic standard case $\langle h_{cs} \geq 0.5 \rangle$=0.75, Table 6, the following estimate can be used

$$H_{eq}(h_{cs} \geq h_{\min}) = d(0.7 - 0.0075d)0.178,\ d = d(h_{cs} \geq 0.5)\ . \tag{164}$$

Thumb rules obtained by neglecting the quadratic term are H_{eq}=0.125d(h_{cs}≥0.5) and the ice consumption per unit ridge density c_{eq}=(π/2)0.7c=300 m.

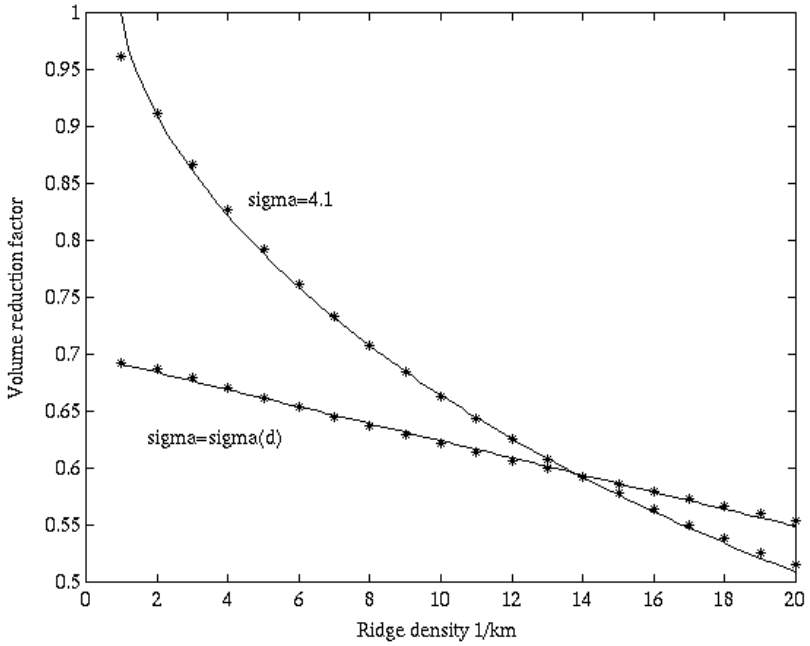

Figure 37. The volume reduction due to ridge clustering.

The equivalent cross-sectional volume $v_{eq}(d)$ is (158) multiplied by $p(d)$. Using (158), (161), and parent ice thickness (157a) in (140), the Baltic standard case relations between Lagrangian ice area and ridge density are

$$CA = C_0 A_0 \frac{d_0 - 0.011 d_0^2 + 3.17}{d - 0.011 d^2 + 3.17}\ ,\ d = \frac{C_0 A_0}{CA} d_0 \frac{93 - d_0}{93 - d} + 3.17 \frac{C_0 A_0 - CA}{CA} \frac{1}{1 - 0.011 d} \tag{165}$$

where d=d(h_{cs}≥0.5) has unit [1/km]. The area decrease per unit change in ridge density (139) is finally

$$\varphi(d) = -\frac{1-0.021d}{d-0.011d^2+3.17} \tag{166}$$

(Figure 38). For low ridge densities the approximation $\varphi(d)$=-1/(d+3.17) may be used.

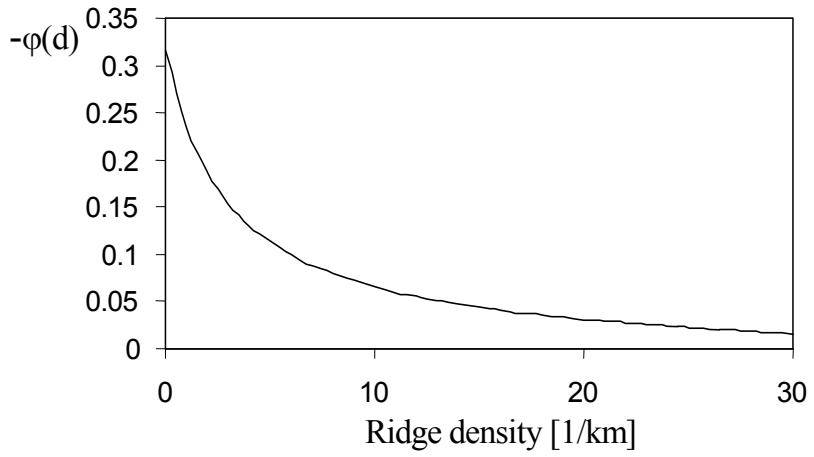

Figure 38. The factor -$\varphi(d)$, or the relative reduction in ice area per unit change in ridge density.

7.5.2.Comparison to ice volume observations

The equivalent thicknesses H_{eq} of ridge rubble from (163) are of the order 0.1d meters and larger than those previously estimated with cross-sectional models from sail statistics. This is due to the volume parameter η=129. Ridge rubble was assumed to lie above and on a parent ice sheet with thickness $\langle H \rangle$. When compared to the conventional definition of equivalent thickness the H_{eq} from (163) are smaller by $\langle H \rangle C_r$ where C_r is keel rubble coverage. The relative magnitude of this difference is small and does not affect essentially the following comparisons where the referred H_{eq} have the conventional definition.

In Kankaanpää (1997) the maximal regional estimates of H_{eq} are 0.14 m. However, the average length 290 m of parent ice per ridge in (151) is a constant determinable from published cross-sectional data and does not change in the scaling (150a-c). One detached ridge per km from parent ice thickness $\langle H \rangle$ contributes then to H_{eq} by $(\pi/2)\cdot 290\langle H \rangle$. This is already of the order of 0.05-0.1 m in the Baltic. Applying (163) to Lewis et al. (1993) results (B88), H_{eq} is estimated

to 0.50 m. This is more than the estimated level ice thickness, and about the same as the highest values in the Baltic Climatological Ice Atlas (1982).

Hibler et al. (1974) proposed a volume model based on isostacy between sail and keel and derived η=20 from cross-sectional geometry. The same value has been applied also by Lytle and Ackley (1991) and Dierking (1995). Lewis et al. (1993) had η=17.2 from Baltic cross-sectional data and extrapolated the negative exponential distribution for h_{cs} to zero. Their H_{eq} varied from 0.03 m to 0.28 m for five regions in the Bay of Bothnia with ridge densities from 1.4/km to 17.4/km. The basinwide average was not given but can be estimated to lie around 0.1 m. These suggested values of η agree with the value η=21 that would be found in the present study if the volume correction factor 6.25 would not be used.

These values of η appear too small and can be compared with direct determinations of the equivalent freeboard F_{eq} of sail ice. It is defined as the volume of sail rubble per unit area. As for other keels sail is not found or is very shallow, and as in general the sail rubble isostatically compensates only a part of the keel (Lensu et al. 1998, Kankaanpää 1997), estimates from sail rubble are lower bounds. In Lewis et al. (1993) profile elevations exceeding h_0 (=0.4 m) had coverage 0.05 and belong to ridges with $h_{cs}>h_0$. As h_{cs}-h_0=0.18 m, the equivalent freeboard F_{eq} of elevations $h_{cs}>h_0$ is estimated to (1-0.21)0.05(0.4+0.18/2)=0.02 m. Here the sail porosity 0.21 from Kankaanpää 1997 is used. This can be converted to equivalent thickness with draft-freeboard ratio. Wadhams (1981) obtained from Arctic submarine sonar and profilometer data set the relationship $draft = 8.35\,freeboard + 3.04$ where 3.04 was interpreted as level ice thickness. The draft/freeboard ratio was further studied by Wadhams et al. (1992) who give the average value is 7.89. Thus the ratio 8 will be used in the present discussion, and assuming the sail porosity 0.21 equivalent thickness is 9(1-0.21) times equivalent freeboard as determined from profilometer data. Thus in Lewis et al. (1993) the equivalent thickness from ice with freeboard exceeding 0.4 m level is around 0.18 m.

The B93 data with $d(h_{cs}\geq 0.5)$=4.9/km is from snow-free conditions. Ice was classified into ten classes by average profile elevation for 2 km segments (Lensu 1993b). Assuming that the average surface elevation of least deformed class corresponds to level ice, the equivalent freeboard F_{eq} of deformed ice varied from 0 cm to 10 cm with the average 2.9 cm. Using thickness/freeboard ratio 9 and porosity 0.21, H_{eq} was up to 0.71 m and 0.21 m on the average. For B94 data with $d(h_{cs}\geq 0.5)$=3.2/km it was estimated that the elevations exceeding 20 cm, with coverage 0.1, are ridge sail ice (Lensu 1995a). For this category F_{eq}=2.9 cm and H_{eq} is estimated to 0.21 m. The B97 data is from snow-free conditions. For elevations exceeding 20 cm, with coverage 0.3, F_{eq}=18.3 cm and H_{eq} is estimated to 1.3 m.

These estimates of H_{eq} for B93, B94 and B97 can be taken as lower bounds. The reference level of the profile data is the local elevation of undeformed ice added by snow thickness. For B94 the snow cover was 0.1 m and zero for the other two surveys, and the level ice thicknesses are about 1.3 m, 0.7 m and 0.7 m (Lensu 1994a, 1994b, Haapala and Leppäranta 1997 resp.). Thus, the level ice thickness multiplied by deformed ice coverage is first added to H_{eq}. It is assumed that the snow cover has not depressed the freeboard in B94. The estimates H_{eq} become 0.34 m, 0.35 m and 1.51 m while from (143) the values 0.58, 0.41 and 1.85 m are obtained for B93, B94 and B97 respectively. The difference is not large as not all surface rubble could be counted and the surface rubble is not expected to counterbalance the keel rubble isostatically. It is concluded that the volume is not necessarily overestimated by (143), and that in any case the estimate is more reliable than the several times smaller values submitted previously.

8. SUMMARY AND CONCLUSIONS

The creation of ridge fields can in a short time multiply the average thickness of ice cover. Their description is important for dynamic ice modelling, ice navigation and estimation of ice induced loads. In this work a theory describing the evolution of ridged ice fields has been formulated.

Ridge sail fields were quantified in terms of sail spacings and in terms of numbers of sails in line segments. Equations governing spacing and sail number distributions were formulated. These are specific versions of a general Kolmogorov-Feller equation and are derived from the basic assumption that a distribution changes through instantaneous transition events. In an evolving ridge field the transitions are due to ridge formation events and are associated, due to ice consumption, with a differential movement which is of the order of 300 m. The observed spacing distributions were related to the solutions of the spacing equation. The explaining of the observed distributions was reduced to the task of explaining the evolution parameters in the equation. Strict quantitative comparison between the statistical parameters of observed and predicted distributions was not possible. This was due to the lack of initial distribution from which the observed distribution has evolved, due to the fact that the transition events are not known well enough, and due to the asymptotic character of the solutions.

The observed spacing distributions indicated that the transition rate, which is the dominant parameter of the equation, has a certain functional form. This rate includes a parameter which in two limit cases gives lognormal and exponential type behaviour. The effective value lies in the range between these limit cases. Using this as a starting point several results were predicted. These concerned spacing correlations, statistics pertaining to concatenations of successive spacings, and sail numbers on segments. Five different process types were considered and their respective rate parameters were linked to the assumed spacing transition rate and to the basic assumptions of the evolution as a sequence of transition events. The observations and interrelations agreed with the predicted behaviour.

The sail number distribution was studied as the principal alternative to the sail spacing distribution. The solutions of the sail number distribution equation were derived also in cases that correspond to the range of spacing distributions mediating between lognormal and exponential. The corresponding solutions of the spacing distribution are not known. The segment length parameter can also be varied in the sail number distribution which generates of scale system of distributions. By applying such system to observed ridge sail data it was possible to separate the relative intensities of two component processes that strive towards lognormality and exponentiality respectively.

The analytical solutions describe Lagrangian ridge fields. Conservation equations for distributions with a continuously varying coordinate were also given. Such equations can then be parameterised by the results and added to dynamic ice models describing ice cover movement and thickness change. Their relation to concentration change and strain rate was discussed. The sail number approach is more readily applicable here also as the scale systems of sail number distributions are parameterised by ridge density and by the relative intensities of the component processes. If the latter are known, a conservation equation for ridge sail density suffices. The density fields can then also parameterise semiempirical distribution models for spacing and sail number that were generated directly from data with 0.5 m sail height cutoff. A more extensive parameterisation was done for the sail density equation. It can directly use sail densities that are determined from data with 0.5 m cutoff. Values of the sail density equation parameters were estimated for Baltic ridge fields for which 0.75 m average sail height in 0.5 m cutoff data was assumed.

The present work introduced a large number of new concepts and results that can be applied outside the field of Kolmogorov-Feller type equations. These were generated as a by-products of the theory formulation and its parameterisation. Tools for the characterisation of ridge clustering or keel contact were formulated. Spacing cross-section was introduced to replace the ridge cross-section in clustered ridge fields. It also provided the basic structural entity of the evolution theory. Several alternative ways to quantify clusters and their statistics were provided. The occurrence and structure of ridge clusters was discussed at length. Clustering decreases equivalent thickness of ridged ice and average ice consumption from values estimated without it. Only few direct measurements of this effect exist and models constructed from known ridge structure data with simple assumptions were used. In the parameterisation of ridge statistics ridge height and spacing were determined from profile data with cutoff. A model for the statistics for ridges below the cutoff was formulated and a correction factor was added to cross-sectional ridge models when they are used in profile data context. This factor was estimated by considering the height variation of a basic unit, ridge sail link.

The following main conclusions were reached in the present work:

1. In most cases the time change of a variable describing ice cover morphology constitutes a discontinuous Markov process. The time continuous equation for its distribution is then of Kolmogorov-Feller type. In ice morphological contexts this equation has the same degree of fundamentality as the general diffusion equation has for stochastic diffusive transport processes.

2. Equations describing the evolution of ridged ice fields are of Kolmogorov-Feller type. There are several formulations, but the variable transitions constituting the discontinuous Markov process are in all cases due to ridge formation events. This also creates theoretical links between the formulations, and the study of several formulations and their interrelations results into a deeper understanding of the underlying processes. Ice consumption in ridge formation event, which is in average about 300 m, is a feature not present in previous applications of the general theory.

3. In a sufficiently large Lagrangian region the observed ridge distributions are analytically derivable solutions of the equations. The predicting of distribution evolution requires knowledge on the evolution parameters, and the problem is best approached through the direct study of the parameters which are also observable quantities. This also provides a solution to the characterisation problem of homogeneity and spatial continuity in ridged ice fields.

4. Ridge sail spacing evolution is a combined Poisson and clustering process and can be characterised by a parameter quantifying the relative intensity of the Poisson process. For small values of this parameter the spacing distribution is asymptotically lognormal, for large values it shows asymptotically exponential tail. For intermediate values, short spacings show lognormal and long spacings exponential features. If the parameter value is small, the lognormality is enhanced in the statistics of spacing concatenations. Sail spacings and sail heights are not correlated and the ridge height cutoff in observed spacing data does not affect the spacing statistics expect by changing the statistical parameters. Adjacent spacings show logarithmic correlations which follow from the developed multivariate spacing equation.

5. The developed alternative description, ridge number distribution scale system, was in several ways superior to the spacing distribution. Within it the relative rates of Poisson and clustering processes were determined and a set of solutions applicable to all studied data sets constructed. The Poisson intensity is typically 10 % from the clustering intensity. New ridges tend to form to areas with high local ridge density and arrange to close groups. The ridge height cutoff does not affect the statistics and the very good fit between the observed distributions and theory demonstrate the predictability of ridge field evolution within the approach.

6. Evolution processes for five kinds of features were considered: spacings, groups of adjacent spacings, spacing concatenations of two kinds, and linear segments. The respective transition rates were linked through the basic assumption of ridging as a combined clustering and Poisson process. This explained the observed statistics in all cases. There were no indications against

the validity of the approach. Thus the evolution of ridged ice fields can be described within the presented framework using the suggested rates.

7. The spatially continuous conservation equations for ridge field distributions can be formulated and parameterised basing on corresponding Lagrangian formulations and data studies. They can be added to dynamic ice models containing a conservation equation for ridged ice concentration. A directly applicable way is to use the provided conservation equation for ridge density and the developed formulations of ridge spacing and ridge number distributions parameterisable by ridge density only.

8. The basic unit of a ridge field is rather a ridge cluster than a formation where one sail corresponds to one keel, and typically five sails correspond to one keel on the average. Wide clusters with tens of sails are found and contain less than 1/3 of the ice volume estimated with cross-sectional models from sail height only. The spacing cross-section and cluster cross-section should replace the ridge cross-section as basic units of description. The cluster concepts have application potential as large clusters are extremal sea ice features encountered by ships or offshore features. The developed statistics for spacing concatenations and sail numbers can be applied to describe the width and occurrence of clusters.

.

9. Proper estimation of ridged ice volume from surface profile data requires the consideration of the effects of ridge height cutoff, clustering, and the height variation of a ridge sail. The given method for 0.5 m cutoff data is not sensitive to the assumptions considering the extrapolation of observed statistics below the cutoff. The volume reduction factor due to clustering is estimated to lie between 0.5 and 0.7. On the other hand, the volume increase factor, to be included when cross-sectional ridge models are applied to the profile data, was estimated to be about 6. These corrections should be made to previous volume estimates combining cross-sectional models and surface profile data. Equivalent thicknesses of ridged ice up to 1.8 m were estimated for the Bay of Bothnia.

10. The ice consumption parameter links ice area decrease to ridge field evolution. It is principally determined by block thickness and the volume of block rubble in ridges, clusters, or spacing cross-sections. The unreliability of cross-sectional data and models linking ridge height to volume and block thickness is the main source of quantitative error in the present theory. These relationships are also insufficiently seized by simple functional relations and should be modeled as distributed quantities.

11. The work on the equation governing the ice thickness distribution has been hampered by its unnecessary nonlinear formulation and by its detachment from the main body of research around Kolmogorov-Feller type equations. More versatile treatment is possible by following the methodologies of the present work. However, in comparison with the presented equations, for ridged ice fields no benefit is gained from the use of thickness evolution equation. The thickness equation is more applicable in larger scales and then parameterisable by more specific evolution equations describing the time change of various ice types which likewise can be formulated within the given framework. The sail number results suggest that in a ridged ice cover described by segment thickness averages thick ice is more likely to grow thicker than thin ice.

12. The general framework can further be applied to formulate conservation equations for cracks, floes, and leads which then can be either included into ice models as external modules driven by standard model output or be used to develop constitutive equations that are more closely related to the basic physical processes in the ice cover.

The present work opens up a field of continued work on the ridge field evolution, on the evolution of other distributed ice morphological quantities, on the reassessing of thickness equation, on the enhancing of ice models, on proper parameterisation methodologies, and on the application of developed concepts and theories in ice navigation and ice-structure interaction. If properly parameterised evolution equations can be formulated for some ice morphological distribution they create a solid basis for applications and further developments.

However, vistas of more fundamental research open up as well. The ice cover as a quasi two-dimensional system has its own peculiarities that are worth studying. From the viewpoint of the present approach this means the explaining of the transition rates from physical principles. For the evolution of ridged ice fields certain rates were suggested but no explanations of the rates were given. The rates are related to the stress propagation in ice cover which is yet poorly known. However, it is clear that ridging is only one manifestation of the process where global stresses from atmosphere and ocean propagate to local scale and induce local deformation processes. Floe fragmentation, cracking, and lead formation are other such processes. As ridging initiates from cracks, floe-floe contacts, refrozen leads and other local inhomogeneities the respective distributions also evolve together. It appears clear that the local stresses change the local ice cover which, in turn, changes the patterns of stress propagation. The description of this coupling and generally the linking of dynamic and morphological evolution is the background scientific programme of the present work.

REFERENCES

Aitchison, J. and Brown, J.A.C. 1957 The Lognormal Distribution. Cambridge University Press.

Alvarez, J., Alvarez, J. and Hernandez, M. 1994 A population balance approach for the description of particle size distributions in suspension polymerisation reactors. Chem. Engng Sci. 49 (1) 99-113.

Ball, J.M. and Carr, J. 1990 The discrete coagulation-fragmentation equations: existence, uniqueness, and density conservation. J. Statist. Phys. 61 (1-2) 203-234

Bendat, J.S. and Piersol, A.G 1986 Random data. John Wiley & Sons.

Bitz, C.M., Holland, M.M., Weaver, A.J., Eby, M. 2001 Simulating the ice-thickness distribution in a coupled climate model, J. Geophys. Res. 106, 2441-2463.

Bowen R.G. and Topham, D.R. 1996 A study of the morphology of a discontinuous section of a first year arctic pressure ridge. Cold Reg. Sci. Technol. 24, 83-100.

Chao, J.C. 1992 Comparison of ridge load prediction methods and experimental data for conical structures. Proceedings of 11th International Conference on Offshore Mechanics and Arctic Engineering (OMAE 1992), Calgary, Vol IV, 195-203

Cheng, Z. and Redner, S. 1988 Scaling theory of fragmentation. Phys. Rev. Letters 60 (24) 2450-2453.

Cheng, Z. and Redner, S. 1990 Kinetics of fragmentation. J. Phys. A: Math. Gen. 1233-1258.

Climatological Ice Atlas 1982. Climatological Ice Atlas for the Baltic Sea, Kattegat, Skagerrak and Lake Vänern (1963-1979). Distributed by Sjöfartsverket, S-60179 Nörrköping. Sjöfartsverkets tryckeri, Norrköping.

Connors, D.N., Levine, E.R., Shell, R.R. 1990. A small-scale under-ice morphology study in the High Arctic. In S.F. Ackley and W.F. Weeks (editors), Sea Ice Properties and Processes, CRREL monograph 90-1, 145-151.

Davis, N.R. and Wadhams, P. 1995 A statistical analysis of Arctic pressure ridge morphology. J. Geophys. Res. 100 (C6) 10915-10925.

Dierking, W. 1995 Laser profiling of the ice surface topography during the Weddell Gyre Study 1992. J. Geophys. Res. 100 C3, 4807-4820.

Dubowskii, P.B. and Stewart, I.W. 1996 Existence, uniqueness and mass conservation for the coagulation-fragmentation equation. Math. Methods Appl. Sci. 19(7) 571-591

Epstein, B. 1947 The mathematical description of certain breakage mechanisms leading to the logarithmico-normal distribution. J. Franklin Inst. 224.

Feller, W. 1936 Zur Theorie der Stochastischen Prozesse. Math. Ann. 113, pp. 113-160.

Fily, M. and Rothrock, D.A. 1990 Opening and closing of sea ice leads: Digital measurements from SAR. J. Geophys. Res., 95(C1), 789-796.

Flato, G.M. and W.D. Hibler III, 1991 An initial numerical investigation of the extent of sea-ice ridging. Ann. Glaciol. 15, 31-36.

Flato, G.M. and W.D. Hibler III, 1995 Ridging and strength in modelling the thickness distribution of Arctic sea ice. J. Geophys. Res., 100, 18,611-18,626.

Granberg, H.B. and Leppäranta, M. 1999 Observations of sea ice ridging in the Weddell Sea. J.Geophys. Res. 104 (C11), 25 735-25 745

Gray, J.M.N.T. and Killworth, P.D. 1996 Sea ice ridging schemes. J. Phys. Oceanogr. 26, 2420-2428.

Gray, J.M.N.T. and Morland, L.W. 1994 A two-dimensional model for the dynamics of sea ice. Philos. Trans. R. Soc. London. A, 347, 219-290.

Gumbel, E.J. 1958 Statistics of extremes. Columbia University Press.

Haapala, J., 2000 On the modelling of the ice thickness redistribution. J. Glaciol. 46, 427-437.

Haapala J. and Leppäranta, M. 1996 Simulations of the Baltic Sea ice season with a coupled ice-ocean model. Tellus 48A, 622-643.

Haapala, J. and Leppäranta, M. (editors) 1997 ZIP-97 data report. Report series in geophysics 37. University of Helsinki, Department of Geophysics.

Harder, M. and Lemke, P. 1994 Modeling the extent of sea ice ridging in the Weddell Sea, The Polar Oceans and Their Role in Shaping the Global Environment, Geophys. Monogr. Ser., edited by O. M. Johannessen, R.D. Muench, and J. E. Overland, vol. 85, pp. 187-197, AGU Washington, D. C.

Hibler, W.D. III 1972 Removal of aircraft altitude variation from laser profiles of the Arctic Ice Pack. J. Geophys. Res. 77 (36), 7190-7195.

Hibler, W.D. III 1979 A dynamic thermodynamic sea ice model, J. Phys. Oceanogr. 9, 815-845

Hibler, W.D., III 1980 Modeling a variable thickness sea ice cover. Mon. Weather Rev. 108 (12) 1943-1973.

Hibler, W.D. III 1984 The role of sea ice dynamics in modeling CO_2 increases. In: Climate Processes and climate sensitivity, Geophys. Monogr. No 29, Vol. 5, 238-253.

Hibler, W.D. III 1986 Ice Dynamics. In: Geophysics of Sea Ice, edited by Norbert Untersteiner, NATO ASI series B: Physics Vol 146, Plenum Press, New York and London.

Hibler, W.D. and Ackley, S.F. 1975 Height variation along sea ice pressure ridges and the probability of finding 'holes' for vehicle crossings. Journal of Terramechanics 12 (3/4) 191-199.

Hibler, W.D. III, Mock, J.S. and Tucker, W.B. III 1974 Classification and variation of sea ice ridging in the western Arctic basin. J. Geophys. Res. 79 (18) 2735-2743.

Hibler, W.D. III, Weeks, W.F: and Mock, S.J. 1972. Statistical aspects of sea-ice ridge distributions. J. Geophys. Res. 77, 5954-5970.

Hopkings, M.A. 1996 On the mesoscale interaction of lead ice and floes. J. Geophys. Res. 101 (C8), 18315-18326.

Hopkins, M.A. 1998 Four stages of pressure ridging. J. Geophys. Res. 103 (C10), 21883-21891

Hopkins, M.A. 1999 A granular sea ice model. Proceedings of the 15th Int. Conference on Port and Ocean Engineering under Arctic Conditions, POAC '99, Vol. 1, pp. 91-96, Espoo, Helsinki University of Technology.

Hopkins, M.A., Tuhkuri J. and Lensu, M. 1999 Rafting and ridging of thin ice sheets. Journal of Geophysical Research 104 (C7), 15815-15825.

Hoyland, K.V., Kjestveit, G., Heinonen, J. and Määttänen, M. 2000 LOLEIF ridge experiments at Marjaniemi; the size and strength of the consolidated layer. The 15th International Ice Symposium, IAHR´00, Gdansk, Poland, 28.8 - 1.9.2000. Gdansk 2000, Institute of Hydroengineering, Polish Academy of Sciences, Gdansk, Poland, Vol 1, p. 45-52

Johnson N. and Kotz S. 1969 Distributions in Statistics:Discrete Distributions. Houghton Mifflin.

Kankaanpää, P. 1997 Distribution, morphology and structure of sea ice pressure ridges in the Baltic Sea. Fennia 175 (2)

Keinonen, A. 1976 The shape and size of ice ridges in the Baltic according to measurements and calculations. Winter Navigation Research Board, Research Report 17. Finnish Board of Navigation. 50 pp.

Keinonen, A. 1979 An analytical methods for calculating the pure ridge resistance encountered by ships in first year ice ridges. Thesis for the degree of Doctor of Technology. Helsinki University of Technology.

Key, J. and McLaren, A.S. 1989 Periodicities and keel spacings in the under-ice draft distribution of the Canada Basin. Cold Reg. Sci. Technol. 16,1-10.

Kolmogorov, A.N. 1931 Über die analytischen Methoden in der Wahrscheinlichkeitsrechnung. Math. Ann. 104, pp 415-458.

Kolmogorov, A.N.1941 Über das logaritmisch normale Verteilungsgesetz der Dimensionen der Teilchen bei Zerstückelung. C.R. Acad. Sci.U.R.S.S. 31, 99

Kovacs, A. 1970 On the structure of pressured sea ice. Publications of U.S. Army Cold Regions Research and Engineering Laboratory (CRREL) Sep. 1970.

Kovacs, A. 1972 On pressured sea ice. In: T.Karlsson (editor), Sea Ice, National Research Council, Iceland, Reykjavik, 276-295.

Kovacs, A. and Sodhi, D.S. 1980 Shore ice pile-up and ride-up: Field observations, models, theoretical analyses. Cold Reg. Sci. Technol. 2, 209-288.

Kreider, J.R. and Thro, M.E. 1981 Statistical techniques for the analysis of sea ice pressure ridge distributions. Proc. POAC'81, 789-798.

Kujala, P. 1994 On the statistics of ice loads on ship hull in the Baltic. Acta Polytechnica Scandinavica, Mechanical Engineering Series No.116.

Landahl, M.T. and Mollo-Christensen, E. 1992 Turbulence and random processes in fluid mechanics. Cambridge University Press.

Lensu, M. 1992 The evolution of floe distributions. - Internal report / Finnish Institute of Marine Research 1992(8):1-43.

Lensu, M. 1993a Morphological distributions in ice geophysics: Basic solutions of the evolution equation. Internal report / Finnish Institute of Marine Research 1993(12) 37 p.

Lensu, M. 1993b Statistics of a ridged ice field in the Bay of Bothnia. Internal report / Finnish Institute of Marine Research 1993(11) 50 p.

Lensu, Mikko 1993c Ice morphology. In Kosloff, P. et al. (eds.): BEERS 92. R/V Aranda base data report II: The measurements. Internal report / Finnish Institute of Marine Research 1993 (5) p.15-47.

Lensu, M. 1994a Field observations during OSIC ice expedition in February 1993. Internal report / Finnish Institute of Marine Research 1994(3), 38 p.

Lensu, M. 1994b Field observations during OSIC ice expedition in March 1994. Internal report / Finnish Institute of Marine Research 1994(9), 38 p.
Lensu, M. 1995a The analysis of laser profilometer data. AEM flights in the Baltic, winter 1994. Helsinki University of Technology/Ship Laboratory report series M-195, 98 p.
Lensu, M. 1995b Ridge link distributions. Proc. of POAC 95 vol III and vol IV, St. Petersburg.
Lensu, M. 1997 Correlations between fragment sizes in sequential fragmentation. J. Phys. A: Math. Gen. 30, p.7501-7507.
Lensu, M. 1998a Distribution of the number of fragmentations in continuous fragmentation. J.Phys. A: Math. Gen. 31, p. 5705-5715.
Lensu, M. 1998b Laser profilometer measurements in the Bay of Bothnia during the ZIP-97 experiment. Helsinki University of Technology, Ship Laboratory Report Series M-232, 148 p.
Lensu, M. 1999a A model for ridge field statistics. Proceedings of the 15th Int. Conference on Port and Ocean Engineering under Arctic Conditions, POAC '99, Vol. 3, pp 1001-1010, Espoo, Helsinki University of Technology.
Lensu, M. 1999b Sea ice ridging in the Kara Sea. Proceedings of the 15th Int. Conference on Port and Ocean Engineering under Arctic Conditions, POAC '99, Vol. 1, pp. 371-379, Espoo, Helsinki University of Technology.
Lensu, M. 1999c Incorporation of distributions for floes, ridges, leads and thickness into mesoscale ice description. In K.Riska and J.Tuhkuri (editors), Local ice cover deformation and mesoscale ice dynamics, Part I: Final scientific report. Helsinki University of Technology, Ship Laboratory Report Series M-242, pp. 62-76.
Lensu, M. 1999d The time evolution of mesoscale morphological distributions. In K.Riska and J.Tuhkuri (editors), Local ice cover deformation and mesoscale ice dynamics, Part I: Final scientific report. Helsinki University of Technology, Ship Laboratory Report Series M-242, pp. 77-99.
Lensu, M. 2002 A downscaling structure for distributions describing ice characteristics. In Dempsey, J.P. and Shen, H.H. (editors), IUTAM Symposium on Scaling Laws in Ice Mechanics and Ice Dynamcis. Solid Mechanics and its Applications 94, Kluwer Academic Publishers.
Lensu, M., Heale, M., Riska, K. and Kujala.P. 1996 Ice envinronment and ship hull loading along the NSR. Insrop Working Paper No. 66 - 1996.I.1.10.
Lensu, M. and Green, J. 1995 Ice tank tests on pressure ridge formation. Helsinki University of Technology, Ship Laboratory Report Series M-202, 83 p.
Lensu, M., Tuhkuri, J. and Hopkins, M. 1998 Measurements of curvilinear ridges in the Bay of Bothnia during the ZIP-97 experiment. Helsinki University of Technology, Ship Laboratory Report Series M-231, 64 p.
Leppäranta, M. 1981a Statistical features of sea ice ridging in the Gulf of Bothnia. Styrelsen för Vintersjöfartsforskning, Forskningsrapport 32 (Winter Navigation Reseach Board, Research Report 32).
Leppäranta, M. 1981b On the structure of pack ice in the Bothnian Bay. Finnish Marine Research 248.
Leppäranta, M. 1981c An ice drift model for the Baltic Sea. Tellus 33 (6): 583-596

Leppäranta, M. 1983 Size and shape of ice floes in the Baltic Sea in spring. Geophysica 19:2, 127-136.
Leppäranta, M. 1998 The dynamics of sea ice. In Physics of Ice-Covered Seas, ed.by M. Leppäranta, University of Helsinki, Department of Geophysics. Vol I, 305-342.
Leppäranta, M. and Hakala, R. 1992 The structure and strength of first year ridges in the Baltic Sea. Cold Reg. Sci. Technol. 23, 279-290.
Leppäranta, M. and Hibler, W.D. III 1987 Mesoscale sea ice deformation in the East Greenland marginal ice zone. J. Geophys. Res. 90 (C6) 11899-11909
Leppäranta, M., Lensu, M., Kosloff, P. and Veitch, B. 1995 The life story of a first-year sea ice ridge. Cold Reg. Sci. Technol. 23, 279-290
Leppäranta, M. and Palosuo, E. 1981 Studies of sea ice ridging with a shipborne laser profilometer. Proc. POAC'81, Vol. II, 1031-1038.
Lewis, J.E., Leppäranta, M. and Granberg, H.B. 1993 Statistical properties of sea ice surface topography in the Baltic Sea. Tellus 45 A, 127-142.
Lowry, R.T. and Wadhams, P. 1979 On the statistical distribution of pressure ridges in sea ice. J. Geophys. Res. 84, 2487-2494.
Lytle, V.I. and Ackley, S.F. 1991 Sea ice ridging in the Eastern Weddell Sea. J. Geophys. Res. 96, C10, 18411-18416.
Lu, Q.M., Larsen, J. and Tryde, P. 1989 On the role of ice interaction due to floe collisions in marginal ice zone dynamics. J. Geophys. Res. 94, C10, 14525-14537
Manninen, A.T. 1996 Surface morphology and backscattering of ice-ridge sails in the Baltic Sea. J.Glaciol. 42 (140), 141-146
Manninen, A.T. 1997 Surface roughness of Baltic Sea Ice. J. Geophys. Res. 102 C1, 1119-1139.
Marchenko, A. 1999 On the construction of kinetic theory of ice cover taking into account the evolution of internal ice structure. Proceedings of The 15th International Conference on Port and Ocean Engineering
McGrady, E.M. and Ziff, R.M. 1987 “Shattering” transition in fragmentation. Phys. Rev.Lett. 58 (9) 892-895.
McLaren, A.S. 1989 The under-ice thickness distribution of the Arctic basin as recorded in 1958 and 1970. J. Geophys. Res. 94, 4971-4983.
Melling, H. and Riedel, D.A. 1995 The underside tophography of sea ice over the continental shelf of the Beaufort Sea in the winter of 1990. J. Geophys. Res. 100(C7), 13641-13653.
Melling, H., Topham, D.R. and Riedel, D. 1993 Topography of the upper and lower surfaces of 10 hectares of deformed sea ice. Cold Reg. Sci. Technol. 21, 349-369.
Mock, S.J., Hartwell, A.D. and Hibler, W.D. III 1972 Spatial aspects of pressure ridge statistics. J. Geophys. Res. 77, 5945-5953.
Multala, J., Hautaniemi, H., Oksama, M., Leppäranta, M., Haapala, J., Herlevi, A., Riska, K. and Lensu, M. 1996 An airborne electromagnetic system on a fixed wing aircraft for sea ice thickness mapping. Cold Reg. Sci. Technol. 24 (1996) 355-373.

Mäkinen, E., Keinonen, A.J. and Laine, A. 1975 Ice resistance measurements in ridges with I/B APU in the Baltic Sea. Proceedings of POAC '75, Fairbanks, Alaska.

Norris, J.R. 1998 Smoluchowski's coagulation equation: Uniqueness, non-uniqueness and a hydrodynamic limit for the stochastic coalescent. Univ. of Cambridge, Statistical Laboratory research reports 1998(1).

Nyman, T., Riska, K., Soininen, H., Lensu, M., Jalonen, R., Lohi, P. and Harjula, A. 1999 The ice capability of the multipurpose icebreaker Botnica - full scale results. Proceedings of the 15th Int. Conference on Port and Ocean Engineering under Arctic Conditions, POAC '99, Helsinki University of Technology., 631-643

Ochi, M.K. 1990 Applied probability and stochastic processes. John Wiley & Sons.

Overland, J.E., McNutt, S.L, Salo, S., Groves, J. and Li, S. 1998 Arctic sea ice as a granular plastic. J. Geophys. Res. 103 (C10) 21845-21867

Palosuo, E. 1971 Ice ridges in a coastal area of Finland. Proceedings of POAC'71, The Technical University of Norway, Trondheim, Norway, 23-30 Aug. 1971.

Palosuo, E. 1975 The formation and structure of ice ridges in the Baltic. Report Nr 12, Winter Navigation Research Board, Helsinki, Finland.

Parmerter, R.R. and Coon, M.D. 1972 Model of pressure ridge formation in sea ice. J.Geophys. Res. 77, 6565-6575.

Parmerter, R.R. and Coon, M.D. 1973 Mechanical models of ridging in the Arctic sea ice cover. AIDJEX bulletin No. 19, Washington.

Prabhu, N.U. 1965 Stochastic Processes. The Macmillan company.

Pritchard, R.S. 1998 Ice conditions in an anisotropic sea ice dynamics model. Int. Journal of Offshore and Polar Engineering 8 (1).

Ramkrishna, D. 1985 The status of population balances. Rev. Chem. Engng. 3. 49-95

Redner, S. 1990 Fragmentation. In H.J. Herrmann and S. Roux (editors), Statistical Models for the Fracture of Disordered Media. North-Holland, Amsterdam.

Reynolds, E. and Lindholm, J.-E. Field measurements of Northern Baltic pressure ridges. Helsinki University of Technology, Arctic Offshore Research Centre, Report Series M-19.

Rothrock, D.A. 1975 The Energetics of the plastic deformation of pack ice by ridging. J. Geophys. Res. 80 (33) 4514-4519.

Rothrock, D.A. 1986 Ice thickness distribution - measurement and theory. In: Geophysics of Sea Ice, edited by Norbert Untersteiner, NATO ASI series B: Physics Vol 146, Plenum Press, New York and London.

Sayed, M. and Frederking, R.M.W. 1988 Model of ice rubble pileup. Journal of Engineering Mechanics 114, 149-160.

Sayed, M. and Frederking, R.M.W. 1991 Ridge sail statistics at the shear edge at Lancaster sound. Ann. Glaciology 15, 271-275.

Schulkes, R.M.S.M. 1995 A note on the evolution equations for the area fraction and the thickness of a floating ice cover. J. Geophys. Res. 100 (C3) 5021-5024.

Shen, H.H., Hibler, W.D. III and Leppäranta, M. 1987 The role of floe collisions in sea ice rheology. J. Geophys. Res. 92, 7085-7096.

Shinohara, Y. 1990 A redistribution function applicable to a dynamic model of sea ice. J. Geophys. Res. 95, 13423-13431.

Smoluchowski, M. van 1916 Drei Vorträge über Diffusion, Brownsche Bewegung und Koagulation von Kolloidteilchen. Physik. Z. 17, 557-585

Steiner, N., Harder, M. and Lemke, P. 1999 Sea Ice Roughness and Drag Coefficients in a Dynamic-Thermodynamic Sea Ice Model for the Arctic, Tellus, 51A (5), 964-978.

Stern, H.L., Rothrock, D.A. and Kwok, R. 1995 Open water production in the Arctic sea ice cover: Satellite measurements and model parameterizations, J.Geophys. Res., 100(C10), 20,601-20,612.

Thomas, D., Martin, S., Rothrock, D. and Steele, M. 1996 Assimilating satellite concentration data into an Arctic sea ice mass balance model, 1979-1985. J. Geophys. Res. 101, 20849-20868

Thorndike, A.S. 1992 Estimates of sea ice thickness distribution using observations and theory. J. Geophys. Res. 97 (C8) 12601-12605

Thorndike, A.S., Rothrock, D.A., Maykut, G.A., and Colony, R. 1975 The thickness distribution of sea ice. J. Geophys. Res 80 (33)

Timco G.W. and Burden R.P. 1997 An analysis of the shapes of sea ice ridges. Cold Regions Science and Technology 25,65-77.

Timco, G.W. and Sayed, M. 1986 Model tests of the ridge-building process of ice. Proceedings of IAHR Ice Symposium Vol I, 591-602.

Timokhov, L.A. 1988 Ice dynamics models. In M. Leppäranta (editor), Physics of Ice-Covered Seas. University of Helsinki.

Treat, R.P. 1997a On the similarity solution of the fragmentation equation. J. Phys. A:Math. Gen. 30, 2519-2543.

Treat, R.P. 1997b Similarity solution for fragmentation with volume change. J. Phys. A: Math. Gen. 30, 7639-7658.

Tucker, W.B. III, and Govoni, J.W. 1981 Morphological investigations of first-year sea ice pressure ridge sails. Cold. Reg. Sci. Technol. 5, 112.

Tucker, W.B. III, Sodhi, D.S. and Govoni, J.W. 1984 Structure of first-year pressure ridge sails in the Prudhoe Bay region. In P.W.Barnes, D.M.Shell and E.Reimnitz (editors), The Alaskan Beaufort Sea: Ecosystems and Environment, Academic Press, San Diego, Calif., 113-135.

Tucker, W.B. III, Weeks, W.F. and Frank. M. 1979 Sea ice ridging over the Alaskan continental shelf. J. Geophys. Res. 84 C8, 4885-4897.

Tuhkuri, J. and Lensu, M. 1998 Ice tank tests on ridging of non-uniform ice sheets. Espoo, Helsinki University of Technology, Ship Laboratory, Report M-236. 130 p.

Tuhkuri, J. and Lensu, M. 2002 Laboratory tests on ridging and rafting of ice sheets. J. Geophys. Res. 107 (C9), 3125.

Wadhams, P. 1980 A comparison of sonar and laser profiles along corresponding tracks in the Arctic Ocean. In R.S. Pritchard (ed.), Sea Ice Processes and Models, pp. 283-299. University of Washington Press, Seattle.

Wadhams P. 1981 Sea ice topography of the Arctic Ocean in the region 70 W to 25 E. Philosophical Transactions of the Royal Society of London, Ser. 1A, 302 (1464), 45-85

Wadhams, P. 1997 Ice thickness in the Arctic Ocean: The statistical reliability of experimental data. J. Geophys. Res. 102 (C13), 27951-27959.

Wadhams, P. and Davy, T. 1986 On the spacing and draft distributions for pressure ridge keels. J.Geophys. Res. 91 (C9), 10697-10708.

Wadhams, P. and Horne R.J. 1980 An analysis of ice profiles obtained by submarine sonar in the Beaufort Sea. J. Glac. 25 (93) 401-424.

Wadhams, P., Tucker, W.B., III, Krabill, W.B., Swift, R.N., Comiso, J.C. and Davis, N.R. 1992 Relationship between sea ice freeboad and draft in the Arctic Basin, and implications for ice thickness monitoring. J.Geophys. Res. 97 (C12) 20325-20334.

Weeks, W.F., Ackley, S.F. and Govoni, J. 1989 Sea ice ridging in the Ross Sea, Antarctica, as compared with sites in the Arctic. J. Geophys. Res. 94 C4 4984-4988.

Weeks, W.F., Kovacs, A. and Hibler, W.D. III 1971 Pressure ridge charactristics in the Arctic coastal environment. Proceedings of POAC'71, Technical University of Norway, Trondheim, Norway, 23-30 August 1971.

Veitch, B., Lensu, M., Riska, K., Kosloff, P., Keiley, P. and Kujala, P. 1991 Field observations of ridges in the northern Baltic Sea. Proceedings of POAC'91, St.Johns, Canada, 381-400.

Vinje, T., Nordlund, N. and Kvambekk, A, 1998 Monitoring ice thickness in Fram Strait. J.Geophys. Res., Vol. 103, C5, 10437-10449.